REPORT

Earth Sciences and Environmental Technologies Division

Study	MPN12	**Division chrono**	R164/n°21/016
Partners		**Contract**	1997C0022

Title	**Assuring integrity of CO2 storage sites through ground surface monitoring (SENSE) - WP2.2: Understanding the mechanism of surface movement (Deliverable D2.2)**		
Author(s) and membership	BOUQUET Sarah, ESTUBLIER Audrey, FOURNO André, FREY Jérémy, MALINOUSKAYA Iryna		
Diffusion	Public	**Publication date**	8/1/2021
Division visa *Scientific authentication*	HERZHAFT Benjamin	**Project visa** *Specification compliance*	ESTUBLIER Audrey

Keywords	Surface displacement – Coupled flow-geomechanical simulation – CO2 storage integrity – Cost-effective monitoring – Conceptual models – Subsurface uncertainties – Risk analysis – Failure criterion

Summary

The project, SENSE, is funded through the ACT program (Accelerating CCS Technologies, Horizon2020 Project No 294766). Its objective is to demonstrate how surface displacements can be used in a monitoring program aimed at verifying the long-term integrity of a CO_2 geological storage site. IFPEN participates as WP2 (work package) leader to coordinate the flow/geomechanics coupling simulation activities in order to understand the surface displacement mechanism in response to pressure changes due to CO_2 injection. In this WP2, IFPEN works both on the conceptual models and simulation activities with synthetic cases and real cases.

This report addresses the Task 2.2: Initial evaluation of the observability of deformation mechanisms and potential for constraining subsurface processes. The objectives of this task are (i) identify whether surface displacements are likely to be "visible" by monitoring tools and for which resolution, (ii) identify which conditions impact surface displacements, (iii) analyze the usefulness of various surface monitoring techniques (based on satellites, tiltmeters, GPS, etc.) and their ability to provide concrete information on subsurface behavior. A coupled flow-geomechanical model is developed and applied to various key scenarios. For each of these scenarios, a statistical analysis of the system responses is performed as a function of the *a priori* uncertain subsurface properties. Statistical analysis is also performed to define the probability to detect surface movement with the various tools in the diverse contexts and thus define the usefulness of each tool for each context. This study reveals to be useful to monitor the subsurface deformations, to predict the long-term CO_2 storage fate, and to be able to give early warning of an unexpected behavior. It also allows to draw some recommendations for the monitoring design.

Earth Sciences and Environmental Technologies Division

Diffusion list (pdf)	E-mail address
DELPRAT-JANNAUD Florence	
SOUQUE Christine	
ESNAULT Vivien	
GERVAIS-COUPLET Véronique	
HERZHAFT Benjamin	
CACAS-STENTZ Marie-Christine	
REINERT BRUCH André	
BOUQUET Sarah	
FOURNO André	
MALINOUSKAYA Iryna	
FREY Jérémy	
ROGGERO Frédéric	
BOHLOLI Bahman (NGI)	Bahman.Bohloli@ngi.no
BOUXIN Alix (ADEME)	alix.bouxin@ademe.fr

For agreement,

Benjamin HERZHAFT :
Accord du Directeur de la Direction Sciences de la Terre et Technologies de l'Environnement

Table of contents

Earth Sciences and Environmental Technologies Division

Project information

Project title: Assuring integrity of CO2 storage sites through ground surface monitoring (SENSE)

Project period: 1 September 2019-30 August 2022

Project Coordinator: Norwegian Geotechnical Institute

Web-site: https://sense-act.eu/

Deliverable No.:	D2.2	***Responsible for deliverable:***	IFPEN
Quality control by:	IFPEN, Frederic Roggero	***Contributing partner(s):***	IFPEN
Deliverable prepared by:	BOUQUET Sarah, ESTUBLIER Audrey, FOURNO André, FREY Jérémy, MALINOUSKAYA Iryna	***Dissemination level:***	Open Access
Project No.:	299664	***Date: 2021-08-01***	Rev. No.: 0

The project, SENSE, is funded through the ACT program (Accelerating CCS Technologies, Horizon2020 Project No 294766). Financial contributions made from The Research Council of Norway, (RCN), Norway, Gassnova SF (GN), Norway, Bundesministerium für Wirtschaft und Energie (BMWi), Germany, French Environment & Energy Management Agency (ADEME), France, US-Department of Energy (US-DOE), USA, Department for Business, Energy & Industrial Strategy (BEIS) together with extra funding from NERC and EPSRC research councils, United Kingdom, Agencia Estatal de Investigación (AEI), Spain, Equinor and Quad Geometrics are gratefully acknowledged.

1 Introduction

For carbon dioxide capture and storage technology (CCS) having a significant impact on climate objectives, significant quantities of CO_2, on the order of several gigatons per year, must be captured and stored. This means that the volume and number of injection sites must be rapidly increased, from today's isolated demonstrations pilots to large-scale storage sites. Monitoring of CO_2 geological storage sites is crucial to verify the behavior of the sites and to enable their long-term closure as well as to gain acceptance of the process as a reliable method of reducing CO_2 emissions. The SENSE project aims to develop reliable and cost-effective monitoring based on the combination of ground motion measurements with geomechanical modelling and inversion (Figure 1).
The objective of this project is to demonstrate how surface displacements can be used in a monitoring program aimed at verifying the long-term integrity of a CO_2 geological storage site.
The proposed research activities include:

- demonstration of continuous monitoring of surface displacements and subsurface pressure distribution using satellite data, water pressure sensors, tiltmeter array, fiber optics, and seafloor geodesy;
- quantitative characterization of critical geomechanical and hydraulic parameters and automatization routine for data processing and interpretation;
- optimization of sampling arrays to offer to storage site operators a cost-effective monitoring option as part of an effective site assurance program and feeding into existing workflows for an early alert system.

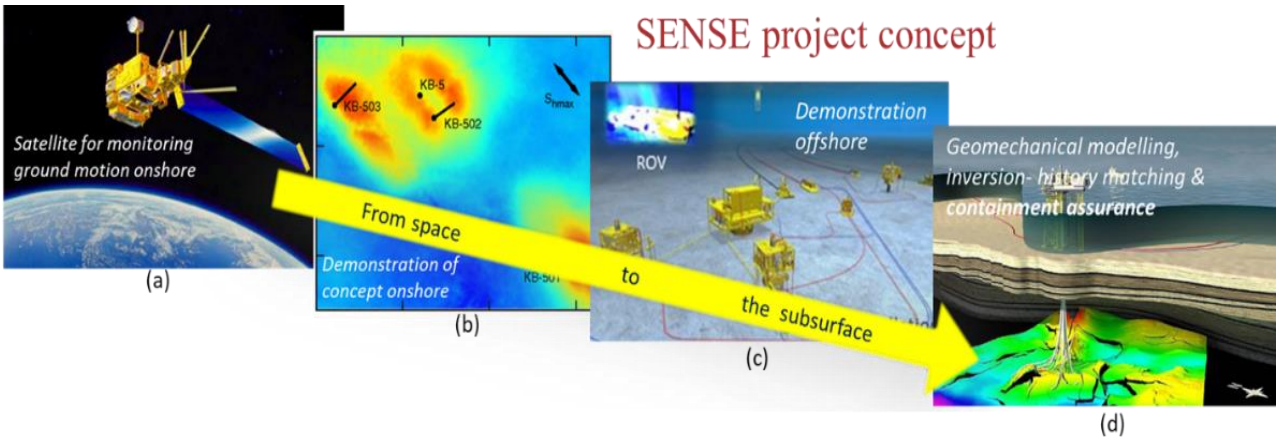

Figure 1 : Key elements of SENSE project with the objective to analyze the usefulness of various surface monitoring techniques and their ability to provide information on subsurface behavior

As WP2 leader, IFPEN coordinates the flow-geomechanics simulation activities to understand the surface displacement mechanism in response to pressure changes due to CO_2 injection. The objective of WP2 is to develop conceptual/theoretical models, possibly based on newly acquired and available data (e.g. In Salah) within the framework of the project and to perform advanced coupled flow-geomechanics simulations to study the geomechanical behavior of these sites in response to reservoir pressure changes. This is summarized in 3 tasks

- Task 2.1: Integration of ground movement datasets and presentation of conceptual models (leader: NGI). Conceptual models are used to identify which conditions induce different surface displacements, require specific surface monitoring strategy and to cover different situations encountered at storage sites.
- Task 2.2: Initial evaluation of the observability of deformation mechanisms and potential for constraining subsurface processes (leader: IFPEN)
- Task 2.3: Numerical simulation of ground movement in response to reservoir pressure change for the candidate sites (leader: LLNL)

This report describes the results obtained from the Task 2.2, *i.e.* **the analysis of surface displacement potential as data for constraining subsurface processes.** From numerical simulations of CO_2 injection for synthetic case studies, the objectives of this task are:

- identify whether surface displacements are likely to be "visible" by monitoring tools and for which resolution,
- identify which conditions impact surface displacements,
- analyze the usefulness of various surface monitoring techniques (based on satellites, tiltmeters, GPS, etc.) and their ability to provide concrete information on subsurface behavior.

Coupled flow-geomechanical models are used to relate surface displacements to subsurface formations parameters. From the uncertainty on the subsurface properties and the uncertainties on the measurements, predictive models (coupled flow-geomechanical simulations) can reproduce the expected measurements obtained with various surface monitoring tools. By carrying out a sensitivity study and considering the advantages and disadvantages of each tool (including their respective accuracies), a design can be defined such that the tools will record potential displacements at the most sensitive periods and locations.
We also must prove that the information acquired by these tools is valuable in terms of monitoring, it means that it can be used to characterize the reservoir and its subsurface environment (unknown fault or heterogeneity), to predict subsurface behavior and to anticipate unexpected behaviors (risk of leakage, risk for formation integrity).
These predictive models can distinguish the type of response expected according to the formations structure, to quickly analyze any type of *a priori* abnormal behavior on the surface and identify structures which might be missed in the first phase of exploration. Differences in displacements, detectable by the selected monitoring tools, must clearly be observed between models and parameter sets in order to define relevant sampling, to discriminate between models and parameter sets and/or to use surface displacement measurements as a monitoring tool to guarantee the storage integrity. Eventually, if they are discriminating, the surface deformation measurements will be used through model inversion to constrain the values of the coupled model parameters (flow and mechanical).
Finally, typical results from these analyses can be used by operators to define what are the necessary requirements for monitoring CO_2 storage at surface.

To achieve these objectives, numerical models coupling flow and geomechanics are developed for different key scenarios. For each specific surface displacement, the potential for surface monitoring in time and space can be evaluate with these numerical results. Numerical coupling is described in the paragraphs 2.1 and 2.2.
IFPEN and Lawrence Livermore National Laboratory (LLNL), the other partner in this task, have designed geological and mechanical scenarios representative of the CO_2 storage sites characteristics. The following scenarios have been selected:

1. "simple" formations, uniform and circular displacements expected at the surface,
2. presence of faults (sealing or draining),
3. reactivation of faults,
4. fracturing of the cap rock.

The task partners have shared the scenarios to be treated. IFPEN worked on scenarios 1, 2. For some cases, facies/flow properties heterogeneities are considered.
The identification of conditions inducing variations in surface displacements relies on the definition of the different scenarios, representative of real potential storage sites. Conceptual models and related scenarios are described in paragraph 2.3.
For each of these scenarios, a statistical analysis of the system responses is performed as a function of the *a priori* uncertain subsurface properties. If differences in observed surface displacements can be related to some model parameters (e.g. subsurface properties), then the measured surface displacements could help to characterize such subsurface properties. Statistical analysis is also performed to define the probability to detect surface movement with the various tools in the diverse contexts and thus define the usefulness of each tool for each context. These results are presented in paragraphs 3 and 5. In paragraph 4, we compared these results from two coupled modelling techniques. Recommendations are drawn in terms of modelling for surface monitoring from this comparison.

2 Methods

This paragraph addresses the methods used in the workflow applied in this study and presents the conceptual models characterizing the chosen scenarios and the surface monitoring tools studied in this project.

This workflow is divided into 6 steps:

1. Building of a Latin Hypercube Sampling (LHS) design (McKay et al., 1979) of experiments of *m* models to be simulated based of the uncertain parameters
2. For each simulation, computation of the storage capacity and surface displacement by a coupled flow-geomechanics model
3. Statistical analysis of the surface displacement observability to define the area where (and the period of time when) surface displacements are measurable with a tiltmeter and INSAR technology using the standard deviation value and the Shannon entropy (cf. section 2.4)
4. Sensitivity analysis to define the most sensitive uncertain parameters for which the soil surface displacement data would be the most informative using the HSIC value or the Sobol indices (cf. section 2.4)
5. Design (location of measurements) of an optimized monitoring plan to better constrain the most sensitive parameters.

   To optimize the monitoring design with the objective to better constrain subsurface properties and, consequently, the subsurface behavior, we propose to select data locations corresponding to a high dependency between data measurements and uncertain properties, *i.e.* **with the highest HSIC values** (cf. section 2.4), and **with the highest variance** for data measurements based on uncertainty analysis and corresponding simulations.

   The efficiency of these measurements is evaluated through a Bayesian approach, similarly to one from Barros et al., 2020 (pre-ACT project). We also suggest using metamodels predictions to investigate further parameters combinations.

   For sensors locations selection with a detection limit, the following method based on simulations results from the training sample for each scenario is applied.
   1 - Remove data below detection threshold.
   2 - Evaluate HSIC values for different uncertain parameters.
   3 - Select coordinates related to the highest values of HSIC.
   4 - Evaluate variance and/or entropy.
   5 - Restrain coordinates for the highest variance and/or entropy.

6. Failure criterion calculation for risk analysis to define additional points of monitoring.

2.1 Coupled flow-geomechanics model

The coupled hydro-mechanical simulation (Baroni et al., 2015) is based on the sequential coupling of the IFPEN reservoir simulator PumaFlow (IFP Energies Nouvelles, 2018) and Code_Aster (EDF, 2020). PumaFlow is a compositional multiphase flow simulator solving the fluid flow and transport equations based on the Darcy velocity. Code_Aster is a finite element-based simulator for solid mechanics and structural analysis.

The simulation is subdivided into several time periods simulated independently with both PumaFlow and Code_Aster codes. Two coupling models are used, the one-way, and the iterative ones. For iterative couplings, the

retroaction of the mechanical effects on the reservoir simulation is based on the difference in pore volumes estimated by the mechanical and reservoir codes, independently. This retroaction directly impacts the porosity and optionally, through the Touhidi-Baghini relationship (1998), the permeability values used in the reservoir simulations.

For the sake of coherence between mechanical and reservoir simulators, the pore compressibility *Cp* is set accordingly to the elastic properties (Young modulus E and Poisson coefficient ν), and the initial porosity ϕ_0 (Mainguy and Longuemare, 2002),

$$Cp = \frac{3(1-2\,\nu)}{\phi_0 E}$$

It should be noted that for the mechanical simulator, the solid matrix is supposed to be incompressible, therefore, induced volume variation is considered as pore volume variation. Under small strain assumption, volume variations ΔV are expressed from deformation tensor $\mathcal{E}_{ii}$, $\mathcal{E}_v = \mathcal{E}_{ii} = \Delta V/V$.

2.1.1 One-way

The one-way is the simplest and the less invasive coupling scheme. It does not involve any retroaction of the mechanical results on the reservoir. The mechanical simulation is used to estimate the additional properties, namely effective and total stress fields as well as displacements fields.

For each injection period, stress and displacements induced by pressure variation are computed as follows (Figure 2):

1. Flow simulation
   ⇒ Pressure field (pressure of the reference phase) at the end of period i, $P(i)$
2. Transfer of the pressure variation during period i, $\Delta P(i) = P(i) - P(i-1)$, to the mechanical simulation
3. Mechanical simulation with the load $\Delta P(i)$ imposed linearly through the period i
   ⇒ Stress field $\Delta\sigma(i)$,
   ⇒ Displacements field $u(i)$,
   ⇒ Volume variation $\Delta V(i)$ and pore volume $V_p^{aster}(i) = V_p^{aster}(i-1) + \Delta V(i)$.

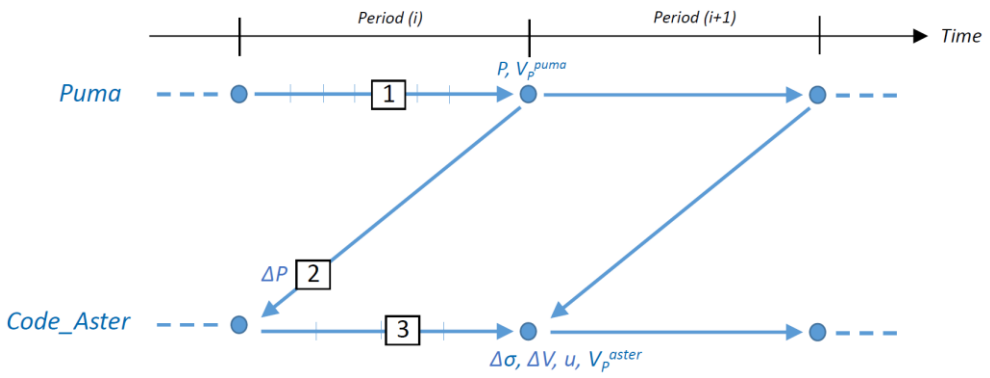

Figure 2 : Schematic representation of the "one-way" coupling between flow and geomechanical simulations.

2.1.2 Iterative

In the iterative coupling model, a convergence test is done after the mechanical simulation. The maximal relative difference between the pore volume obtained with both codes is compared to the given convergence criterion. If the criterion is satisfied, the simulations continue to the next period. Otherwise, the obtained pore volume difference $\Delta V_p(i)$ is prescribed linearly to the reservoir simulator and the same period is repeated till convergence is reached as shown in Figure 3.

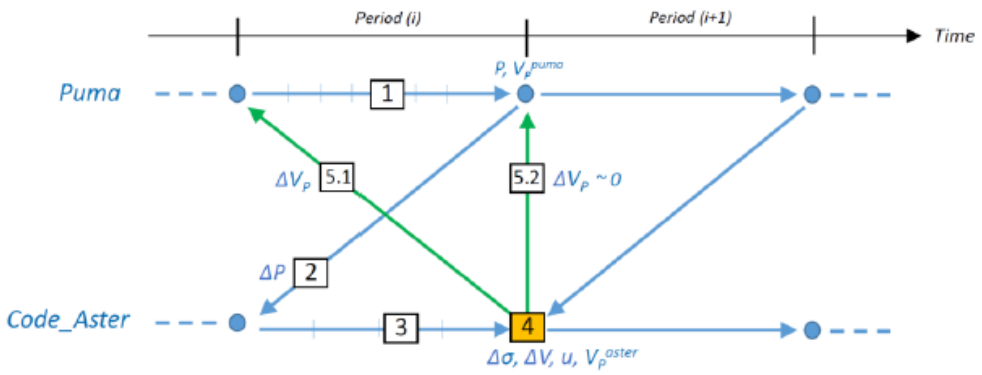

Figure 3 : Iterative coupling model.

Thus, the iterative coupling model can be summarized in the following steps.

1.-3. Identical to One-way model

4. Test of convergence

$$\max \frac{\Delta V_p(i)}{V_p^{puma}(i)} \leq \epsilon, \text{ where } \epsilon \text{ is a convergence criterion}$$

5. If convergence criterion is not satisfied, then 5.1, else 5.2

5.1. $\Delta V_p(i)$ is linearly applied during period i, restart the step 1.

5.2. $\Delta V_p(i)$ is linearly applied during next period $i+1$.

2.1.3 Mechanical problem description

For each period, the quasi-static mechanical equilibrium equation is given by

$$\frac{\partial \sigma_{ij}^{tot}}{\partial x_j} = \rho f_i$$

With σ^{tot} the total stress et ρf_i the volumic forces.

Decomposing the total stress into the Terzaghi effective stress σ and the fluid pressure P , (based on soil mechanics sign convention) $\sigma_{ij}^{tot} = \sigma_{ij} + P\delta_{ij}$.

Under the assumption of linear elasticity, effective stress variation $\Delta\sigma$ in response to pressure variations ΔP is computed independently at each period. Thus, the resulting stress at the end of the period i is obtained as

$$\sigma(i) = \sigma(0) + \sum_{j=1}^{i} \Delta\sigma(j)$$

With $\sigma(0)$ the initial stress estimated through geostatic equilibrium or imposed from given data. This decomposition of the stress expression allows to analyze the impact of the initial stress on the resulting stress field, by considering several initial stresses for one injection scenario.

2.2 Coupled model validation

2.2.1 Analytical solution

The considered problem corresponds to a consolidation of soil layer as described in Coussy (1991). A horizontal soil layer of thickness h is placed on a rigid and impermeable bedrock. The soil is modelized as a thermo-poro-elastic homogeneous isotropic medium. At the reference state, the total stress σ^{tot} is zero and the pressure is uniform $P = P_0$ (Figure 4). There are no thermal effects, thus, the temperature is uniform and constant as a function of time. The vertical mechanical load $\sigma_z^{tot} = -W$ is imposed at initial time step $t = 0$ maintaining a constant pressure $P = P_0$ on the top of the soil layer (Figure 4).

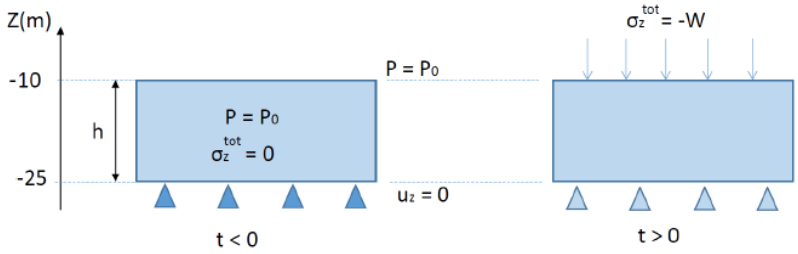

Figure 4 : Consolidation layer problem formulation (Coussy, 1991).

The evolutions of pore pressure $P(z)$ and vertical displacement $Uz(z)$ with time are studied. The analytical solution is given for the following parameters:

- Biot coefficient $b = 1$,
- drained Poisson coefficient $\nu_0 = 0.25$,
- fluid density $\rho_f = 10^3$ kg/m^3,
- fluid incompressibility modulus $K_f = 2.15$ GPa,
- drained Young modulus $E_0 = 1$ GPa,
- intrinsic permeability $k_i = 9.869 \times 10^{-16}$ m^2,
- initial porosity $\phi_0 = 0.2$,
- fluid viscosity $\eta_f = 10^{-3}$Pa·s.

The layer thickness h is set to 15 m. The applied load W is equal to 10^7 Pa. A constant pressure is applied at the top $P_0(z^{top}) = 0.9806 \times 10^5$ Pa. The characteristic consolidation time τ is estimated to be equal to 0.211×10^6 s, and the isotherm diffusion coefficient of the fluid mass is $C_m = 0.106 \times 10^{-2}$ cm^2/s .

Then, for time $t \gg \tau$, the analytical solution is written as

$$P(z) \to P_0(z),$$
$$Uz(z) \to -\frac{\left(z - z^{bottom}\right)W}{\lambda_0 + 2\mu_0} = -0.833 \times 10^{-2}\left(z - z^{bottom}\right),$$
$$\sigma_z(z) \to -W = -10^7 \text{ Pa},$$

Where λ_0 and μ_0 are the Lamé coefficients obtained from the Young modulus and the Poisson coefficient, $\lambda_0 + 2\mu_0 = E_0\left[\frac{1}{3}(1 - 2\nu_0) + \frac{4}{6}(1 + \nu_0)\right]$

For various z, the resulting pressure and vertical displacement are found

$$z = -10 \text{ m} : P = 0.9806 \times 10^5 \text{ Pa}, Uz = -0.1250 \text{ m},$$
$$z = -11 \text{ m} : P = 1.0787 \times 10^5 \text{ Pa}, Uz = -0.1189 \text{ m},$$
$$z = -17 \text{ m} : P = 1.6671 \times 10^5 \text{ Pa}, Uz = -0.0666 \text{ m},$$
$$z = -24 \text{ m} : P = 2.3535 \times 10^5 \text{ Pa}, Uz = -0.0083 \text{ m},$$
$$z = -25 \text{ m} : P = 2.4516 \times 10^5 \text{ Pa}, Uz = 0 \text{ m}.$$

2.2.2 Coupling model

The iterative scheme described in section 2.1 is used for the coupled simulation. The considered consolidation problem requires a few specific adaptations. First, in Code_Aster, the load W is applied on the top of the layer for the first period. Second, the retroaction of the pore volume modification on the permeability via Touhidi-Baghini is inactive since the analytical solution implies a constant permeability. Then, the coupled simulation is performed as follows

- For $t \to 0$
    1. Since the imposed load W is transparent in the reservoir simulator, the pore volume and pressure variations are zero for the first iteration.
    2. Vertical compaction of the soil under the load W results from the mechanical simulation

3. The retroaction on the flow, induce a pressure increase to equilibrate the load.

- For $\tau < t < 0$
  1. The boundary condition on the top of the layer $P = P_0$ allows to progressively dissipate the generated overpressure.
  2. The pressure variation ΔP induces soil compaction.
- For $t > \tau$
  1. The overpressure due to the load W is entirely dissipated
  2. The pressure variation transferred to the mechanical code tend to zero, thus, no more deformation are observed (the asymptotic values for the vertical displacements are shown in Figure 5).

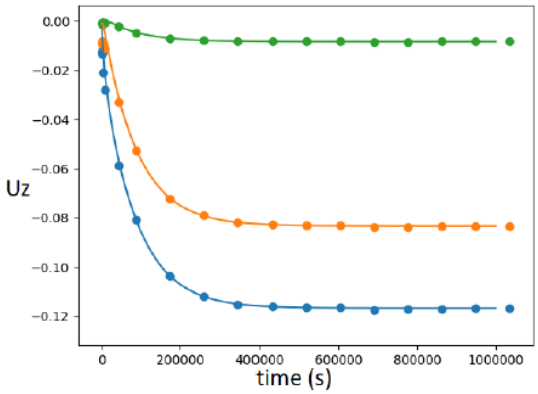

Figure 5 : Vertical displacements resulting from the coupled simulation (points) compared to the analytical solution (lines) for $z = -11$ m (blue), $z = -15$ m (orange) and $z = -24$ m (green).

2.2.3 Validation

In Figure 5, vertical displacements resulting from the coupled simulation are compared to the analytical solution. After time of about $2\tau = 0.422 \times 10^6$ s, the displacements tend to the expected value $Uz(z) = -\frac{(z-z^{bottom})W}{\lambda_0+2\mu_0}$. The coupling results are in very good agreement with the analytical predictions. These results validate the iterative coupling model.

2.3 Formation integrity: Failure criterion calculation for risk analysis

2.3.1 Chosen criteria

To evaluate formation integrity, a double Drucker-Prager criterion is used Drucker (1952). Drucker-Prager criterion is commonly expressed in term of hydrostatic stress p and equivalent stress q as:

$$q = A + Bp$$

With hydrostatic stress p and equivalent stress q as functions of stress tensor σ_{ij} and deviatoric stress tensor s_{ij}:

$$p = \frac{1}{3}\sigma_{ii}, \qquad q = \sqrt{\frac{2}{3}s_{ij}s_{ij}}, \qquad s_{ij} = \sigma_{ij} - p\delta_{ij}$$

A and B are material parameters that can be expressed in term of material cohesion c and friction angle φ.
For our study, there are two Drucker-Prager yield surfaces for a given set of parameters (c, φ) They correspond to the outer and inner Drucker-Prager yield circumscribe and inscribe the Mohr-Coulomb surfaces, respectively, as illustrated in Figure 6.

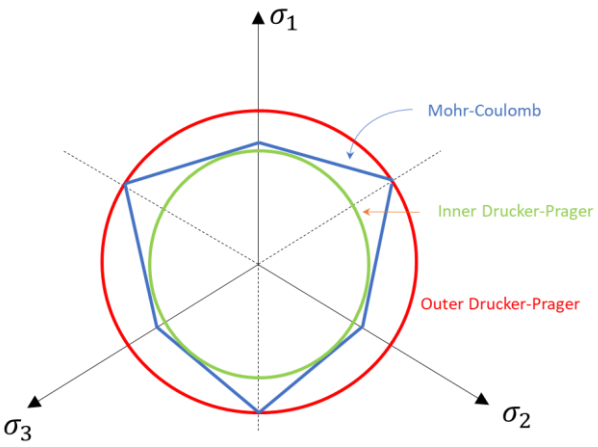

Figure 6 : Mohr-Coulomb and Drucker-Prager yield surfaces in deviatoric plane.

Expression for the double Drucker-Prager criterion, denoted hereafter DP, is written as:

$$q = A_1 + B_1 p, \qquad q = A_2 + B_2 p$$

With A_1 and B_1 parameters of the outer DP expressed as follows:

$$A_1 = \frac{6c\ \cos\varphi}{3 - \sin\varphi}, \qquad B_1 = \frac{6\ \sin\varphi}{3 - \sin\varphi}$$

And A_2 and B_2 parameters of the inner DP:

$$A_2 = \frac{3\sqrt{3}c\ \cos\varphi}{\sqrt{9 + 3\sin^2\varphi}}, \qquad B_2 = \frac{3\sqrt{3}\ \sin\varphi}{\sqrt{9 + 3\sin^2\varphi}}$$

With c and φ material cohesion and friction angle, respectively. The methodology adopted to define these parameters is discussed in section 2.3.2.

At the end of the simulation period i, the hydrostatic stress $p(i)$ and the equivalent stress $q(i)$ are computed from obtained stress field $\sigma(i)$. The stress result of each cell is projected on a (p, q) representation and compared to the criteria as shown in Figure 7. The risk analysis will be addressed based on the "distance" to both criteria defined as difference between stress results and their projection on the DP criteria, as discussed in section 3.5.

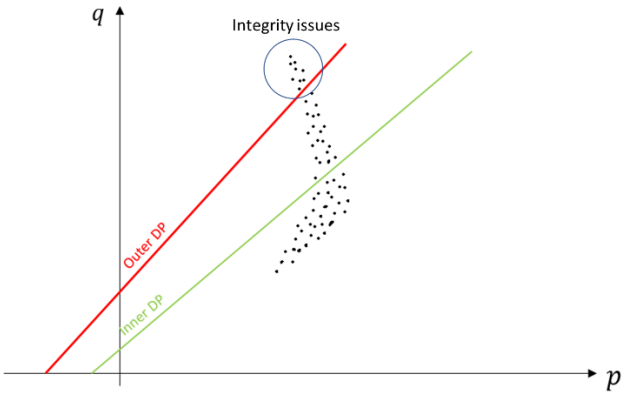

Figure 7 : Stress state projection in (p, q) representation

2.3.2 Evaluation of cohesion and friction angles

Cohesion c (MPa), and friction angles φ (°) are expressed as function of porosity $\phi(\%)$. For the cohesion, an exponential empirical law is used:

$$c = \alpha_c \, e^{\beta_c \phi}$$

For the friction angle a linear empirical law is used:

$$\varphi = \alpha_f \phi + \beta_f$$

With $\alpha_c, \beta_c, \alpha_f, \beta_f$ coefficients of the empirical laws identified from available literature data (see paragraph 2.5.1 for specific values used in our models).

2.3.3 Initial stress states

The adopted stress decomposition expression can evaluate the sensitivity of the initial stress $\sigma(0)$ on the formation integrity for the considered injection scenario.

$$\sigma(i) = \sigma(0) + \sum_{j=1}^{i} \Delta\sigma(j)$$

The initial effective stress tensor $\sigma(0)$ can be expressed in the principal direction as:

$$\sigma(0) = \begin{pmatrix} \sigma_1 & 0 & 0 \\ 0 & \sigma_2 & 0 \\ 0 & 0 & \sigma_3 \end{pmatrix}$$

With $\sigma_1 > \sigma_2 > \sigma_3$ the principal effective stress components. Based on Terzaghi definition of effective stress, total principal stress tensor is given by:

$$\sigma^{tot}(0) = \sigma(0) + P(0) = \begin{pmatrix} \sigma_1 + P & 0 & 0 \\ 0 & \sigma_2 + P & 0 \\ 0 & 0 & \sigma_3 + P \end{pmatrix} = \begin{pmatrix} {\sigma_1}^{tot} & 0 & 0 \\ 0 & {\sigma_2}^{tot} & 0 \\ 0 & 0 & {\sigma_3}^{tot} \end{pmatrix}$$

We assume that one of these total principal stress components is vertical (Sv), the two remaining components are respectively the maximum (SH), and minimum total horizontal stresses (Sh).

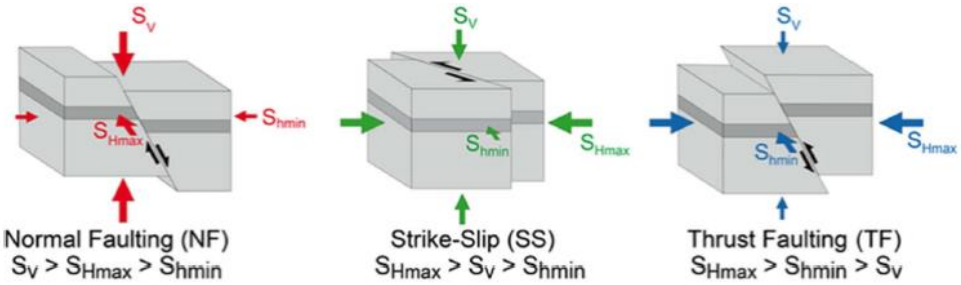

Figure 8 : Main fault regimes Anderson's classification (Heidbach and al. 2016)

Considering the main fault regimes illustrated on Figure 8 :

- In normal faulting (Extensive) regime: $\sigma_1{}^{tot} = \mathrm{Sv} > \sigma_2{}^{tot} = \mathrm{SH} > \sigma_3{}^{tot} = \mathrm{Sh}$
- In StrikeSlip regime: $\sigma_1{}^{tot} = \mathrm{SH} > \sigma_2{}^{tot} = \mathrm{Sv} > \sigma_3{}^{tot} = \mathrm{Sh}$
- In thrust faulting (Compressive) regime: $\sigma_1{}^{tot} = \mathrm{SH} > \sigma_2{}^{tot} = \mathrm{Sh} > \sigma_3{}^{tot} = \mathrm{Sv}$

(see paragraph 2.5.3 for stress ratio values used in this study).

2.4 Statistical Analysis

The statistical analysis of surface displacements function of uncertain parameters brings us recommendations for the design of the monitoring plan by targeting the most sensitive locations and periods and/or presenting the most significant variations in response. *In fine*, this evaluates the required time and space resolutions for the surface monitoring by a given tool according to the considered scenario.

The statistical analysis includes a sensitivity analysis and an uncertainty analysis on surface displacements. Uncertainty analysis consists of evaluating the uncertainty in the predictions of displacements given the *a priori* distribution of uncertain parameters (e.g. statistics of surface displacement maps). Sensitivity analysis is used to quantify the influence of model parameters on the model-simulated outputs of interest. These analyses require a large sampling of combinations of parameters and outputs, too costly in computational time to be carried out from coupled flow/geomechanics simulations only. Here, simulations results are replaced by metamodels (also called response surface model or surrogate model) which approximate the relationship between parameters and simulation outputs (Feraille and Marrel, 2012; Douarche et al., 2014).

These mathematical approximations of the responses of interest in studied parameters space are built by applying kriging methods on simulated data (Scheidt et al., 2007). For each studied time period, a response surface based on Gaussian process technique is used for Sobol index calculation or for statistical evaluation for example. Parameters values are sampled using the Latin Hypercube Sampling method (LHS (McKay et al.,1979)). This design of experiments is a space-filling design, with a flexible number of evaluations and considers every domain of the input space while varying simultaneously every parameter.

The strategy used here (Figure 9) consists first of defining the uncertain parameters and their uncertainty intervals (1- in Figure 9, as described in paragraph 2.3.). Then a design of *m* experiments for the coupled simulation is built (2- in Figure 9). This will be used as a learning sample for metamodels. From the simulation results of the *m* experiments, we compute HSIC criteria (3- in Figure 9) and metamodels (4- in Figure 9) are used to compute statistics information on a quantity of interest, the Shannon entropy maps and the Sobol indices (5- in Figure 9).

HSIC (Hilbert Schmidt Independence Criterion, Da Veiga et al. 2015, De Lozzo and Marrel, 2017) criteria are computed for spatial and temporal properties.

- HSIC criteria are used to quantify the dependence between two random variables from the transformation covariance of these variables.
- The computation of this criterion can be based on a limited number of couples (inputs, outputs), i.e. on a limited number of simulations.

- We obtain HSIC maps, as well as a global value per map (at a given time) or per chronology (at a given point). These criteria allow to distinguish, for example, where and when the surface deformations are the most dependent on the values taken by the uncertain parameters.

Metamodels (Feraille and Marrel, 2012) are constructed for the surface displacement maps function of uncertain parameters and for different time periods. We use LOOCV (Leave-One-Out Cross-Validation) to control metamodels quality and, if necessary, simulation points could be added to improve it. Then, from these metamodels, we compute:

- The **statistics** of surface displacement maps (mean, quantiles, etc) from a Monte-Carlo sampling on metamodels. We are interested in the maps of variances or standard deviations of surface displacements as a function of uncertain parameters for different time periods. Monitoring tools will be used if the predicted displacements are above the detection thresholds, preferably for standard deviations above the tools accuracy and favoring the most uncertain locations and periods (e.g. highest variances and entropy *cf.* below) so that these measurements reduce the uncertainties on the model responses and thus constrain it.
- The statistics of the injected CO2 volume from a Monte-Carlo sampling on metamodels to evaluate the distribution of expected storage capacity from different storage models.
- **Shannon entropy maps** (Leibovici, 2009; Schweizer et al., 2017) of surface displacement that complement the information provided by statistical maps. Shannon entropy can be viewed as a measure of information value:
  - If the same value is always found at a specific location then **the entropy will be zero, a measurement at this location will provide little information**.
  - On the contrary, **if we can record different categories of measurements at a specific location, then the entropy will be positive**. The Shannon entropy is also considered as a measure of uncertainty since if the categories are equiprobable (uniform distribution), i.e. the most uncertain case, then the entropy is maximum.
  - To construct these maps, a discrete variable is defined by categorizing the displacement values according to the tool detection limit.
    - For example, for INSAR data, the categories could be:
      - values below the detection threshold, i.e. of -1 to 1mm/year;
      - values from 1 to 3 mm/year, which, given the accuracy of the tool, globally represents a single type of measured value;
      - values from -1 to -3 mm/year;
      - values above 3 mm/year;
      - values under -3 mm/year.

- **Sobol indices** (Sobol, 1993) which estimate the sensitivity of the response to uncertain parameters from a variance decomposition of the outputs of interest. They are computed from a massive sampling on metamodels
  - Compared to HSICs, Sobol's indices allow **to distinguish the main effects of the parameters from the effects linked to the interactions between parameters**. However, they require the use of a metamodel for the sampling to limit the computational cost.
  - It can be assumed that **a measurement can be informative about the value of an uncertain parameter if the sensitivity of the measurement to this parameter is high**.
- Finally, from metamodels, it will be possible to predict (and visualize) expected surface measurements according to parameters values (and vice-versa).

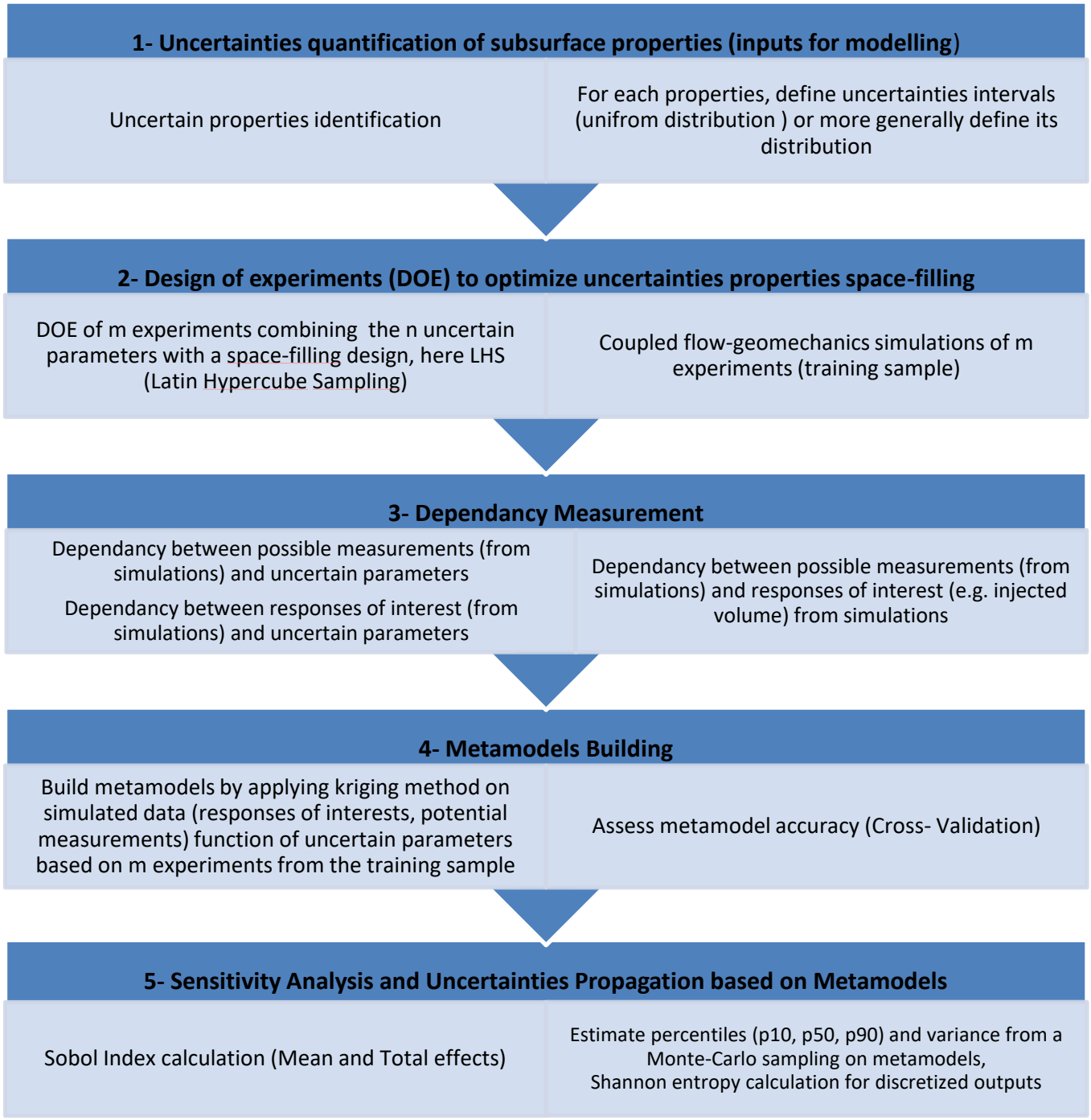

Figure 9 : Workflow of the statistical analysis performed between potential measurements and model parameters, responses of interest to define recommendations on surface monitoring design

2.5 Definition of conceptual models

2.5.1 Structural models and subsurface properties scenarios

Two structural models are considered in this study as potential structures for CO_2 storage. The first one is an anticline structure (Bouquet at al. 2021a) without fault shown in Figure 10 and Figure 11 (left), and the second one is an anticline structure with faults shown in Figure 10 and Figure 11 (right). The faults are either sealing or draining. The sealing faults represent a barrier for the flow, while the draining faults let flow go through the core zone. A

third fault is defined as sub seismic without throw. This sub seismic fault is representative of the type of problematic geological objects, often undetectable by geophysical tool, that may behave in unpredictable ways.

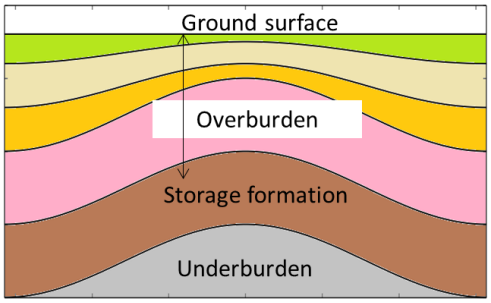

Figure 10 : Schematic representation of the anticline model

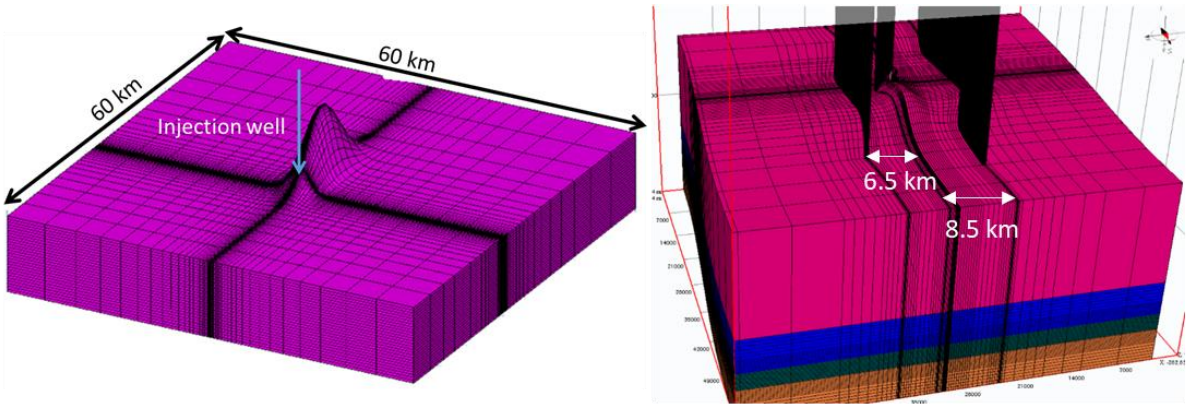

Figure 11 : Anticline conceptual models. Left, anticline trap without fault; right, anticline trap with two major faults and a sub seismic fault.

For both structural models, the injection site is considered as **onshore**. Thus, surface information is directly available and only monitoring tools in onshore context are studied.

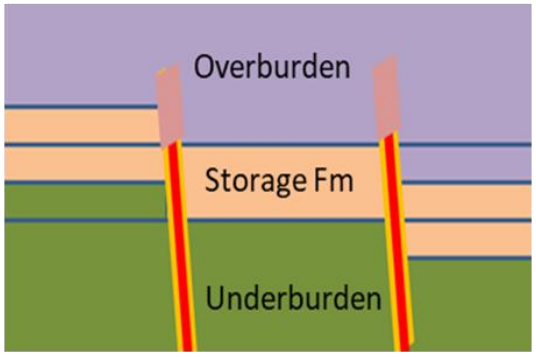

Faults (core and damage zones) with throw

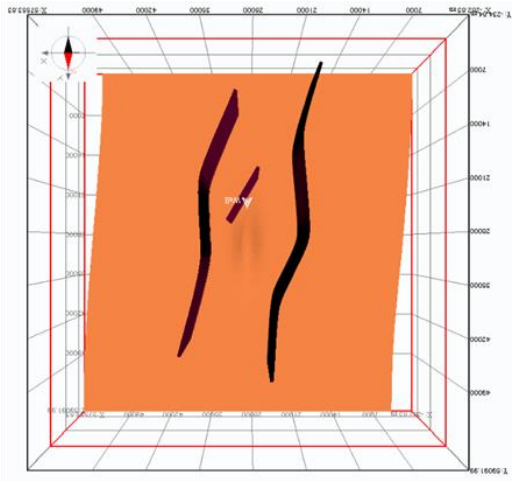

Figure 12 : Conceptual model with faults. Left, schematic representation of the main faults with throw and with explicit modelling of core and damage zones. Right, top view of fault models with two main faults and the smallest and closest sub-seismic fault.

Several scenarios are considered to represent different types of sedimentary formations and therefore corresponding to different subsurface properties. These scenarios are defined to generate realistic intervals of uncertainty of the properties. Three scenarios are defined.

- **Carbonate Case**, inspired from Brindisi (Baroni et al., 2015) and Michigan Basin (MRCSP Michigan Basin, Michael et al., 2010) storage sites.
- **Sandstone I case**, inspired from In Salah (Baroni et al., 2011; Deflandre et al., 2013; Tremosa et al., 2014) and Gorgon (Michael et al., 2010; Flett et al., 2008; Schembre-McCabe et al. 2008) projects.
- **Sandstone II case**, inspired from Snohvit (Estublier et al. 2009; Niemi et al. 2017), Decatur (Mt Simon, Zhou et al. 2010; Ruqvist et al. 2019) and Otway (Cook 2014) storage sites.

More detailed description of conceptual models and petrophysical and geomechanical data are contained in the deliverable D2.1 of the SENSE project (Bouquet et al, 2021b).

2.5.2 Injection design

The exact same injection design is defined for all models and scenarios for the sake of comparison.
A single injector well is modeled, injecting CO_2 on the flank of the anticline, to facilitate the dissolution of CO_2 in the water during its migration towards the anticline summit. CO_2 injection is controlled by a maximum pressure increase of 50 bar at the bottom of the well. The maximum injection rate is 1,500,000 m^3/day under surface conditions, or approximately 2800 t/day (about 1 Mt/year). Well is perforated along a 20-m section from the reservoir bottom for all scenarios. CO_2 is injected for 10 years and up to five years post-injection are studied.

2.5.3 Stress Regime scenarios

Based on literature data (Kempka and al. 2014), (Taghipour and al. 2019*),* 4 scenarios are studied in the formation risk analysis discussed in paragraphs 3.6 and 5.3 3. The considered total stress ratio are summarized in Table 1.

Stress regime	SH/Sv	Sh/Sv
Extensive	0.8	0.8
StrikeSlip 1	1.1	0.6
Strike-Slip 2	1.3	0.8
Compressive	1.6	1.1

Table 1 : Total stress ratio for different fault regimes

For all considered scenario the initial stress ratio is uniformly applied to the model.

2.6 Definition of surface monitoring tools and related limitations

Two kinds of monitoring tools are considered, local measurements and large areas. For local measurements with fine temporal sampling, tools such as tiltmeters, GNSS, i.e. Geolocation and Navigation by Satellite System can be used. For covering large areas but with a limited displacement and time resolutions, scanning systems (satellite data acquisition) like InSAR can be used (McColpin et al., 2009 and Vasco et al., 2019).

After processing, InSAR data can provide displacement maps covering at least the entire storage area, at low cost and with low hardware constraints. However, the usefulness of these data may be limited by their spatial and temporal resolution, the duration of data processing (computational cost and high memory requirements) and their sensitivity to land cover (e.g. vegetation). Typical limitation of displacement detection by InSAR will be 1 mm/yr. This may be improved with corner-reflectors installation in the area of interest.

Point measurements from tiltmeters provide spatially and temporally accurate but local, expensive information, with measurements accuracy 5 to 50 nanorads, which can be affected by weather conditions and necessarily require the installation of surface tools.

3 Workflow application to anticline cases – One-way coupling

The workflow described in paragraph 2 is applied to the 3 scenarios for the anticline model without fault: Carbonate, Sandstone I and II. From the uncertainty ranges of the nine subsurface properties of interest (defined in section 2.5), a LHS design of experiments of 115 models to be simulated is built for each scenario (i.e. 3 x 115 simulations). Statistical and sensitivity analyses are performed on coupled flow-geomechanical simulations result from these designs.

First, the storage capacity is analyzed as a function of the geological context, i.e. function of the considered scenario. Results are expected to be significantly different to describe typical CO_2 storage behaviors within a large scope.
Knowing the storage capacity of each scenario, we then evaluate the geomechanical behavior in response to pressure changes and the observability of surface displacements for each. Surface displacements relationship with subsurface behavior and consequently subsurface properties is studied to assess the value of such information to better constrained the subsurface behavior. This evaluation will lead to recommendations in terms of monitoring design. Finally, a risk analysis of the storage integrity is carried out with different stress regimes to define if the storage site is jeopardized during the injection period.

3.1 Storage capacity

Usually, the main characteristic of a storage site is its storage capacity, and storage sites are classified according to it. Thus, the first analysis on simulation results is performed in order to characterize and classify each scenario as a function of this storage capacity.
Here, storage capacity is both constrained by the injection design, described in section 2.5, with a maximum BHP (Bottom-Hole Pressure) as well as by a maximum injection rate (similar for all scenarios) and by subsurface properties. BHP and injection rate result for the 115 simulations of each scenario are shown in Figure 13.

Due to a low injectivity for **Sandstone I** case, all simulations reach the BHP limit, leading to a large variation in injection rates for the 115 simulations and thus a large spreading in storage capacity (80% of storage capacity are predicted **between 0.4 Mt to 4.7 Mt** of CO_2 in 10 years of injection).
On the contrary, for **Sandstone II** case, all simulations reach the maximum injection rate due to the high injectivity properties for this scenario. For the same injected volume, this leads to a same storage capacity for all simulations of **10.7 Mt** of CO_2 but different results in terms of BHP, depending on subsurface properties.
With intermediate injectivity properties, the **Carbonate** scenario is the intermediate case with some simulations constrained by the BHP while others, reaching the maximum injection rate, exhibited different BHP results. This leads to the largest spreading in storage capacity results, most of them are in between **1.9 and 10.7 Mt** of CO_2.These variations are due to different values in subsurface properties between simulations. More specifically, this is mainly related to the storage formation permeability value according to the sensitivity analysis on storage capacity. **A clear and predominant relationship between storage capacity and storage permeability is observed** in Figure 14.

To summarize, with these three conceptual models we cover different kind of storage behaviors that may be encountered in real storage sites. In that sense, we expect to characterize different surface behaviors in relation with these storage capacities.

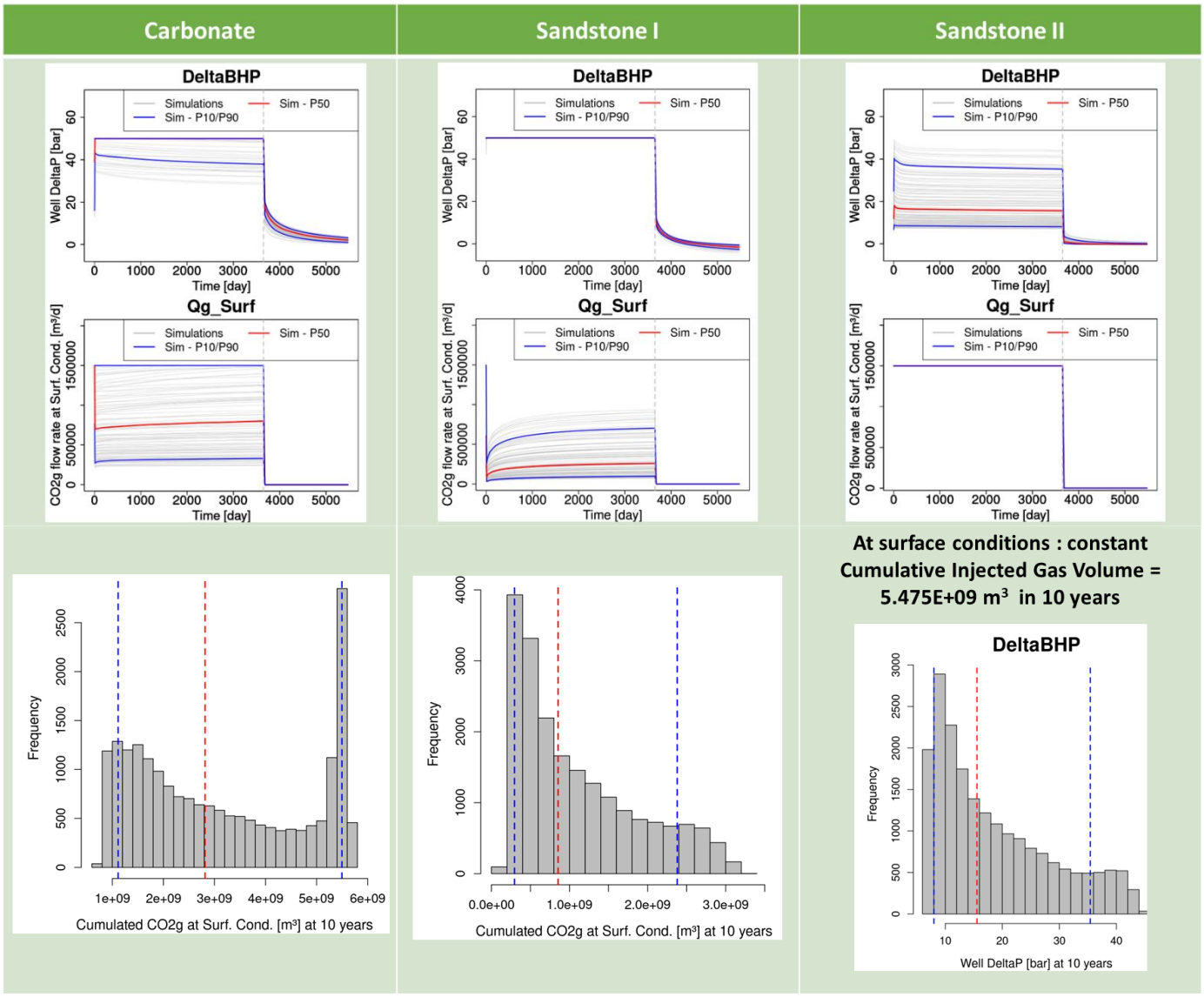

Figure 13 : Top: Increase in pressure at the well (delta BHP), injection rates function of time for the 115 simulations (grey lines) for each scenario and corresponding median, percentiles (p10 and p90) from the 115 simulations results. Bottom: Distribution of storage capacity (cumulative injected gas volume at surface conditions) or of increase in pressure at the well at 10 years of injection from a Monte-Carlo sampling of metamodels predictions (LOOCV Q2 > 0.95).

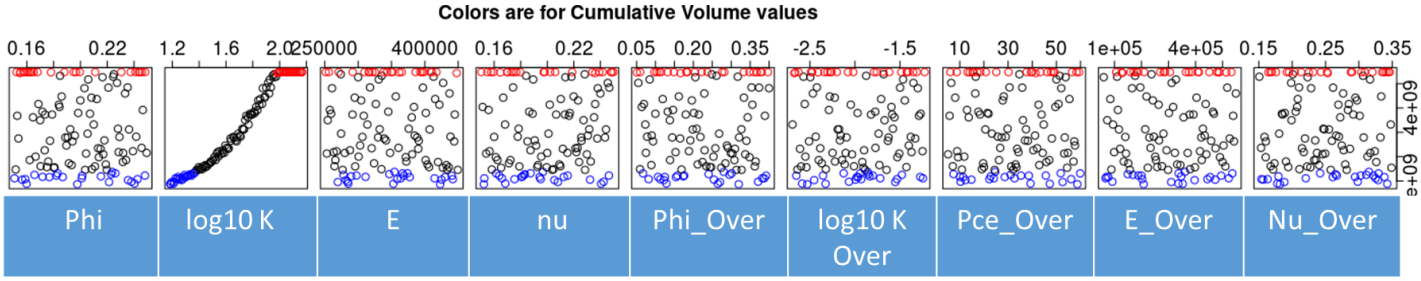

Figure 14 : Cumulative injected Gas volume results, after 10 years of injection, at surface conditions [sm^3] function of parameters values for the carbonate case (one-way coupling) for the 115 simulations from the Carbonate scenario. In blue, the 20% lowest values in storage capacity; in red, the 20% highest values in storage capacity.

3.2 Geomechanical behavior in response to pressure changes in the storage structure

Figure 15 and Figure 16 illustrate the cumulative surface displacements at the end of injection (10 years) and at three years post-injection (13 years) in a YZ cross-section, along the anticline axis and at the well location. Results are significantly different between scenarios with an expected uplift (Figure 15) which reaches the **centimeter-scale for Sandstone I** , while for **Sandstone II** most of the expected uplifts are far **below the centimeter** at the end of injection.

These results are consistent with the observations at real storage sites that can be related to our scenarios with for example an uplift of about 1 cm for In Salah site in 6 years (Baroni et al., 2011; Deflandre et al., 2013 ; Tremosa et al., 2014), that can be related to Sandstone I results and on the other non-observable surface uplift at sites such as Sleipner or Decatur sites (Mt Simon, Zhou et al. 2010; Ruqvist et al. 2019) that can be related to Sandstone II case.

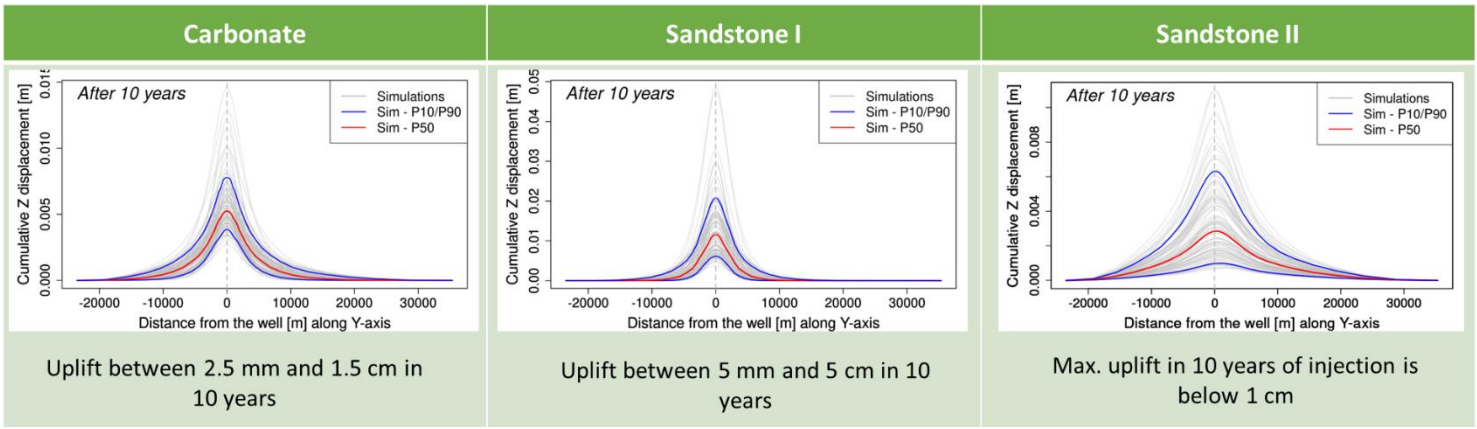

Figure 15: Cumulative surface displacement [m] in 10 years of injection. Indicated values are related to the uplift at the well location. Notice that scales are quite different between scenarios.

In the post-injection period, a subsidence is observed in all cases but with an intensity, and spatial response (extent, shape) quite different between scenarios (Figure 16). Again the highest intensity is expected for Sandstone I case in a limited area around the well while for Sandstone II, it extends further at a lower intensity and more importantly, we observe an asymmetrical shape, with a highest uplift toward the anticline summit. The Carbonate case gives intermediate results between both Sandstone scenarios.

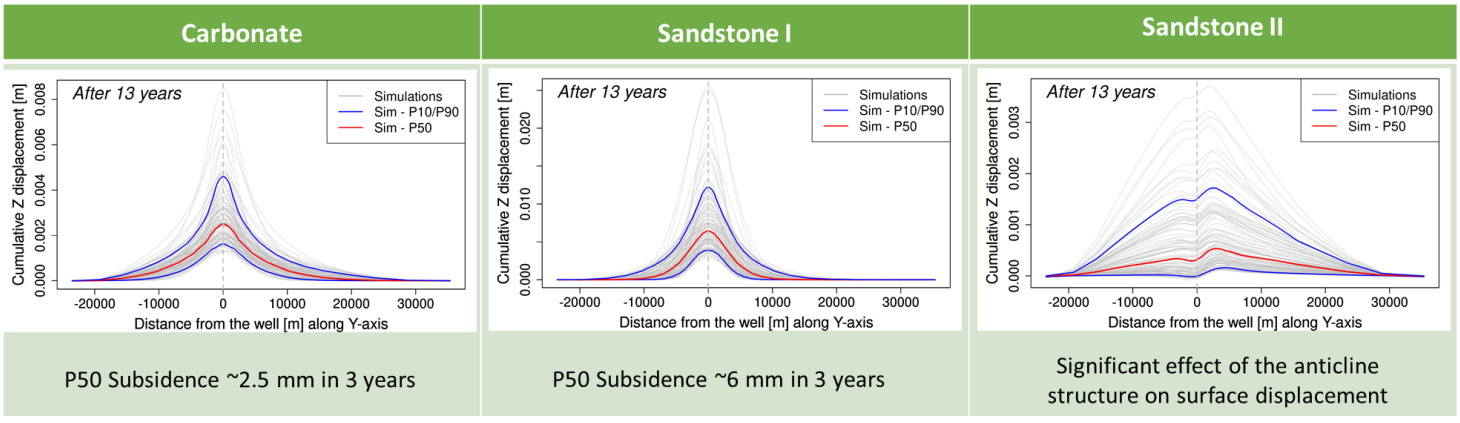

Figure 16 : Cumulative surface displacement [m] after 13 years: 3 years post-injection. Indicated values are related to the uplift at the well location. Notice that scales are quite different between scenarios.

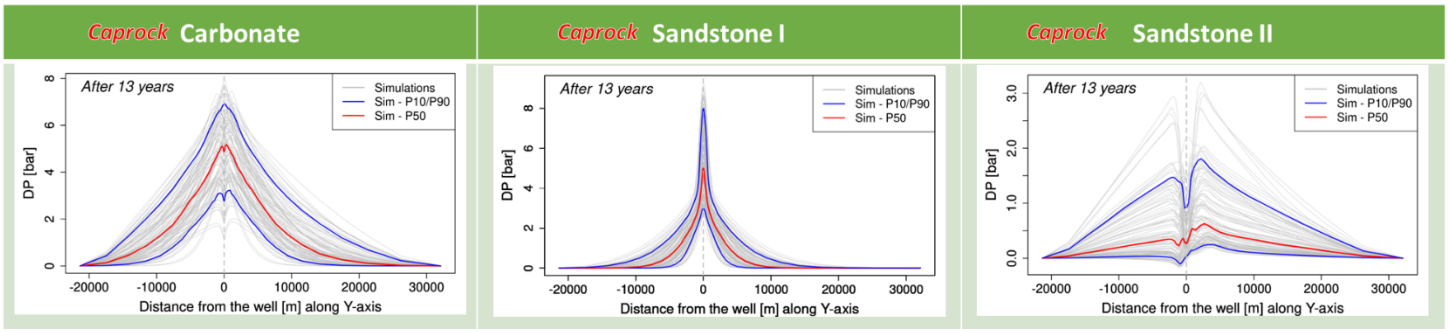

Figure 17 : Pressure variations (relative to the initial state) in the caprock at 13 years, i.e. 3 years post-injection.

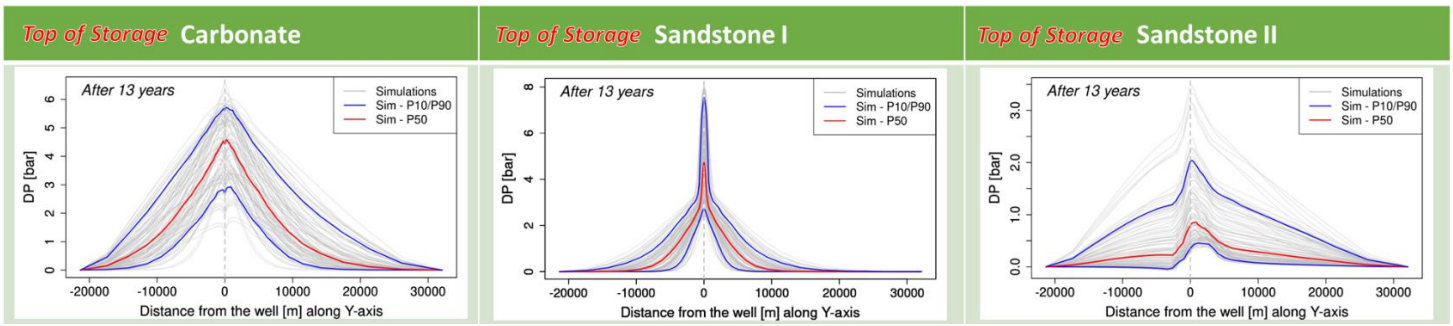

Figure 18 : Pressure variations (relative to the initial state) at the top of the storage formation (interface with caprock) at 13 years, i.e. 3 years post-injection.

The uplift intensity, its extent and shape are directly related to subsurface behavior. The extent and shape of surface displacements are directly related to pressure variations and extents in subsurface. In addition to the reservoir, pressure variations are observed in the caprock due to water entering. Indeed, the caprock is characterized by a low permeability and a high capillary pressure that allows water penetrating in the caprock but not gas. Similarly to surface displacements, for Sandstone I, a major increase in pressure is observed in the well vicinity and at most extending up to 10 km from the well (Figure 17 and Figure 18). On the contrary, for Carbonate case, the increase in pressure is more diffuse over the entire domain.

A particular pressure behavior is observed for Sandstone II case with an asymmetrical increase in pressure towards the anticline summit in the storage formation (Figure 18) and a lower increase in pressure above the well in the caprock (Figure 17)which directly impacts surface displacement results in Figure 16. This behavior is explained by the CO_2 plume migration for this scenario and its impact on pressure response (Figure 19 and Figure 20). Due to its high permeability properties, a large amount of CO_2 is injected and migrates quickly towards the caprock/storage interface. Because the interface is saturated with CO_2, and the corresponding capillary pressure is relatively high compared to the increase in pressure, no more fluids propagate towards the caprock above the well. This leads to a lower increase in pressure in caprock and a lower surface displacement at the top of the well. At the end of injection, CO_2 plume begin to migrate towards the anticline summit leading to the asymmetric shape of pressure and surface displacement.

To conclude, surface displacements can be directly related to the subsurface behavior: pressure and CO_2 migration but without directly identifying the geological formations where the pressure and gas saturation variations are located. If surface displacements are high enough to be detected by the surface monitoring tools, then these tools appear to be efficient for subsurface monitoring as well.

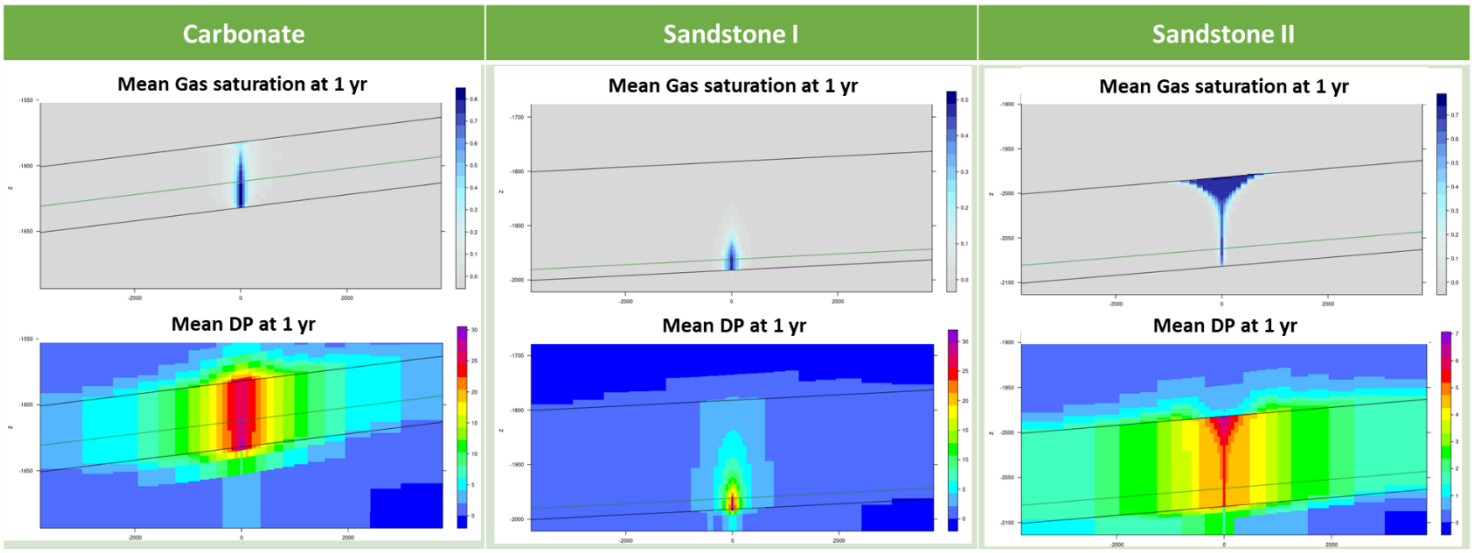

Figure 19 : 2D view (YZ plane) of gas saturation and pressure perturbations for the three scenarios at 1 year of injection. Two horizontal black lines figure the storage formation thickness, horizontal green line figure the top of injection perforation.

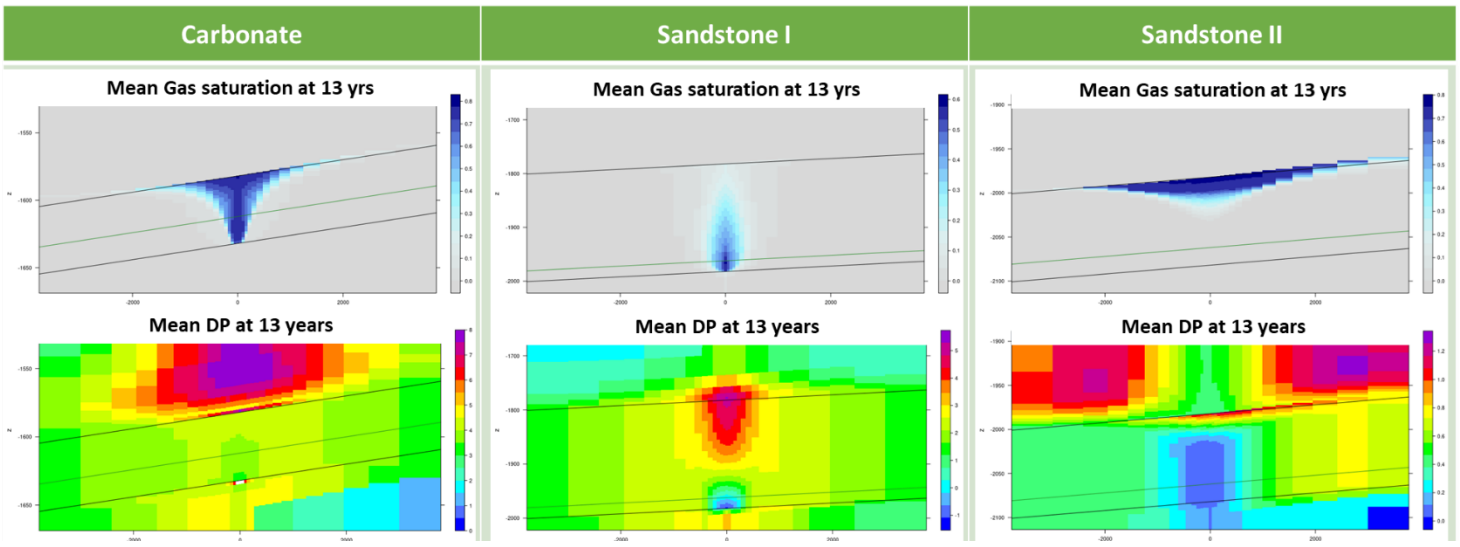

Figure 20 : 2D view (YZ plane) of gas saturation and pressure perturbations for the three scenarios at 13 years, 3 years post-injection.

3.3 Evaluation of the observability of surface displacements

3.3.1 Observability with InSAR measurements

Depending on the scenario, we obtain significantly different results in term of potential use of surface monitoring via InSAR measurements (Figure 21) for which the detection limit is 1 mm/year.
Thus, for Sandstone I case, most of surface displacements are expected to be detectable, especially close to the well. On the other hand, for Sandstone II case, the probability to detect surface displacements via InSAR is much slower and the corresponding detection area is much larger (Figure 21).

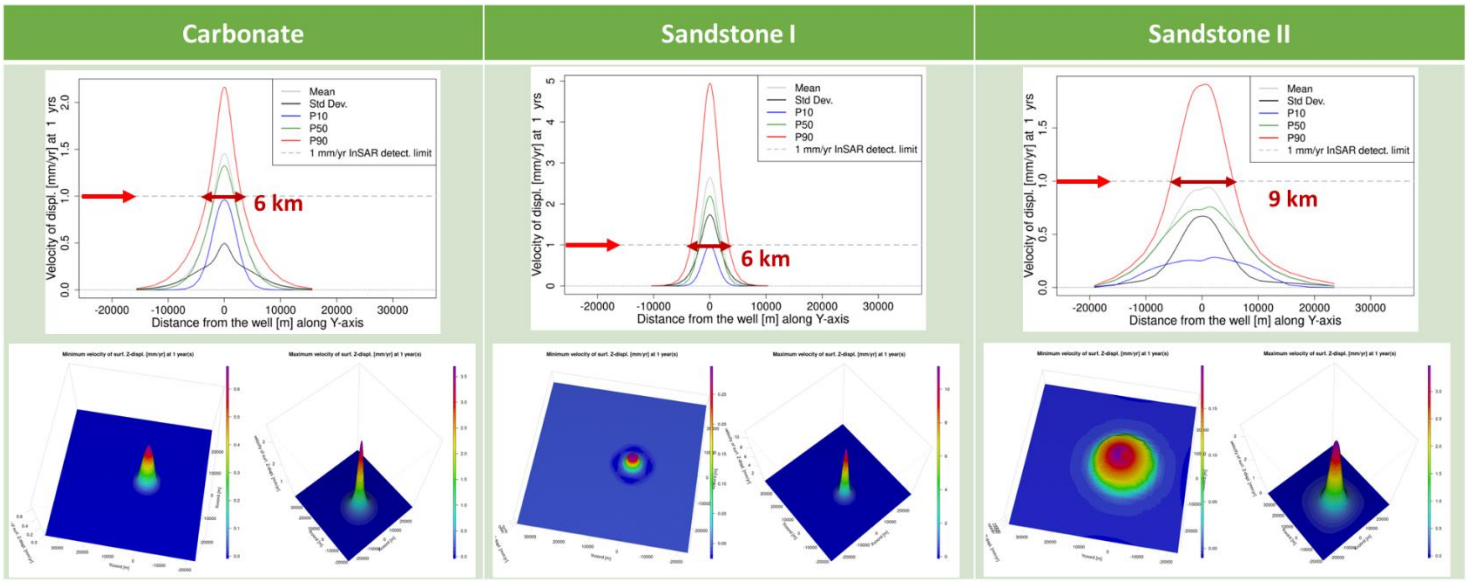

Figure 21 : Spatial differences in InSAR detection capability function of the scenario. Top: Cross section along the well of uncertainties on the surface displacement velocities (mean, standard deviation, median, quantiles 10% and 90%) after one year of CO_2 injection, related to the uncertainties on the subsurface properties. Statistical calculations are performed from a Monte-Carlo sampling on metamodels built from the training sample. The detection threshold of InSAR measurement is estimated at 1 mm/year (red arrow). Bottom: 3D views of surface displacements, minimum (left) and maximum (right) over 115 simulations.

Therefore, the probability to detect displacements via InSAR and their relevancy strongly dependent on the scenario, and the monitoring design have to be adapted. For example, a monitoring area of 3 km around the well would be appropriate for the Carbonate and Sandstone I scenario while for Sandstone II the monitoring area could reach 4.5 km around the well (see the dark red arrows for the distance from the well to have at least 10% of probability to detect surface displacements via InSAR in Figure 21) .

In case of **Sandstone I**, InSAR measurements are very promising with most of values above threshold during and after the injection. In addition, the standard deviation of surface results due to uncertainties in subsurface properties is higher than the threshold thus **we can expect to obtain discriminating results for subsurface properties characterization**.

On the other hand, for **Carbonate and Sandstone II** scenarios, **the constraint brought by these data will be limited since the standard deviation is lower than the precision of the tool**. Still, it is most plausible to record surface displacements in the case of Carbonate than Sandstone II. **It should be noticed that for Sandstone II, the effect of anticline structure to CO_2 migration may be visible on surface results** and may be recorded in some cases (asymmetrical displacement relatively to the well location).

Thus, spatial monitoring design recommendations are based on this statistical analysis as a function of the scenario. The monitoring area based on statistics results according to a tool precision, and on standard deviation and Shannon entropy results (Figure 22)is determined in the most uncertain area where the measurements would be the most insightful.

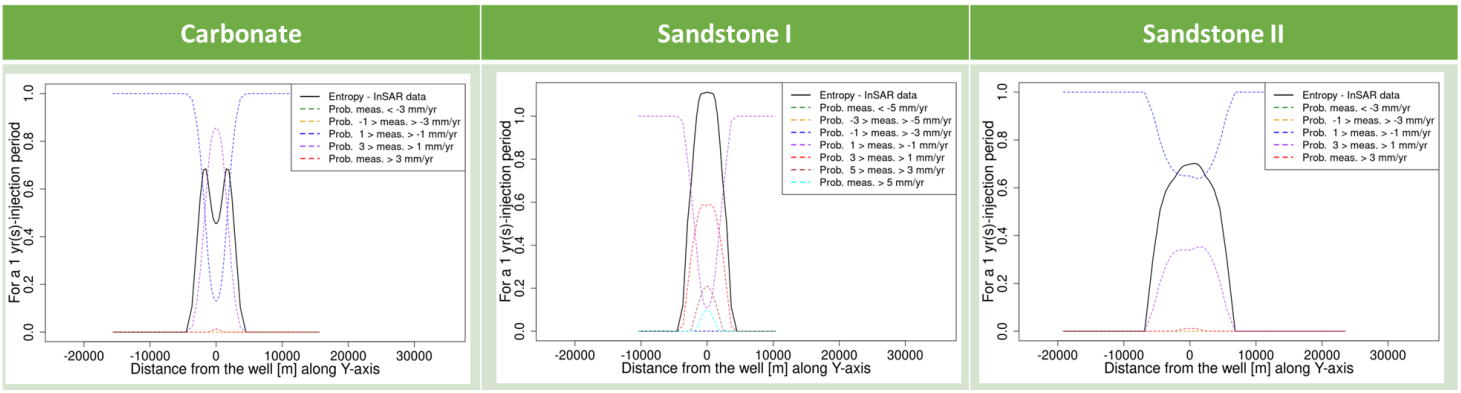

Figure 22 : Shannon entropy for categorical InSAR data (surface displacement velocities) after one year of injection. Measurement error is estimated at +/- 1 mm/yr.

Temporal monitoring recommendations are also based on statistics results, in particular on vertical displacement velocities over the well as a function of time. For all simulations and scenarios, the fastest vertical displacements occur near the well. In Figure 23, one can distinguish the limits of the InSAR tool over time as a function of the considered scenario. For the **Sandstone II and Carbonate** scenarios most of the displacements occur at the early stage of the injection with values **above the detection limit until 2 or 3 years of injection**, respectively. For the **Sandstone I** case there is **no restrictions with time** since most of the results remain above the detection limit during the injection.

Subsidence behavior (post-injection) could be monitored via InSAR data in most cases for Sandstone I and Carbonates.

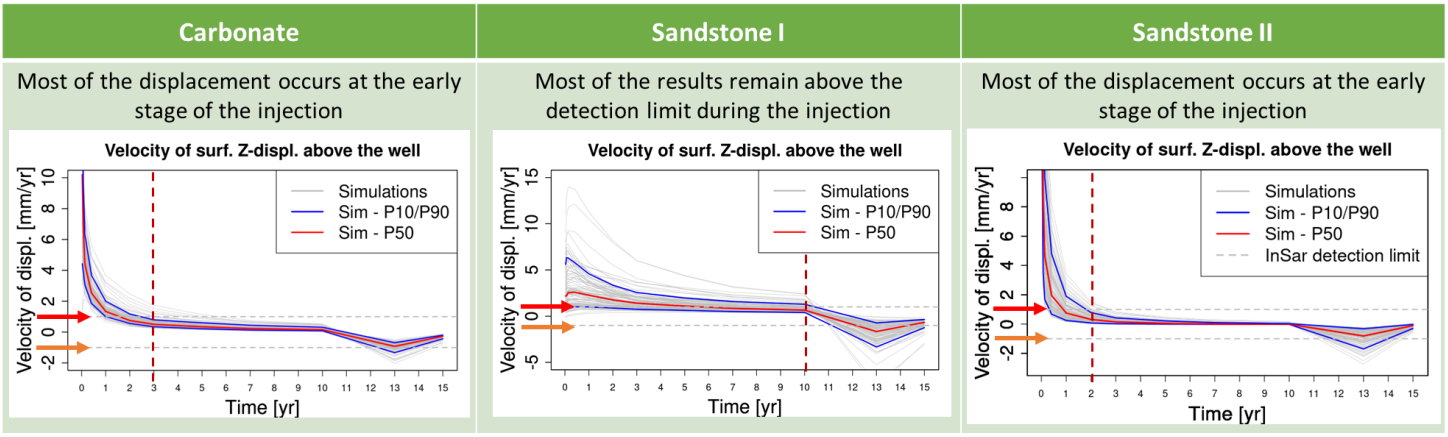

Figure 23 : Temporal differences in InSAR detection capability function of the scenario. Surface displacements velocities results above the well function of time from the training sample (115 simulations, grey lines; median in red, P10 and P90 percentiles in blue) with respect to the range of values for the scenarios parameters. The detection threshold of InSAR measurement is estimated at 1 mm/year (red and orange arrows). Dashed vertical lines figure the end in time of most of surface displacements.

Monitoring strategy with InSAR data should be adapted according to the considered context as follows.

- Temporal definition
  - short period for Carbonate and Sandstone II,
  - all over the injection period for Sandstone I.
- Spatial definition
  - limited around the well survey area for Carbonate and Sandstone I,
  - Extended survey area for Sandstone II.

- InSAR precision
  - specific high precision requirements for Sandstone II, for example, using corner-reflectors or satellite data with better resolution, such as TerraSar_X,
  - due to the small variations, for the Carbonate case, the corner-reflectors would improve the accuracy in the areas of high uncertainties,

Implementing these specifications improves the InSAR data processing in terms of time and cost taking into account type of data, use of corner-reflectors and other additional monitoring techniques.

3.3.2 Observability with tiltmeters measurements

Tiltmeter measurements are estimated by transforming surface displacements results by

$$\tan(\alpha) = \frac{\Delta x}{1 - \Delta z}$$

with α = tilt,
Δx = horizontal displacement
Δz = vertical displacement

The last two values are obtained by simulation. Tiltmeter length is supposed to be one meter. Tilts are expressed in nanorads.
With its high accuracy (from few nanorads to few dozen of nanorads), **tiltmeter is more sensitive in time and in space to surface displacements** due to CO_2 injection compared to InSAR data.

Tilt variations are of the order of fifty to few hundred nanorads in all cases after one year of injection (Figure 24), over distances of several kilometers around the well. We noted that near the well, tilts are null because of mostly vertical displacements (no dip), so **tiltmeters should preferentially be placed where both vertical and horizontal displacements are expected**.

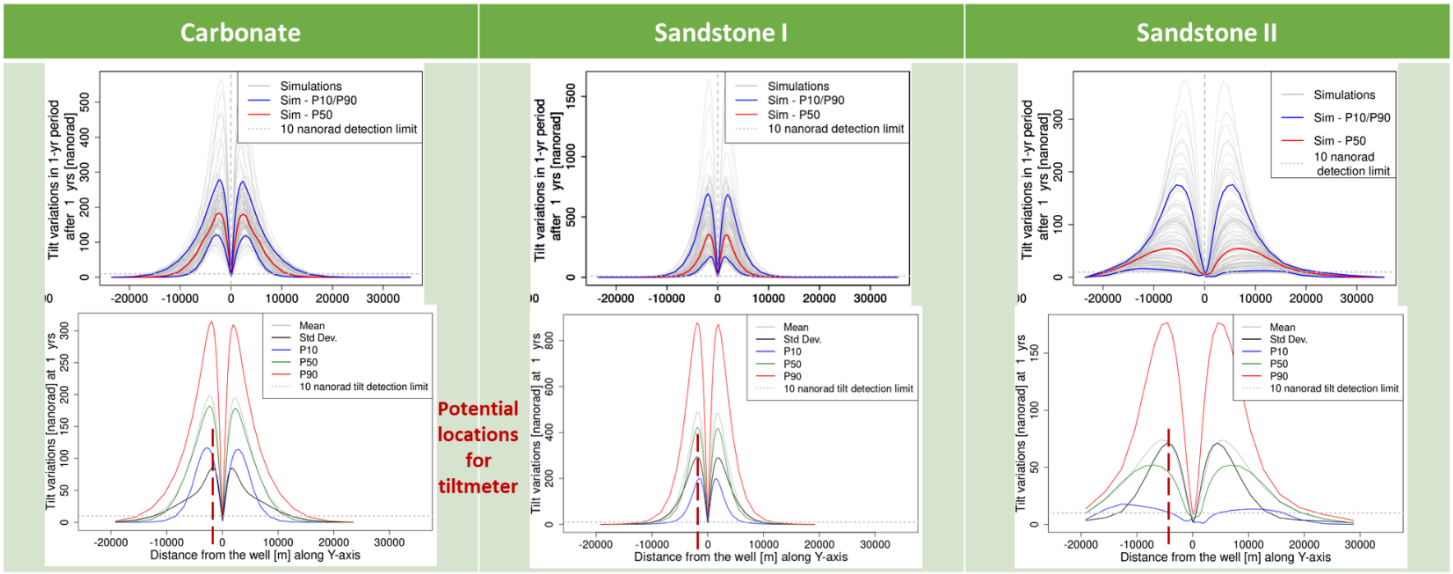

Figure 24 : Spatial variations in tiltmeters data function of the scenario after one year of CO_2 injection. Top: Cross section along the well of tiltmeters data for 115 simulations (grey curves) and related median (red curve), 90 and 10 percentiles (blue curves). Bottom: Cross section along the well of uncertainties on tiltmeters measurements (mean, standard deviation, median, quantiles 10% and 90%) related to the uncertainties on subsurface properties. Statistical calculations are performed from a Monte-Carlo sampling on metamodels built from the training sample. The detection threshold of tiltmeters measurement is estimated at 10 nanorads.

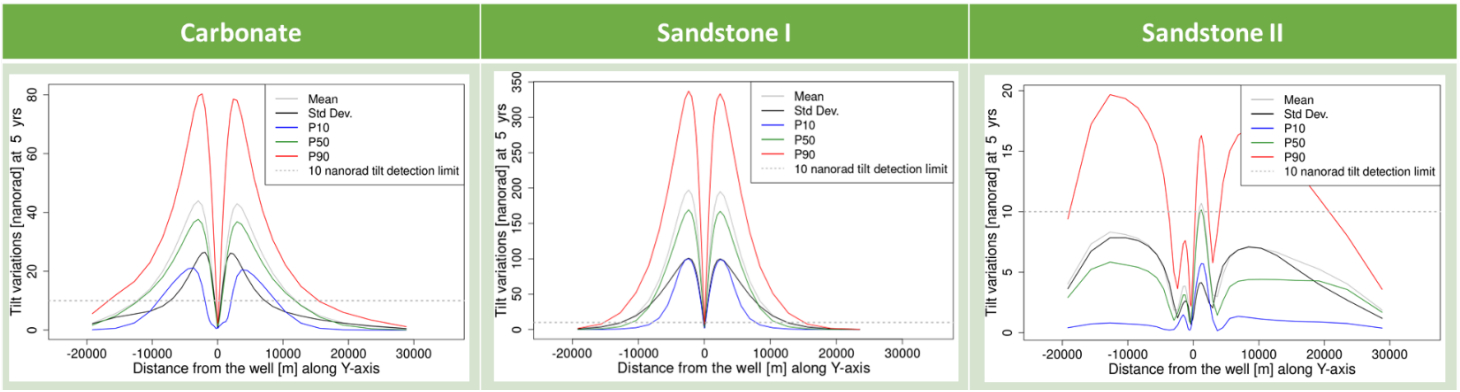

Figure 25 : Spatial variations in tiltmeters data function of the scenario after five years of CO_2 injection. Cross section along the well of uncertainties on tiltmeters measurements (mean, standard deviation, median, quantiles 10% and 90%) related to the uncertainties on subsurface properties. Statistical calculations are performed from a Monte-Carlo sampling on metamodels built from the training sample. The detection threshold of tiltmeters measurement is estimated at 10 nanorads.

After five years of injection, tilt data values remain high enough (above 10 nanorads) to ensure a surface monitoring with tiltmeters located in a few kilometers from the well over time (Figure 25).

For tiltmeters, monitoring design consists on the optimal sensors positioning in order to make the surface monitoring insightful, *i.e.* to be above the precision limit over time and reduce the uncertainty in subsurface behavior.
According to the entropy calculation (Figure 26) and standard deviation results (Figure 24), the high uncertainties on tilt measurements are close to the well and at short period of time. For Sandstone I and Carbonate scenario, they are in between 1 and 3 km at 1 year of injection time.
Therefore, for **Carbonate case**, it is recommended to **locate tiltmeters about 1.5 km from the well for short- and long- term monitoring**. The same recommendation is valid for **Sandstone** I but, taking into account the Shannon entropy results, an extra-tiltmeters are required at about 8 km from the well. For **Sandstone II** case, the recommendations are to locate sensors further away from the well, at about **5 km and 10 km from the well,** for surface displacements monitoring over time.

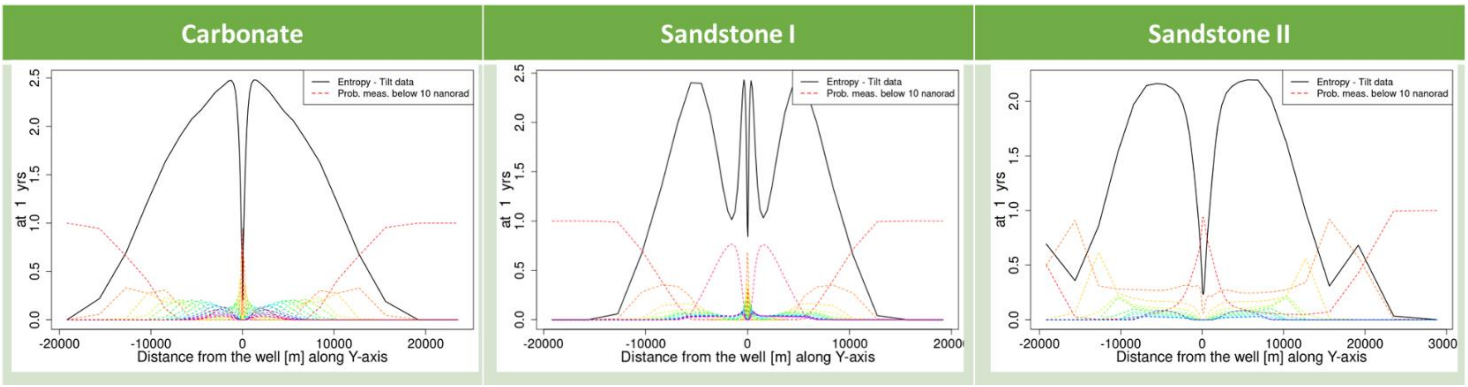

Figure 26 : Shannon entropy for categorical tiltmeter data with a measurement error of +/-10 nanorads: categories are defined from 10 nanorads up to 600 nanorads with an interval of 20 nanorads.

3.4 Sensitivity Analysis

For all scenarios, the results of the sensitivity analysis performed on displacement velocities with respect to model parameters uncertainties suggest a spatial and temporal variation of this sensitivity (Figure 28 and Figure 27). The results are consistent either from the dependency calculation (HSIC, Figure 27) or from Sobol indices(Figure 28).
For the **Carbonate** scenario, we have a **high sensitivity to the permeability** value of the storage formation over the entire model and a **significant sensitivity to the overburden parameters (mostly Young modulus) near the well**. For both **Sandstone scenarios**, the sensitivity is mainly related to storage formation properties, such as **permeability and Young modulus**.
The highest sensitivity to overburden parameters such as Young modulus for the Carbonate scenario can be explained by its *a priori* values interval which is much larger than the one from the storage formation (6-55 GPa *vs.* 25-45 GPa) This reflects the highest uncertainty which more often occurs in overburden compared to storage formation properties.

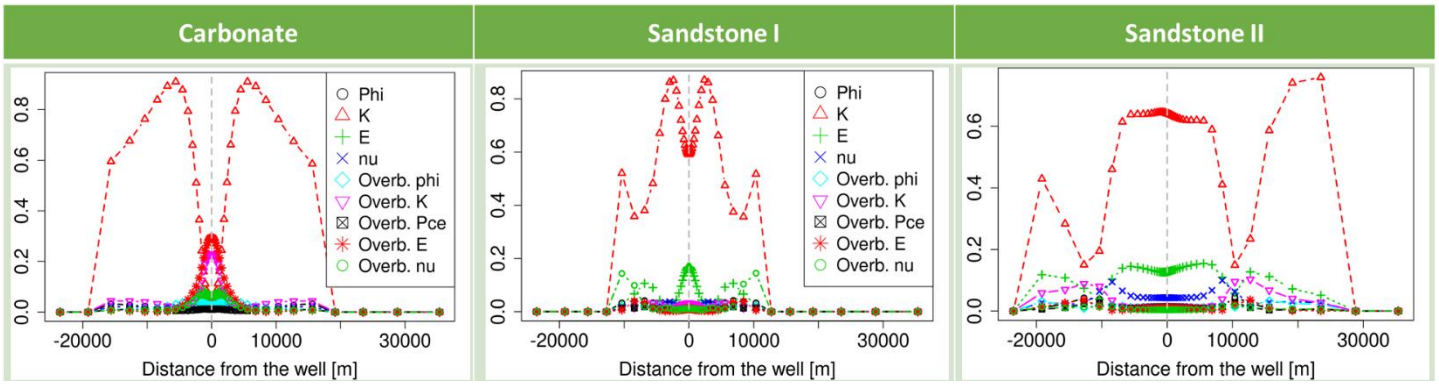

Figure 27 : Dependency criterioa (HSIC) between uncertain parameters and surface displacement velocities after one year of injection.

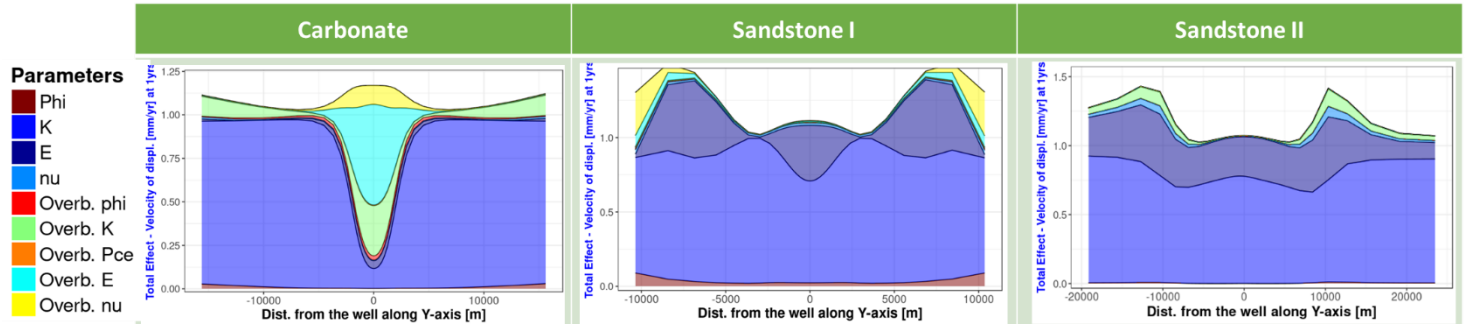

Figure 28 : Results of the sensitivity analysis (Sobol Indices), across the model, performed on the displacement velocities after one year of injection with respect to the different scenarios parameters.

Based on the sensitivity analysis, a monitoring strategy can be designed as the surface tools recording potential displacements at the most sensitive periods and locations, taking into account their accuracies. If surface displacements are measurable and sufficiently sensitive to subsurface properties then this monitoring will help to better constrain subsurface properties (useful for the inverse-problem) and possibly subsurface behaviour, such as plume migration, pressure propagation and storage capacity.

In addition to the far from the well measurements, the accurate near-well displacements data **contribute to constrain over time** the values of **overburden Young modulus** or storage formation Young modulus (depending on the scenario) and **storage formation permeability**. If we project predictions of vertical displacement velocities over the well and at distances from the well as functions of these parameters (Figure 29, Figure 30, Figure 31), we see that these measurements could significantly constrain the values of this couple of parameters. For both Sandstone

scenarios, most of the variations of surface displacements is explained by storage formation Young modulus and permeability values (*e.g*. up to 1 cm for Sandstone I) while other parameters induce an average variation of one to two orders of magnitude lower (*e.g.* max. 0.8 mm for Sandstone I)

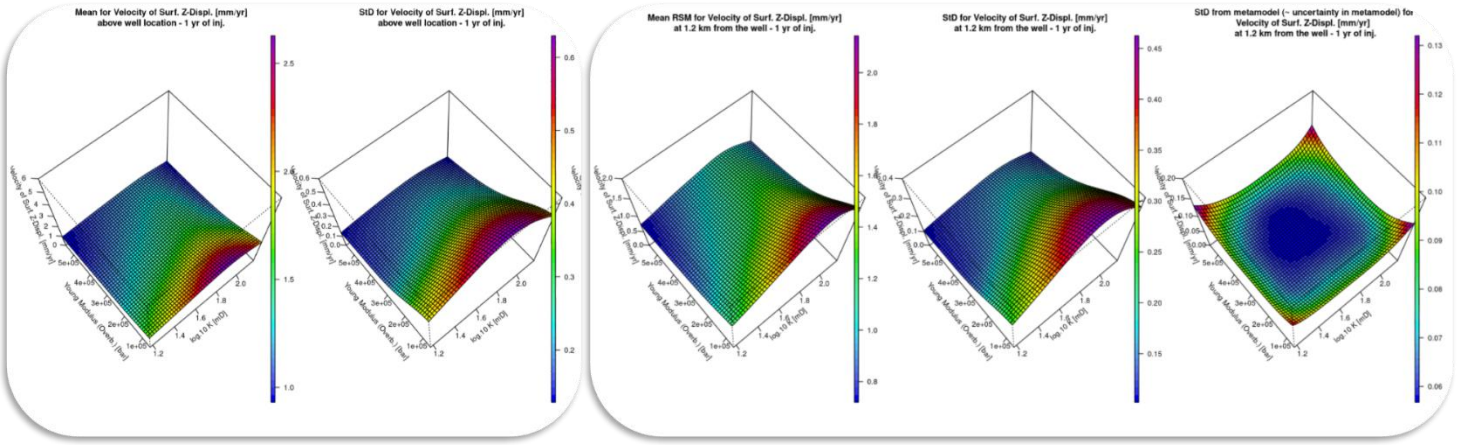

Figure 29 : Carbonate scenario – one year of injection. From metamodels: velocity of surface displacement above the well (left) and at 1.2 km from the well (right) function of Young's modulus value and permeability value of storage formation. For each location, the averaged values with respect to variations due to other parameters are on the left, the standard deviation associated with the variation of other parameters is on the middle and the uncertainty associated with the metamodel on the right.

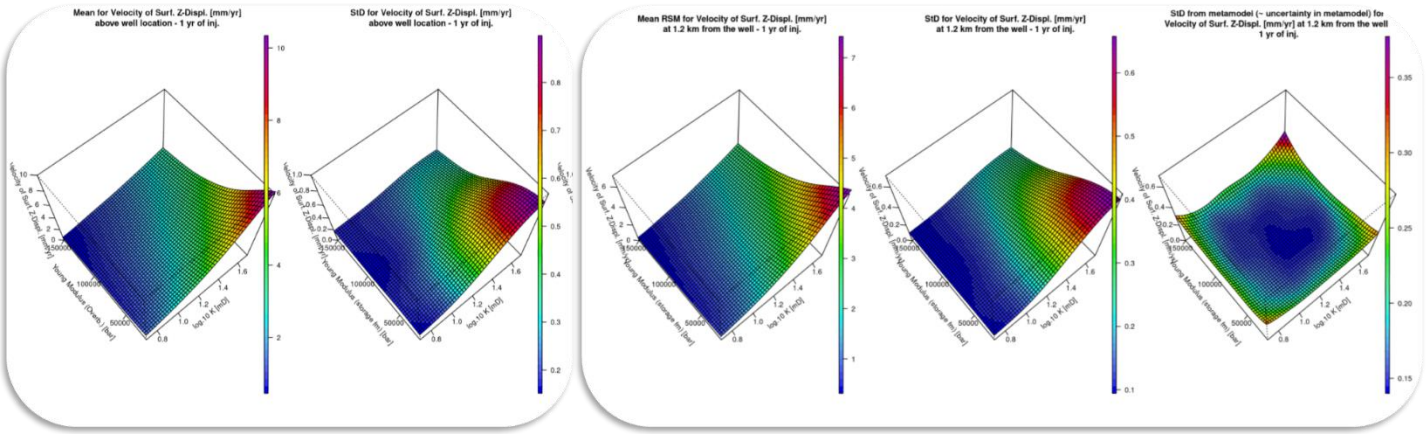

Figure 30 : Sandstone I scenario – one year of injection. From metamodels: velocity of surface displacement above the well (left) and at 1.2 km from the well (right) function of Young's modulus value and permeability value of storage formation. For each location, the averaged values with respect to variations due to other parameters are on the left, the standard deviation associated with the variation of other parameters is on the middle and the uncertainty associated with the metamodel on the right.

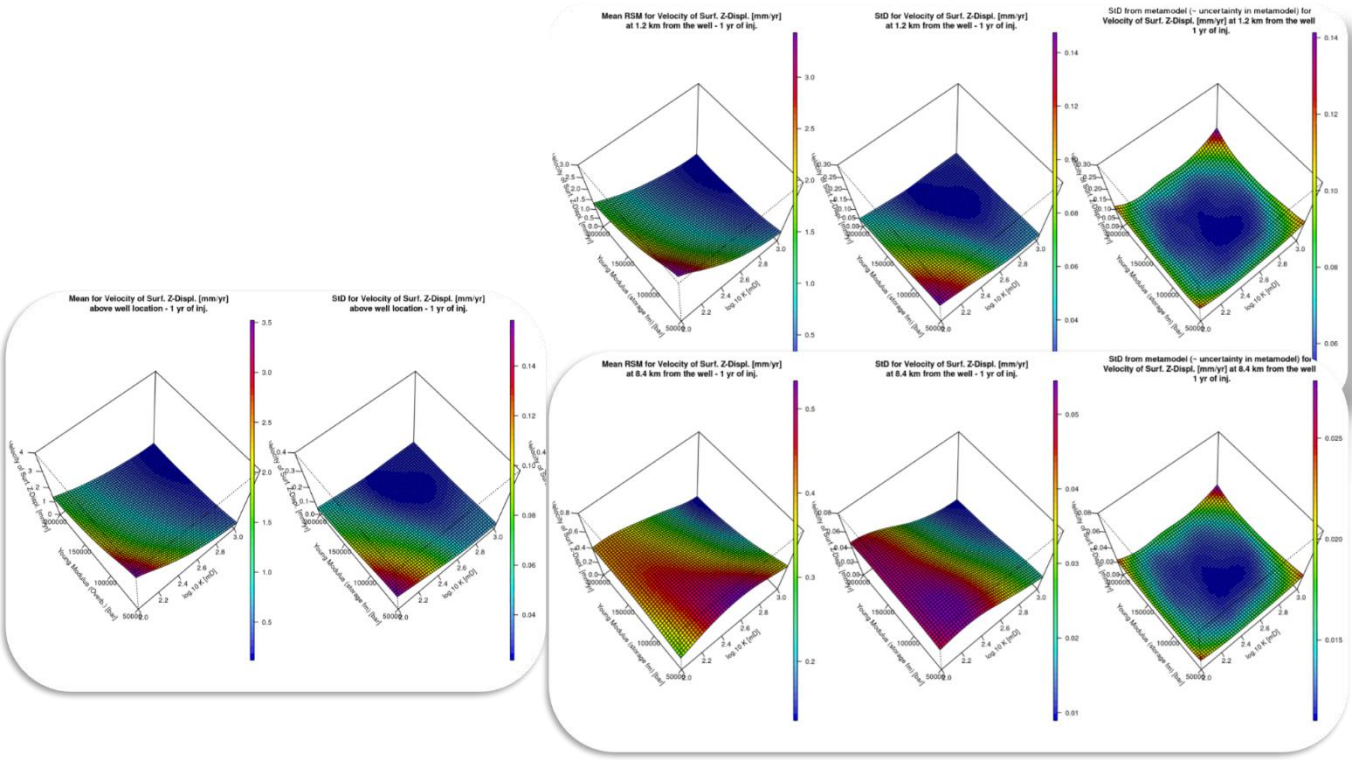

Figure 31 : Sandstone II scenario – one year of injection. From metamodels: velocity of surface displacement above the well (left) and at 1.2 km from the well (top, right) and 8.4 km from the well (bottom, right) function of Young's modulus value and permeability value of storage formation. For each location, the averaged values with respect to variations due to other parameters are on the left, the standard deviation associated with the variation of other parameters is on the middle and the uncertainty associated with the metamodel on the right.

3.5 Optimized monitoring for better constraint of subsurface behavior

The optimization of the monitoring design allows to obtain a better constraint on the subsurface properties and, thus, the subsurface behavior. In this purpose, for the tiltmeters locations we select the locations corresponding to a high dependency between tiltmeters measurements and uncertain properties, *i.e.*, the locations with the highest HSIC values, in addition to the highest variance for tiltmeters measurements based on uncertainty analysis and corresponding simulations.

We applied step 5 of the workflow described in section 2 for tiltmeters locations selection with a 50 nanorads detection limit based on simulations results from the training sample of the Carbonate scenario.

From the HSIC and standard deviation results obtained at 150 days, 1 year (Figure 32), 5 years of injection and 3 years of post-injection, seven locations (see Figure 33) were selected along the Y-axis for constraining the storage formation permeability and the Young modulus of the overburden. From a previous analysis, we know that subsurface and surface behavior for the Carbonate scenario are mainly sensitive to these parameters.

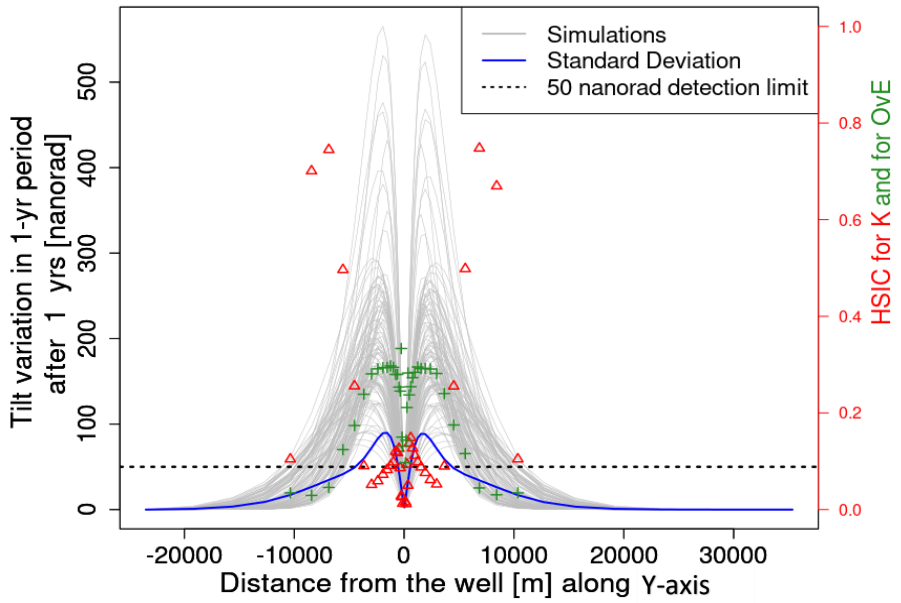

Figure 32 : Tilts simulations results from the training sample (grey lines) and its related standard deviation (blue line) and HSIC results between tilts and storage formation permeability (K, red) or caprock Young Modulus (OvE, green) for the Carbonate scenario after one year of injection.

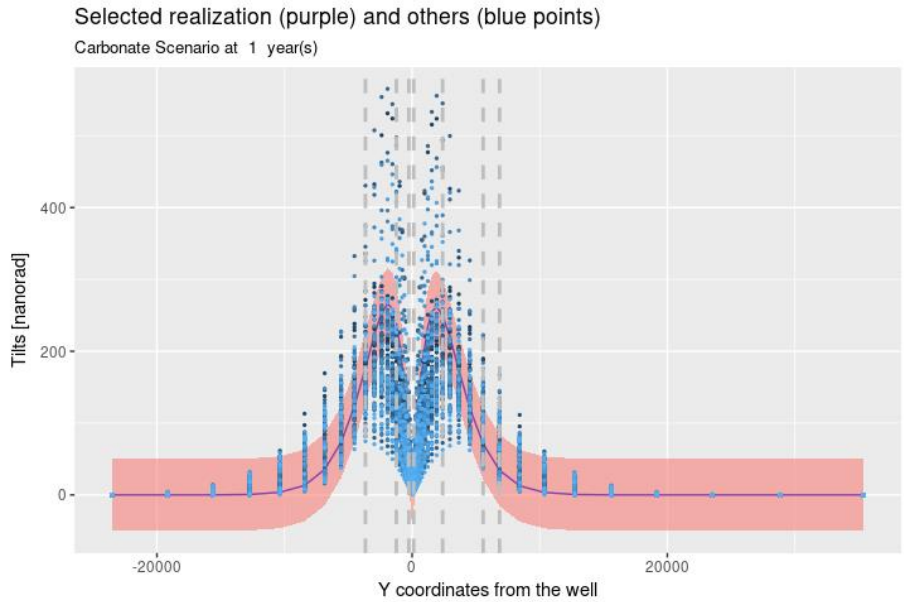

Figure 33 : Selected locations (vertical grey dashed lines) are based on results from the 115 simulations (HSIC for permeability and Young modulus, plus standard deviation results). The purple line represents tilts results from a randomly selected pseudo-reality with an observation error of +/- 50 nanorads (pink area). The blue points are tilts results that would be obtained from the 114 remaining simulation results.

To check the quality of the observations at the chosen locations, we compare *a posteriori* distributions of permeability values based on observations from these locations and on several random locations with pseudo-real observations data, *i.e.* by picking one of the 115 simulations as a real case (Figure 33).
To roughly estimate *a posteriori* distributions, we compare results obtained from the remaining simulations at the different locations with the pseudo-real observed data. If simulation results are equal to pseudo-real data within +/- 50 nanorads, then the corresponding parameters are taken into account for the distribution calculation. *A posteriori* distributions can then be compared to the values from the pseudo-real case. This quality check is applied for several pseudo-real cases.

From a few examples in Figure 34, we obtain **a better constraint** on *a posteriori* distribution **from the selected locations than from random locations**. At best, random locations can give similar results than the selected locations. In Figure 35, the *a posteriori* distributions results from a higher number of random locations (aggregated from 50 random locations) are clearly undefined compared to those from the selected locations which are always constraining the *a posteriori* distribution close to the real-pseudo value.

To investigate further the value of the selected locations through the proposed method, we compare *a posteriori* distributions obtained with a larger sampling of the observation data; we randomly sampled observation data through predictions of metamodels with 5000 random combinations of uncertain parameters. Again, a randomly selected simulation is used as pseudo-real observation data. This selected simulation is removed from the training sample used to build metamodels.
A posteriori distributions based on observation at selected locations and at four sets of random locations are illustrated in Figure 36 for three pseudo-real observation data. On these examples, the selected locations of observation data allow to better constrain the *a posteriori* distribution close to the real subsurface properties than using random locations.

The use of dependency values (HSIC), here associated to standard deviation results, could be a quick assessment method (without requiring the resolution of the inverse problem for each possibility) to estimate the value of observation data and optimize the monitoring design. Here, the proposed monitoring design gives valuable information to reduce uncertainties on subsurface properties and, consequently, for history-matching.

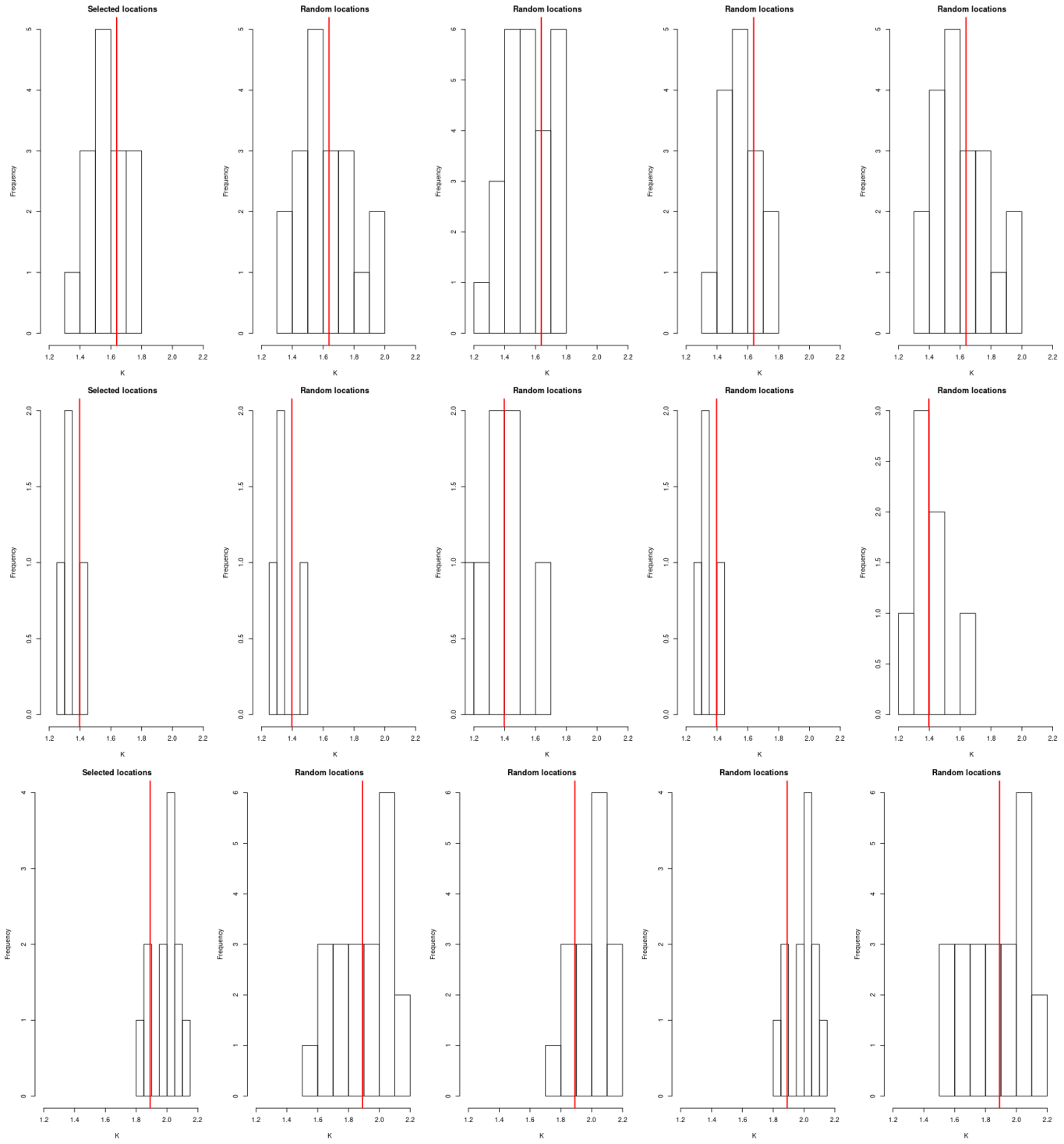

Figure 34 : *A posteriori* distribution estimations for storage formation permeability based on observation data at selected location for tiltmeters (left) or at random locations (four random combinations, right) for three different random pseudo-real cases (pseudo-real value to be matched in red). *A priori* distribution was uniform between 1.2 and 2.2.

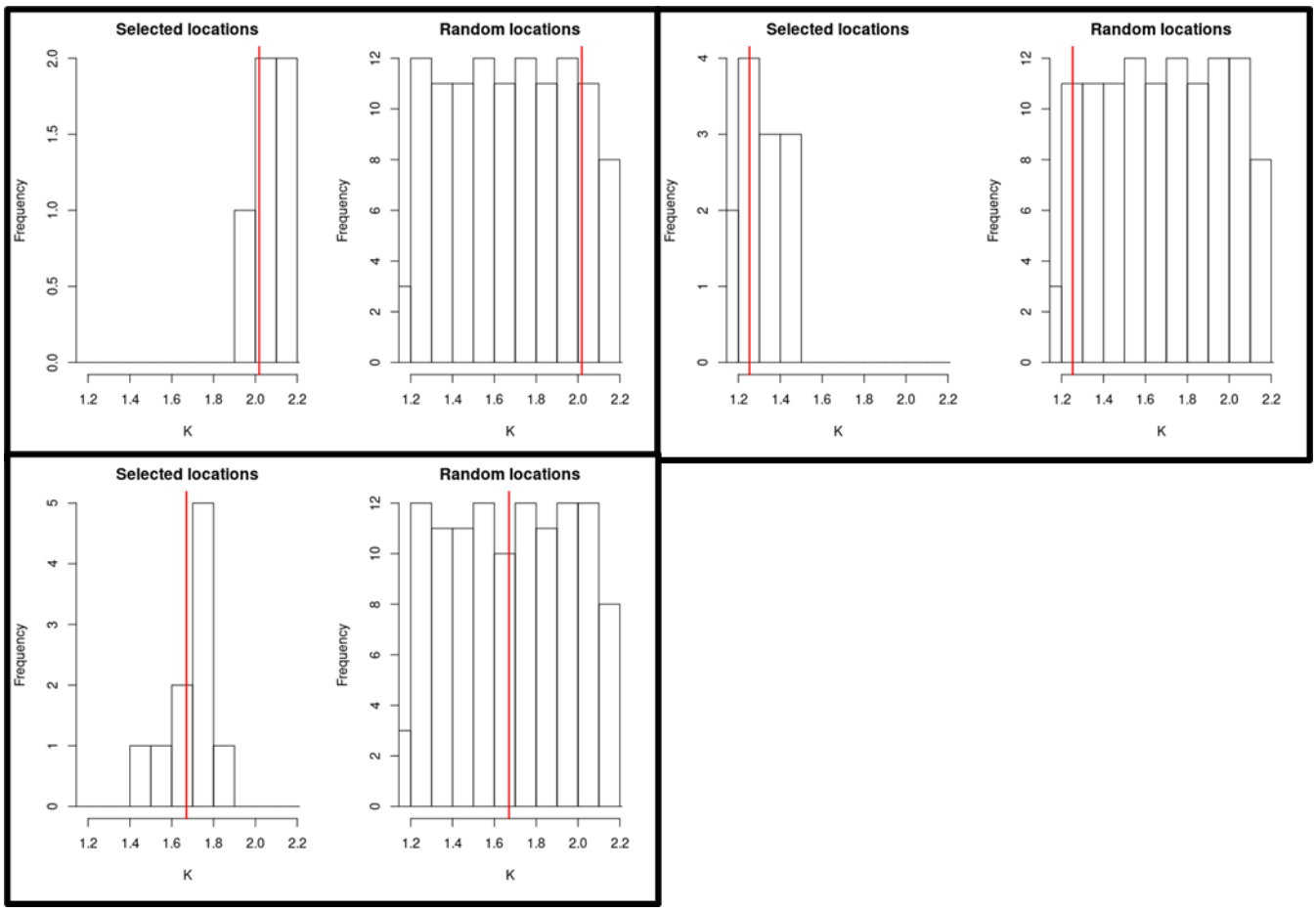

Figure 35 : *A posteriori* distribution estimations for storage formation permeability based on observation data on simulation results at selected location for tiltmeters (left) or at random locations (aggregated results for 50 random locations, right) for three different random pseudo-real cases (pseudo-real value to be matched in red). *A priori* distribution was uniform between 1.2 and 2.2.

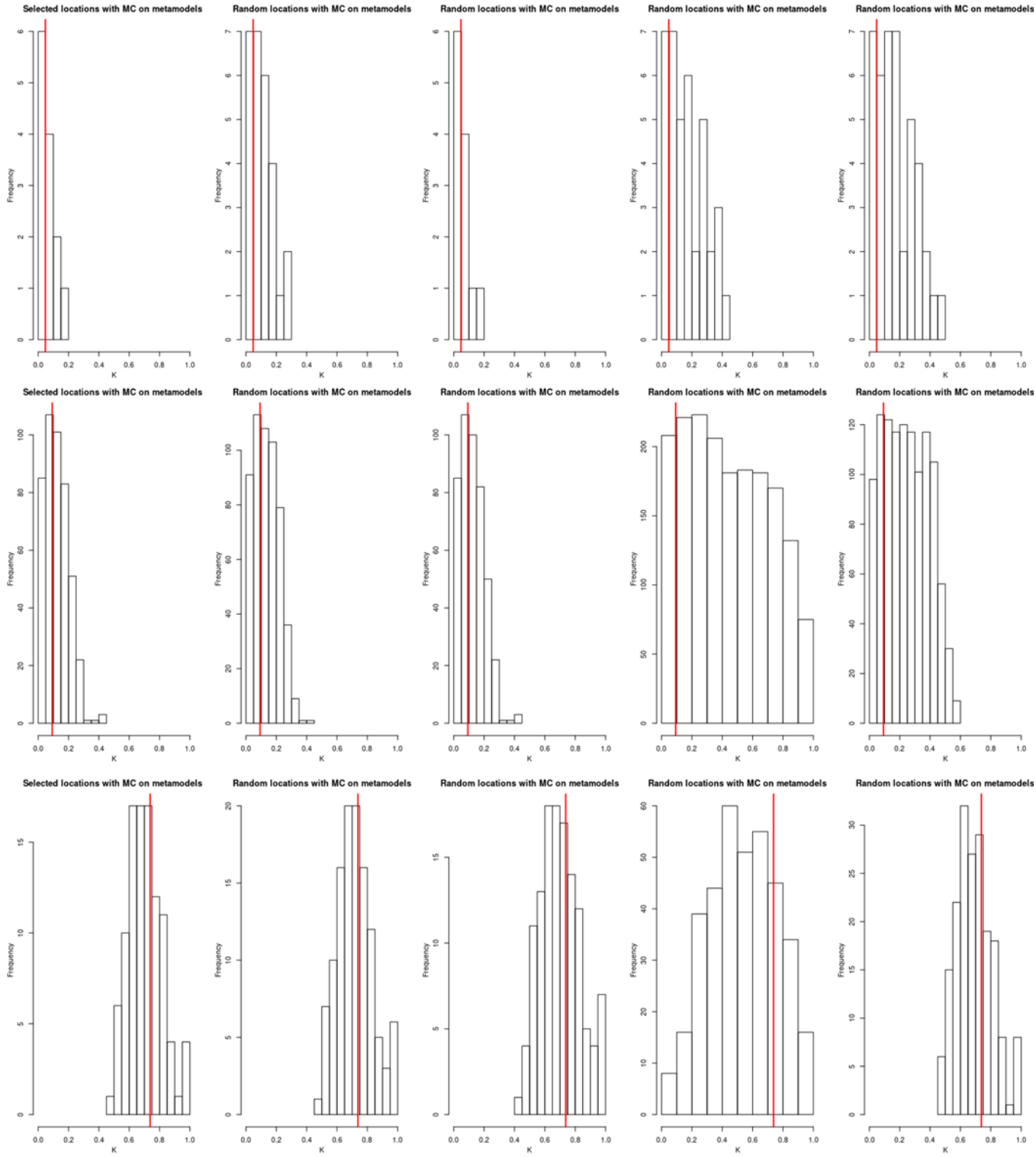

Figure 36 : *A posteriori* distribution estimations for storage formation permeability based on observation data on 5000 samples, predicted by metamodels, at selected location for tiltmeters (left) or at random locations (four random locations, right) for three different random pseudo-real cases (each line, pseudo-real value to be matched in red). *A priori* distribution was uniform between 1.2 and 2.2.

3.6 Risk Analysis of storage integrity with failure criterion

The risk analysis is performed according to the stress regime and subsurface properties scenarios based on the distance to both Drucker-Prager criteria. if they are reached, we consider that the storage integrity is jeopardized. It should be noticed that calculations are performed with the assumption of elastic deformation and that the Drucker-Prager surfaces are considered only to address risk analysis of caprock and faults integrity. This means that for scenarios crossing the outer Drucker-Prager surface, obtained stresses are plastically not admissible, therefore simulation based on an elasto-plastic constitutive law should be considered.

In Figure 37, Figure 38 and Figure 39, we illustrate stress results, relatively to Drucker-Prager criteria, obtained for one specific simulation (simulation #70, *cf.* Table 2) for different scenarios, such as geological properties[1] and stress regime.
Figure 37 illustrates the important differences that we can obtain only with different stress regime context for the most exhaustive example corresponding to the Carbonate scenario.

- In the Extensive regime, neither the inner nor outer criteria are reached in the caprock formation at any time.
- On the contrary, in the StrikeSlip 1 regime, even at the initial state, stress results are above the inner criterion for whole caprock. It means that the CO_2 injection is at risky regarding the caprock integrity.
- In Compressive and StrikeSlip 2 regime, at the initial state, no criteria are exceeded. But later, with CO_2 injection, the inner criterion is exceeded in some caprock regions. It means that the storage integrity is not ensured anymore.

These results are valid for one specific simulation for the Carbonate scenario. However, the same important differences between stress regime are observed for the Sandstone I and II scenarios, e.g. inner criterion reached for StrikeSlip 1 in Figure 38. For the other scenarios and for other simulations, we may not cross the inner criterion in Compressive or StrikeSlip 2 contexts (Figure 38 and Figure 39).

[1] Important notice : caprock porosity are exactly the same between simulations in Sandstone I and Sandstone II (same uncertainty interval for caprock porosity and same sampling) thus cohesion values for caprock are also the same between Sandstone I and Sandstone II (same relationship between porosity and cohesion for shales). Consequently, differences in caprock integrity between both scenarios will be due to other parameters effects.

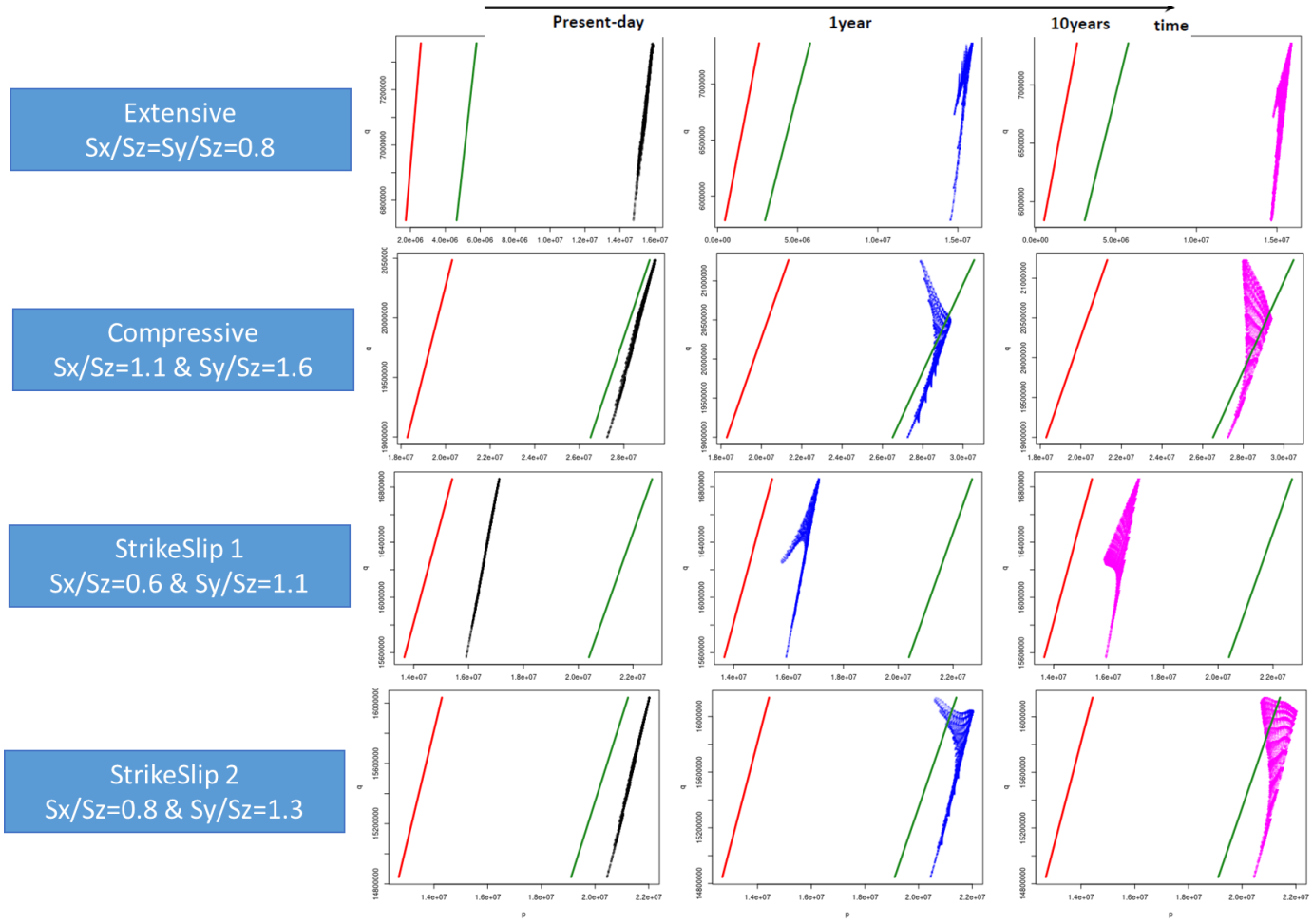

Figure 37 : Example of stress results for the caprock for one simulation (simulation #70, cf. Table 2) for the Carbonate case. Results are presented before injection (present-day), after one year of injection and after ten years of injection and for different stress regimes. Each point represents a cell result from the caprock and are to be compared to both Drucker-Prager criteria (outer in red, inner in green).

	Phi [-]	K [log10 mD]	E [bar]	nu [-]	Overb. Phi [-]	Overb. K [log10 mD]	Overb. Pce [bar]	Overb. E [bar]	Overb. nu [-]	Overb. Cohesion [MPa]	Overb. Friction [°]
Carbonate #70	0.21	1.46	3.E+05	0.18	0.36	-2.60	31.30	5.1E+05	0.22	2.56	19.26
Sandstone 1 #70	0.22	0.98	5.E+04	0.23	0.14	-2.86	29.13	1.8E+05	0.25	3.84	21
Sandstone 2 #70	0.16	2.28	8.4E+04	0.18	0.14	-3.86	26.52	3.9E+05	0.24	3.84	21

Table 2 : Parameters values for simulation #70 for all scenario, used as an example in failure criterion calculation

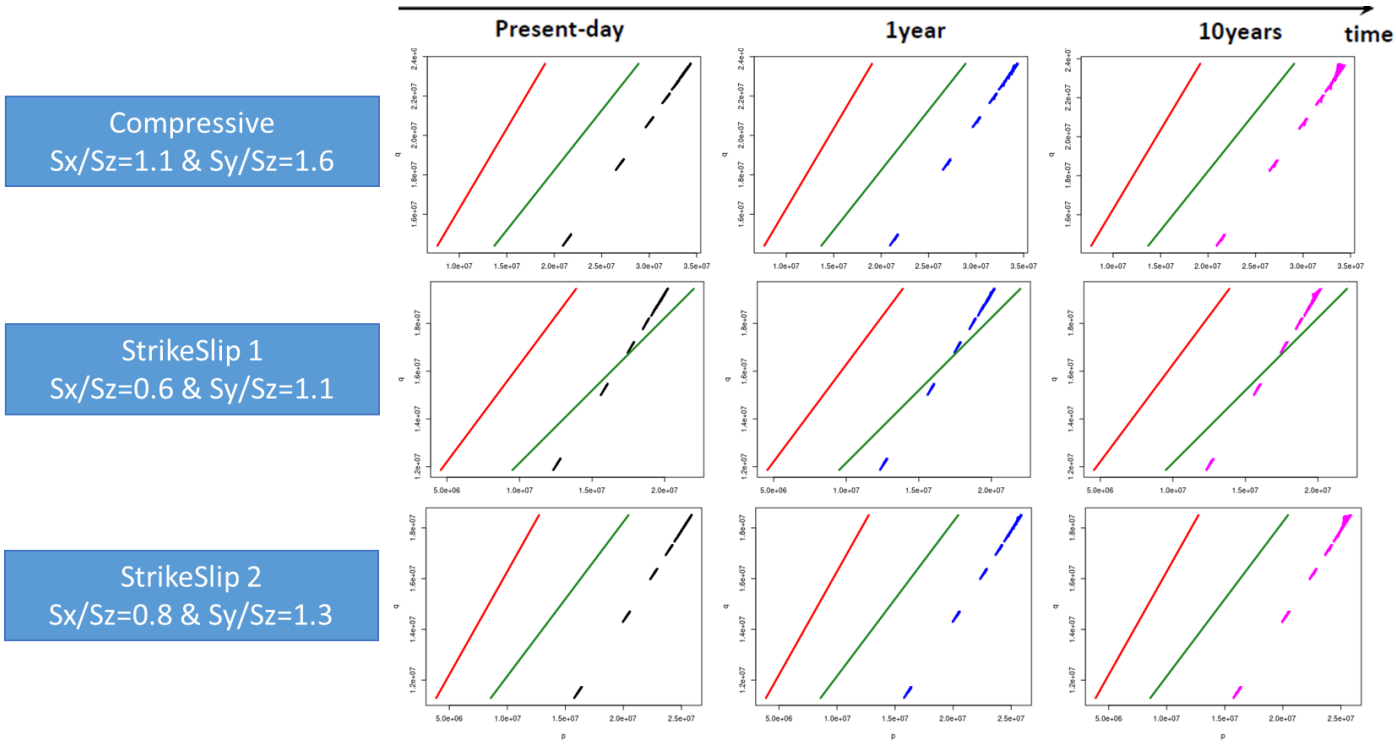

Figure 38 : Example of stress results for the caprock for one simulation (simulation #70, cf. Table 2) for the Sandstone I case. Results are presented before injection (present-day), after one year of injection and after ten years of injection and for different stress regimes. Each point represents a cell result from the caprock and are to be compared to both Drucker-Prager criteria (outer in red, inner in green).

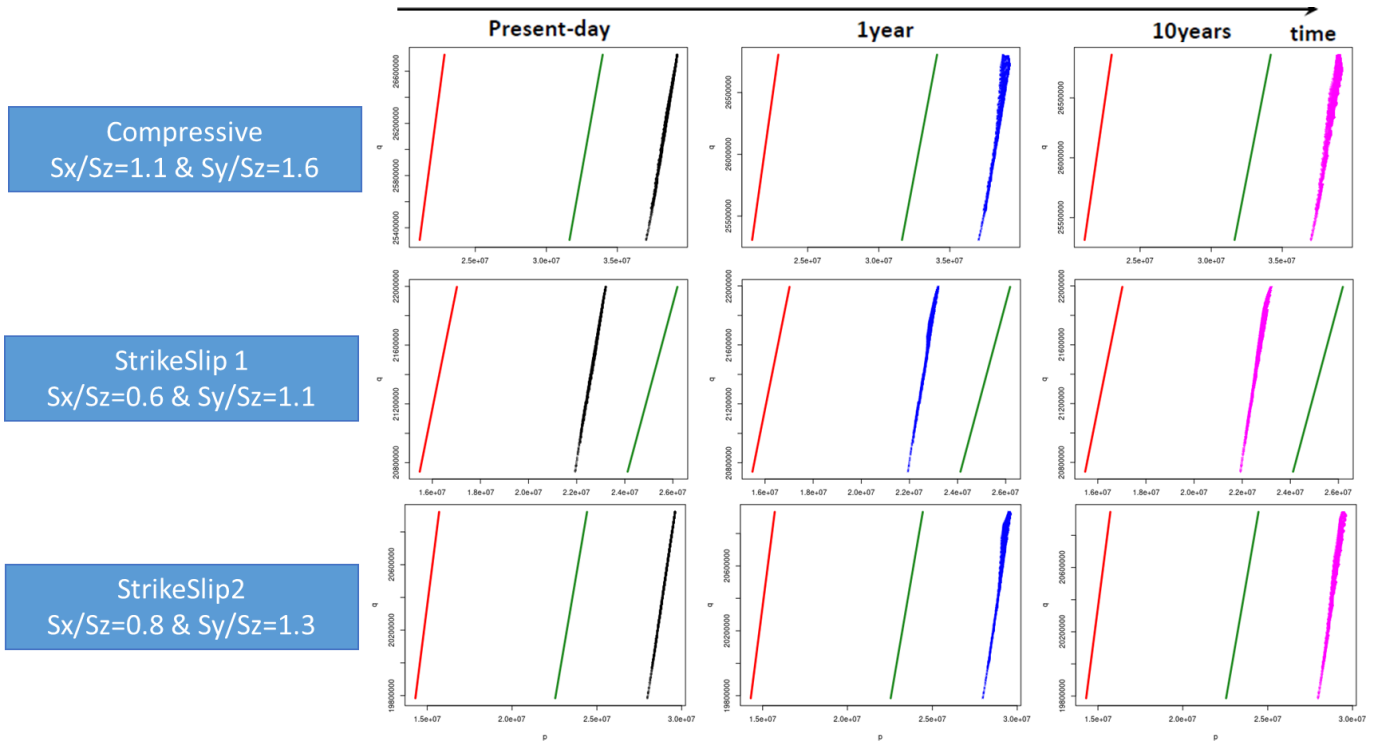

Figure 39 : Example of stress results for the caprock for one simulation (simulation #70, cf. Table 2) for the Sandstone II case. Results are presented before injection (present-day), after one year of injection and after ten years of injection and for different stress regimes. Each point represents a cell result from the caprock and are to be compared to both Drucker-Prager criteria (outer in red, inner in green).

For all scenarios and all simulations, the failure criteria are **never reached in the Extensive regime**. In this case, we can consider that the risk for the storage integrity is negligible. These results are valid for the specific studied contexts, scenarios and studied injection design (with maximal overpressure of 50 bar), *etc*. However, the Extensive stress regime would be the most favorable for CO_2 storage regarding the caprock integrity.
On the contrary, for all scenarios, **the inner failure criterion is reached for a significant part of simulations, even at the initial state in the StrikeSlip 1 context** (Sx/Sz=0.6 & Sy/Sz=1.1). This context is the most unfavorable for which CO_2 storage may not be sustainable whatever the injection design.
These differences according to the stress regime emphasize the importance of properly defining the initial stress regime before considering CO_2 injection.
For the two others stress regimes, as for storage capacity and surface displacements, the risk of failure is quite different depending on the considered geological scenario.

The following analysis focuses on regime contexts where the risk for storage integrity is more uncertain and/or important, *i.e.* StrikeSlip 1 stress regime (Sx/Sz=0.6 & Sy/Sz=1.1) and Compressive stress regime (Sx/Sz=1.1 & Sy/Sz=1.6). Results from StrikeSlip 2 regime are very similar here to those obtained with the compressive stress regime.
The analysis is performed as a function of distances to criteria, more precisely, with a normalized distance to the inner criterion. It is calculated according to the distance between both criteria. If the normalized distance becomes above one, then both criteria are reached. Therefore, the risk for storage integrity is assessed function of this normalized distance, closer it is to one, higher the risk for storage integrity.

In Figure 40, an example of results from one simulation (simulation #70, Table 2) for the Compressive stress regime, shows the impact of the anticline structure on the integrity risk. For all scenarios, there is a higher risk to exceed failure criteria at the summit/crest of the anticline and vice-versa for the anticline flank. As seen before, the containment storage is jeopardized only for the Carbonate case for the Compressive stress regime, with the high-risk area being located closed to the well. As for surface displacements and pressure results, risk is much more located near the well for Sandstone I (but it propagates through the anticline). For Sandstone II, it goes further away from the well. Finally, we obtain an intermediate case for the Carbonate scenario.
The specificity from the Sandstone II scenario is that a lower risk is recorded in the vicinity of the well compared to few hundred meters from the well. This is to be related with the pressure behavior in the caprock described in paragraph 3.2, fluid pressure does not propagate through the caprock above the well because the storage formation is saturated in CO_2 at this location with a high capillary entry pressure in the caprock.
Similar behavior in space is observed for the StrikeSlip 2 context.

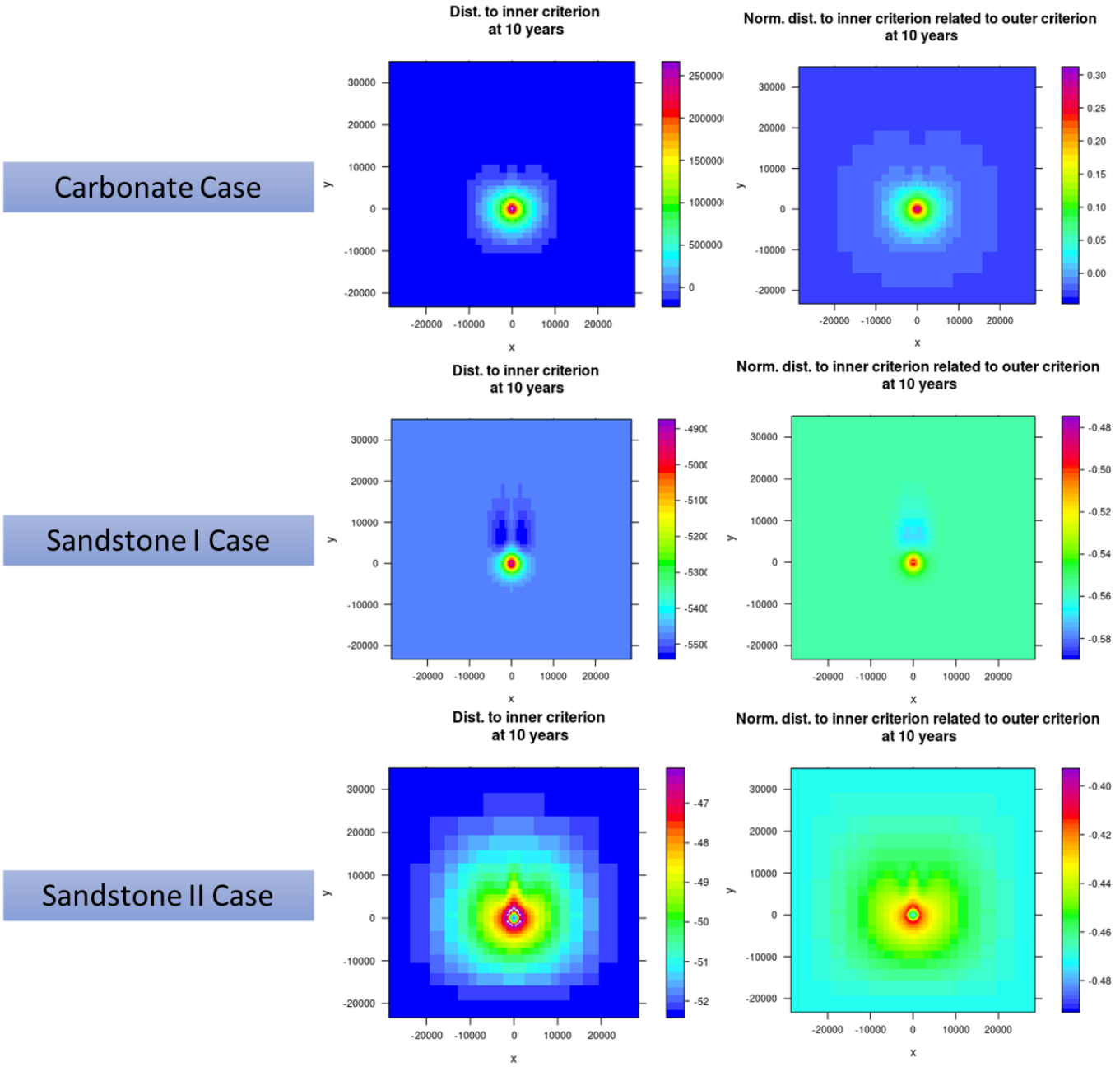

Figure 40 : 2D views (XY plane) of distances to criteria for the first layer of the caprock (interface storage formation / caprock) for one simulation (simulation #70, *cf.* Table 2) for three scenario in Compressive context after ten years of injection. Coordinates are function of distance from the well (in meters).

The maximum normalized distance over the caprock domain, for all simulations for all scenarios and for the Compressive and StrikeSlip 1 contexts are summarized as a function of time in Figure 41.
For the Compressive stress regime, only the injection in the Carbonate case could be risky for storage integrity with some simulations exceeding the inner criterion. For this stress regime, injection in Sandstone cases can be considered as safe since none of the criteria are reached (values remaining below 0).
Nevertheless, we observe a significant evolution of the distances with time for the Sandstone I case. If the injection would be continued beyond 10 years, the inner criterion could be reached and the storage integrity could be compromised. Sandstone I case is the most sensitive to the dynamic conditions of injection. On the contrary, for Sandstone II case, the risk is mainly driven by the initial condition of the storage (evolutions with time are not significant).

For the StrikeSlip1 regime, all cases present some risks for the integrity with some simulations reaching at least the inner criterion. The Carbonate case is the critical one, reaching for some simulations both criteria and being plastically not admissible, even at the initial state for some extreme simulations. On the other hand, Sandstone II case has the highest probability to present some risks for the storage containment given the uncertainties in subsurface properties (more than half of simulations exceed the inner criterion, see also Table 3).

With the color legend, Figure 41 clearly shows that the difference in results between simulations is driven by the initial porosity values that define the cohesion values of the caprock.
Finally, the risk of integrity depends mainly on the initial state with the initial stress regime and the cohesion values (as a function of the initial porosity values), more than on the dynamic subsurface behavior due to CO_2 injection. This integrity analysis is summarized in Table 3.

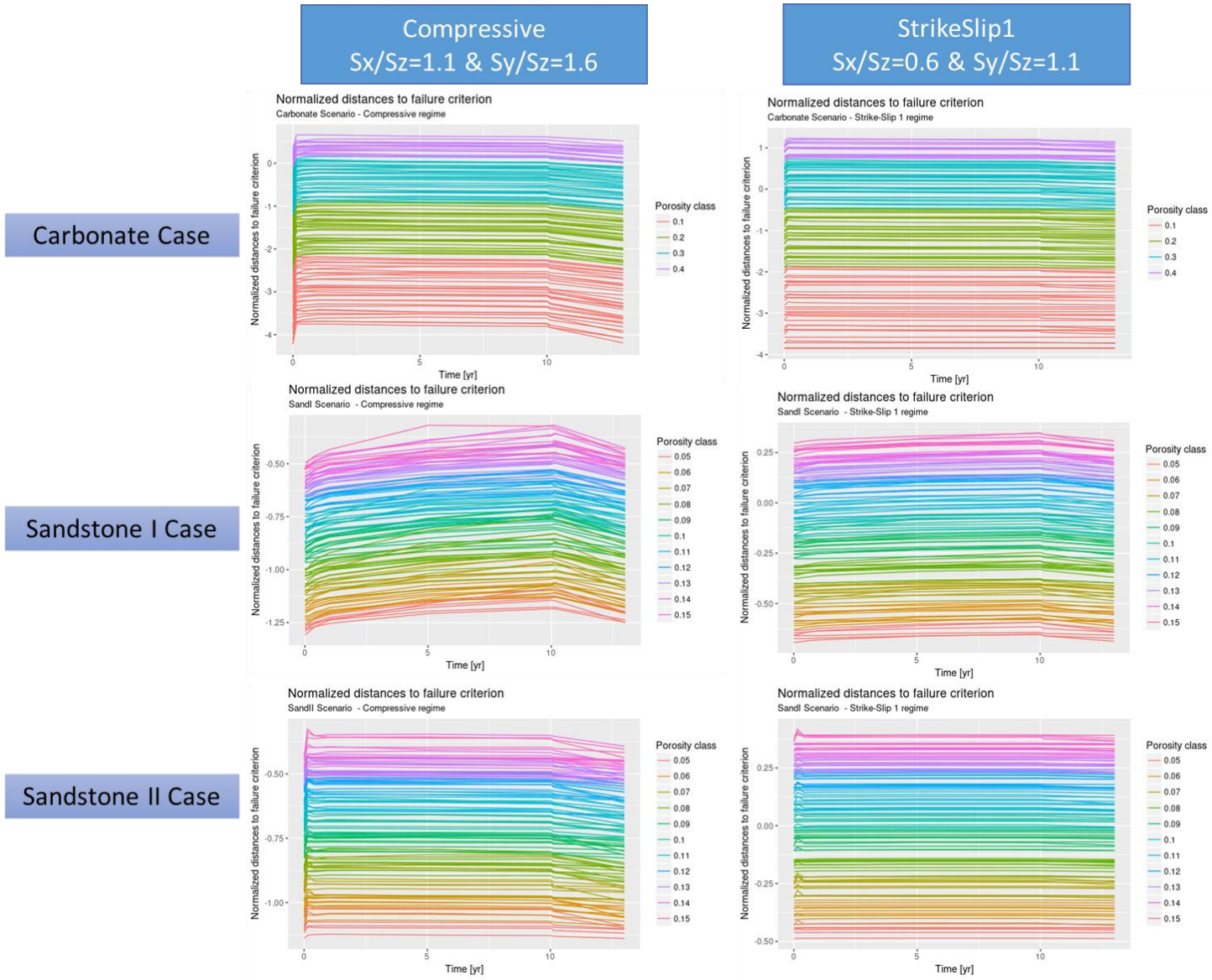

Figure 41 : Maximum normalized distance to failure criteria over the caprock domain function of time for 115 simulations (each line represent a for Carbonate scenario, Sandstone I scenario and Sandstone II scenario. Results are applied to the Compressive context (left) and StrikeSlip 1 context (right). Colors are function of caprock porosity values. If values are above or equal to 0, then the inner criterion is reached, if values are above or equal to 1, both criteria are reached. Otherwise, we would consider that the injection is safe for storage integrity.

	Carbonate		*Sandstone I*	*Sandstone II*
Compressive	18%			
Extensive				
StrikeSlip 1	34%	6%	39%	52%
StrikeSlip 2				

Table 3 : Integrity analysis results for all scenarios. Green: all stresses are below inner Drucker-Prager criterion for all simulations, yellow: some stresses are between inner and outer Drucker-Prager criterion for some or all simulations, red: some stresses are beyond outer Drucker-Prager for all or some simulations. Percentages are the ratio of simulations that has reached one or both criteria.

There is no direct links between the surface displacement resulting from elastic deformation, and this proposed risk analysis. However, such an analysis can be carried out to better constrain injection conditions, to identify where and when a storage may be at risk, and to localize critical points/areas that need to be accurately monitored.

4 Surface displacements comparison between iterative and one-way coupling and its consequences

One-way coupling simulations were performed for the previous statistical and sensitivity analyses. However, one-way coupling may lack of accuracy in terms of surface displacement or flow simulation results compared to more intensive computational methods such as iterative coupling (see paragraph 2.1, p.8, for a description of methods differences). To quantify the loss of accuracy and the gain in computational time, we compare performances between both methods for the Carbonate and Sandstone II scenarios.

4.1 Flow and Mechanical results comparison

The same 115 simulations were performed with one-way and iterative coupling methods to compare statistical and sensitivity results with various parameters combinations. The objective is to determine if both coupling methods lead to the same conclusions in terms of risk analysis, monitoring design recommendations and sensitivity results.

4.1.1 Comparison between one-way and iterative coupling – Carbonate scenario

4.1.1.1 Flow simulation results

Globally, both one-way and iterative coupling lead to similar capacity storage predictions (see distributions in Figure 42). Amplitude of pressure perturbations in the injection area remains similar between both coupling methods (Figure 43). On the other hand, predictions of CO_2 plume extent or pressure propagation are different (Figure 44 and Figure 45), specifically at short-term periods (*e.g.* 1 year). With one-way results we may **underestimate** the extent of CO_2 plume or the pressure propagation by the order of several hundreds of meters for CO_2 plume, and several kilometers for pressure perturbation (increase of 1 bar).

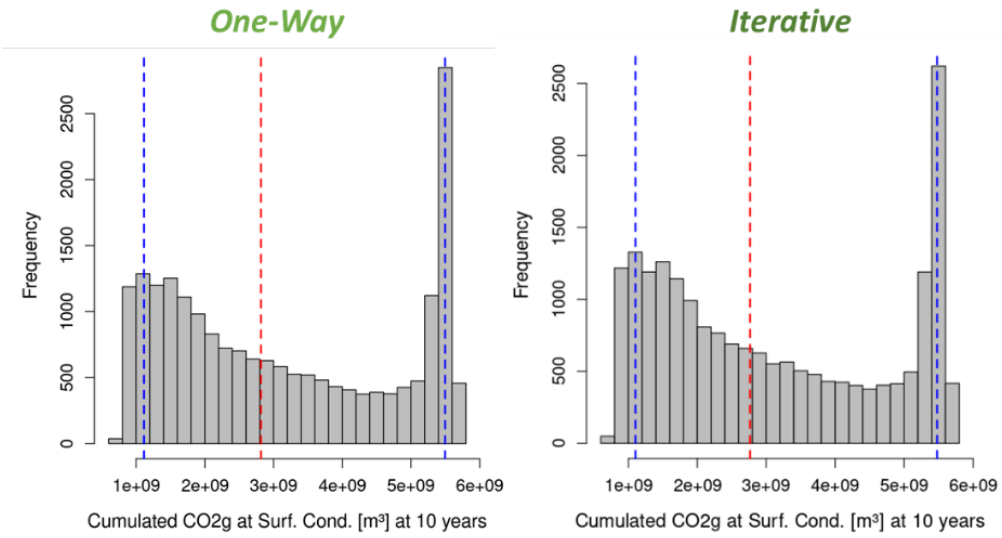

Figure 42: Distribution of storage capacity (cumulative injected gas volume at surface conditions) for 10 years of injection from a Monte-Carlo sampling of metamodels predictions. Left, results based on one-way coupling simulations. Right, results based on iterative coupling simulations.

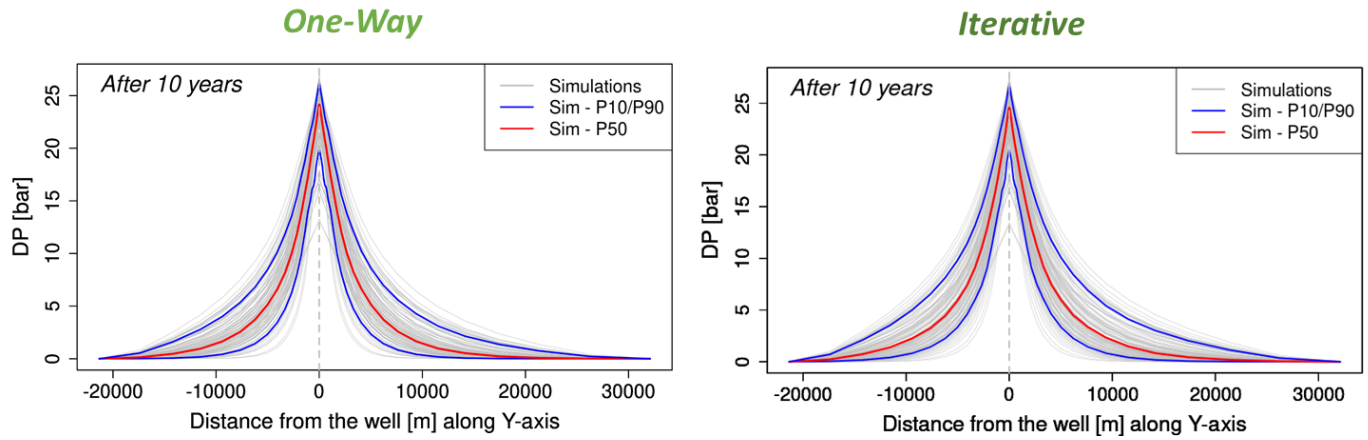

Figure 43 : Pressure perturbations (increase in pressure relatively to the initial conditions) after 10 years of injection for 115 simulations. Left, results from one-way coupling; right, results from iterative coupling.

The estimation of CO_2 plume migration extent or pressure propagation can be crucial to evaluate a potential risk of leakage or contamination (either CO_2 or water-in-place up to shallower aquifer) through abandoned wells, faulted areas, spill-points, *etc.*, or a potential risk of interferences between wells in the area.
Here, the differences may remain acceptable between both methods, however, it should be reminded that one—way coupling may underestimate the extents predictions and thus have to consider an uncertainty of about few hundred meters for CO_2 plume and few kilometers for pressure perturbations. Consequently, if any element at risk exists in the uncertainty range, then the iterative coupling should be used to improve the risk analysis.

Figure 44 : Box plots (describe results distribution with the median (bold line), percentiles 25 and 75 % (box) and dispersion (segments)) of the maximum extent of CO_2 plume for 115 simulations for several injection periods (1 year, 5 years, 10 years) or post-injection (13 years) at the top of storage formation.

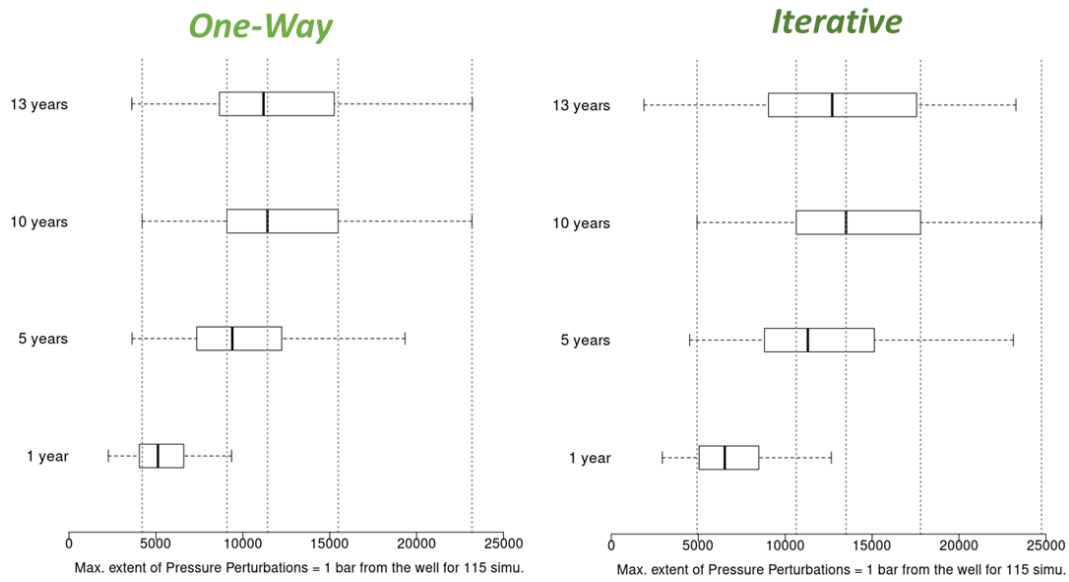

Figure 45 : Box plots (describe results distribution with the median (bold line), percentiles 25 and 75 % (box) and dispersion (segments)) of the maximum extent of a pressure increase of 1 bar for 115 simulations for several injection periods (1 year, 5 years, 10 years) or post-injection (13 years) at the top of storage formation.

4.1.1.2 Surface displacements results

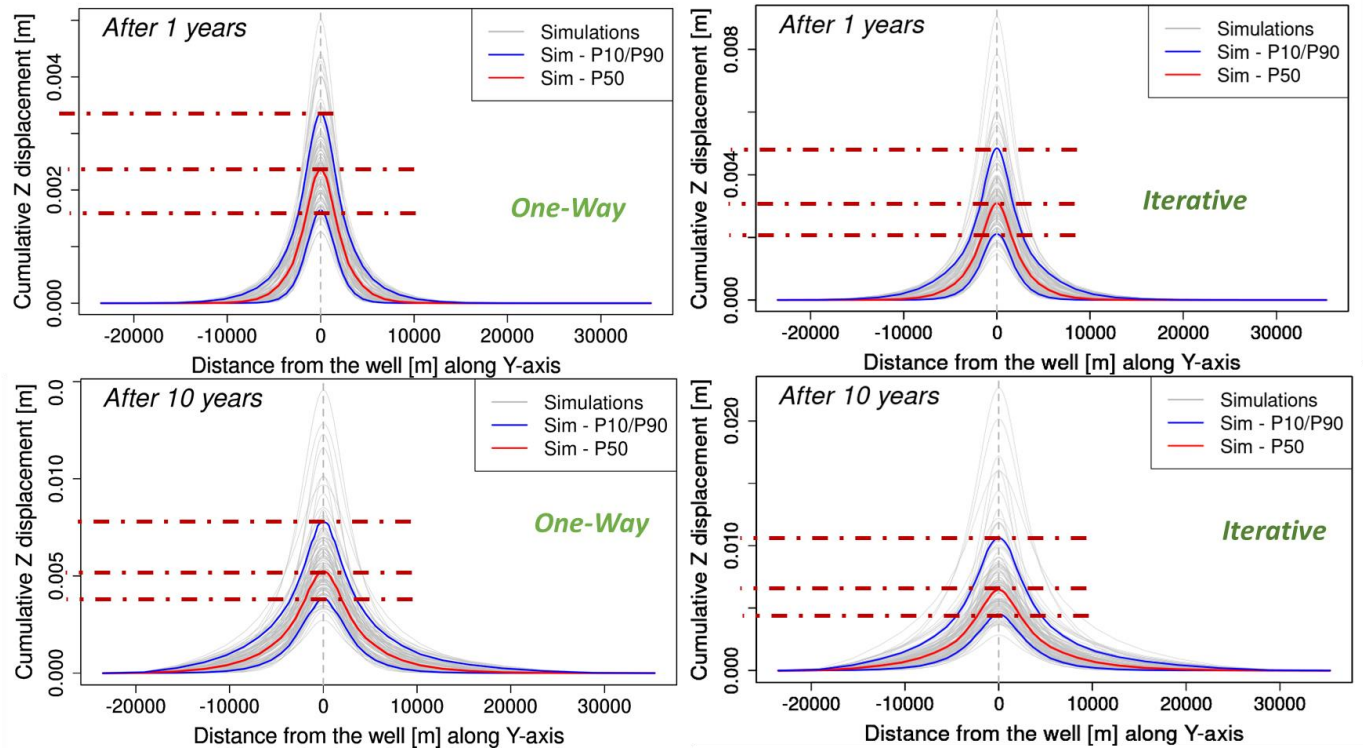

Figure 46 : Cumulative surface displacements function of the distance from the well along the Y-axis (i.e. along the anticline) after one year of injection (top) and after ten years of injection (bottom). In red, the median, in blue P10 and P90 percentiles of the 115 simulations (in grey). Left, results from one-way simulations; right, results from iterative-coupling simulations.

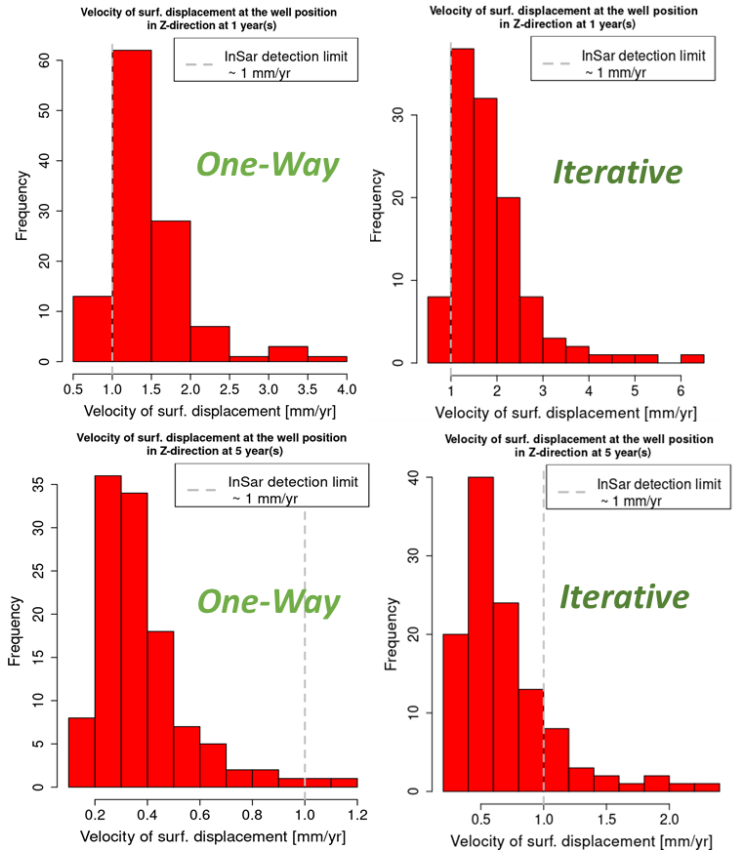

Figure 47 : Distribution of surface displacement velocities above the well after one year of injection (top) and after five years of injection (bottom) with one-way simulations results (left) and iterative-coupling results (right).

Results from one-way simulation **underestimate** the surface displacements compared to iterative-coupling results (Figure 46). For example, the difference in cumulative displacements in the injection area can reach 2 mm after one year or ten years of injection for the 90th percentile. The highest difference can be up to 5 mm if we consider the maximum obtained from the 115 simulations.

Thus, **the loss in information with one-way coupling method can be substantiable** when comparing surface displacements predictions from simulations with tool detection limit and eventually defining recommendations for monitoring strategy (Figure 48). **With iterative results, surface displacements would be detectable on a larger area and for a longer time period**. Moreover, results variability is higher, closer to the detection threshold in the iterative case, leading to a more promising potential to discriminate subsurface properties with surface monitoring. For example, considering the results from one-way coupling, we would recommend to study an area of 6x6 km^2, but considering the iterative coupling, it would be an area of 9x9 km^2 (P90 results at one year of injection).
Consequently, Shannon entropy results, which are calculated according to the tool accuracy will lead to some differences in monitoring design recommendations (Figure 49). **A larger extent for the monitoring area will be recommended if simulations are performed using the iterative method**. On the other hand, one can also consider that the monitoring recommendations resulting from a numerical study using one-way coupling are the minimum and primary ones.

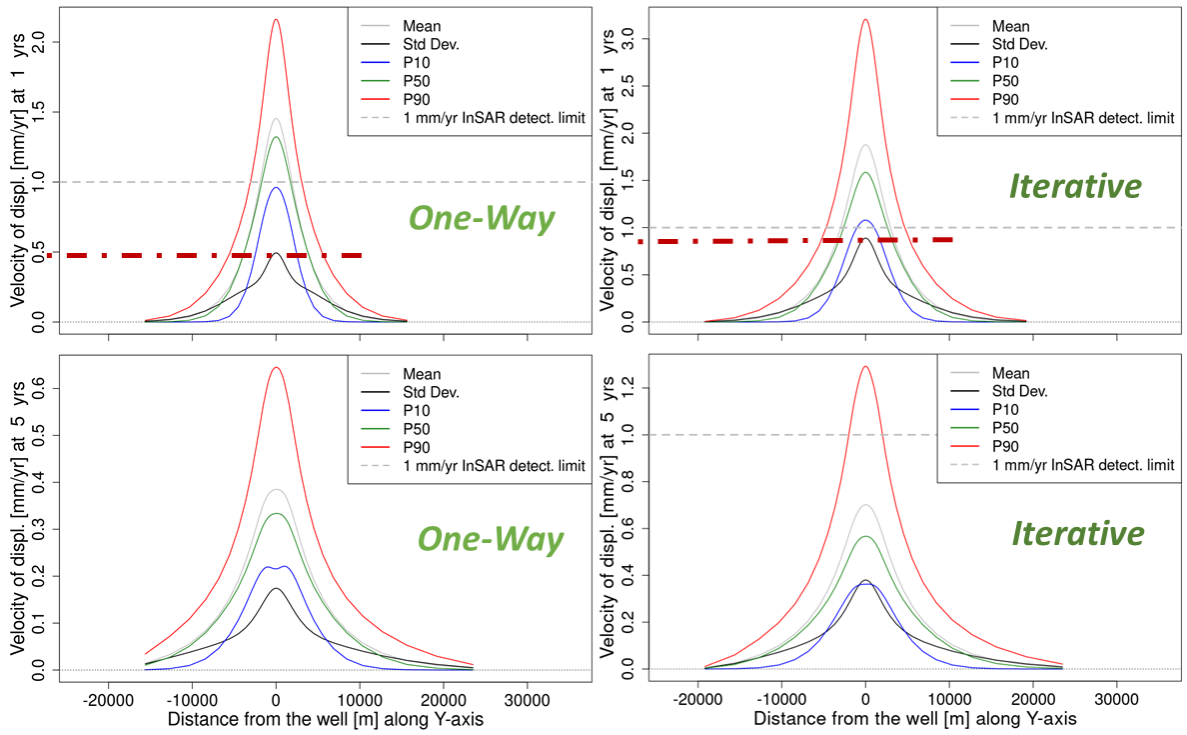

Figure 48 : Uncertainties on the surface displacement velocities (mean, standard deviation, median, quantiles 10% and 90%) related to the uncertainties on the subsurface properties after one year of injection (top), after five years of injection (bottom). Left, results from one-way coupling; right, results from iterative coupling. Statistical calculations performed from a Monte-Carlo sampling on metamodels built from the training sample. The detection threshold of the measurement is estimated at 1 mm/year.

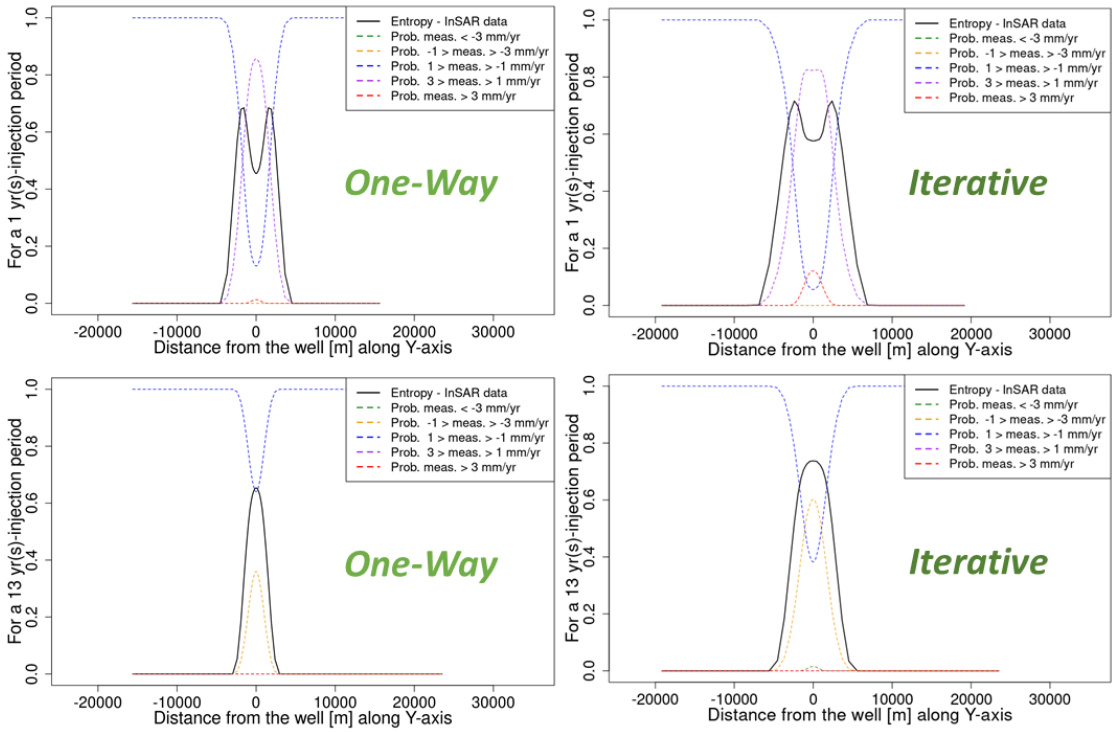

Figure 49 : Shannon entropy for five categories of InSAR surface displacement velocity measurements after one year of injection (top) and three years of post-injection (bottom). The measurement error is estimated at +/- 1mm/year. Shannon entropy is calculated based on one-way results (left) or iterative-coupling results (right).

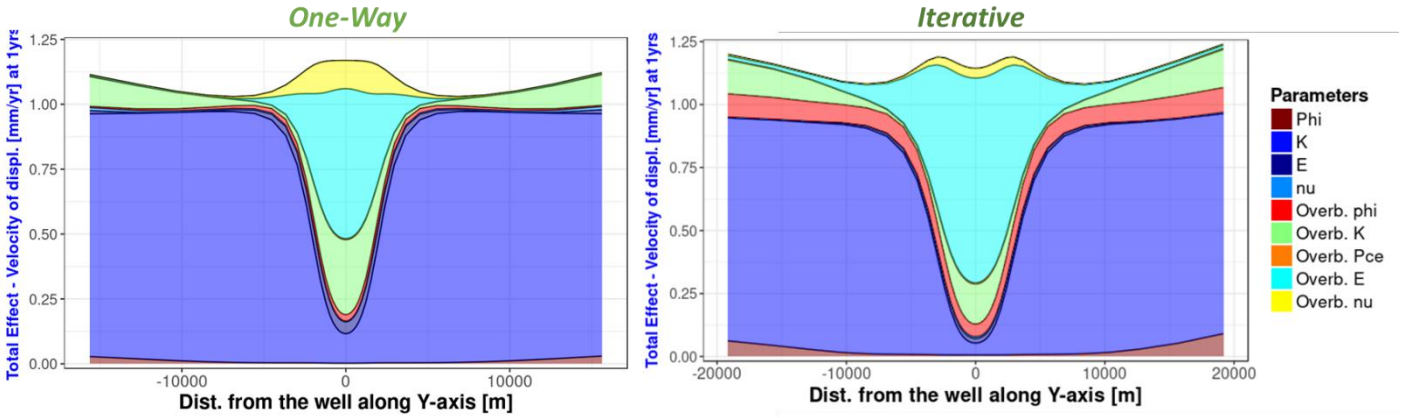

Figure 50 : Total Sobol Indices calculated between uncertain parameters and surface displacements velocities variations after one year of injection based on one-way simulations (left) and iterative-coupling simulations (right).

From sensitivity results (Figure 50), same global conclusions can be drawn from both simulation methods. For the Carbonate case, surface results are mostly sensitive to permeability of the storage formation, and to Young modulus and permeability for the overburden in the injection area. Therefore, one-way coupling can be considered as sufficiently accurate for the sensitivity analysis.

4.1.2 Comparison between one-way and iterative coupling – Sandstone II scenario

Similarly to the Carbonate scenario, comparison between one-way and iterative coupling is performed for Sandstone II. The purpose is to verify that the differences between coupling models are of the same order of magnitude as previously, and to confirm our conclusions are not related to considered parameters values.

4.1.2.1 Flow simulation results

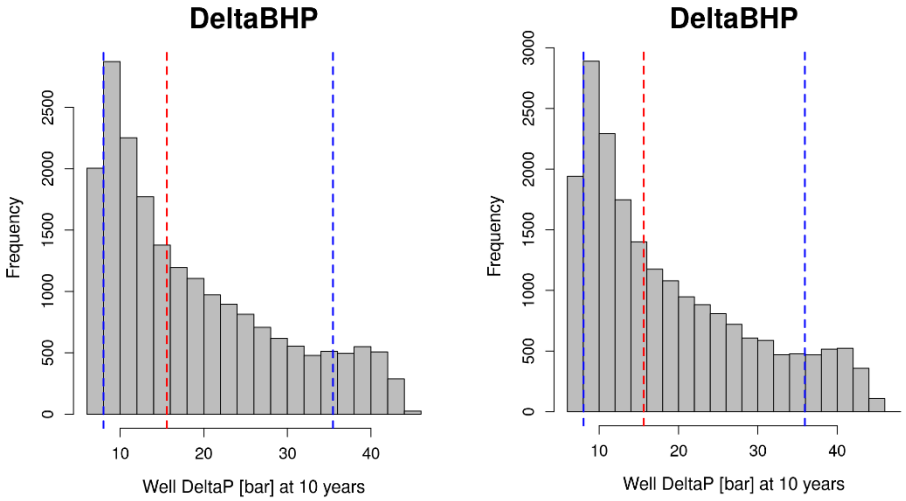

Figure 51 : Distribution of well bottom-hole pressure variations for 10 years of injection from a Monte-Carlo sampling of metamodels predictions. Left, results based on one-way coupling simulations. Right, results based on iterative coupling simulations.

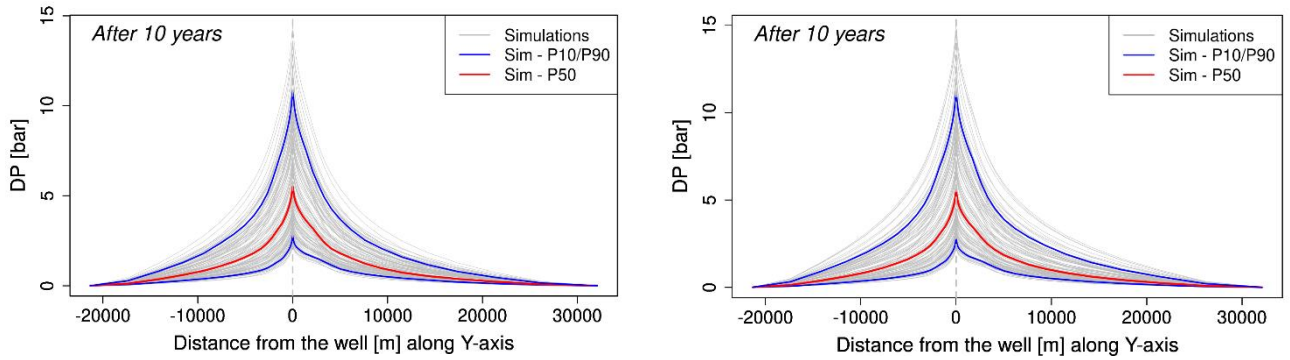

Figure 52 : Pressure perturbations (increase in pressure relatively to the initial conditions) after 10 years of injection for 115 simulations. Left, results from one-way coupling; right, results from iterative coupling.

For Sandstone II scenario, the maximum injection flow rate is reached for all cases, therefore the injection is pressure driven. The one-way and iterative coupling models yield similar distribution of the bottom-hole pressure (BHP) variations and the amplitude of pressure perturbations in the injection area as shown in Figure 51 and Figure 52.

On the other hand, predictions of CO_2 plume extent or pressure propagation are different for both coupling models (Figure 53 and Figure 54). As for the Carbonate scenario, one-way results **underestimate** the extent of CO_2 plume and pressure propagation by the order of several hundreds of meters for CO_2 plume, and several kilometers for pressure perturbation (increase of 1 bar).

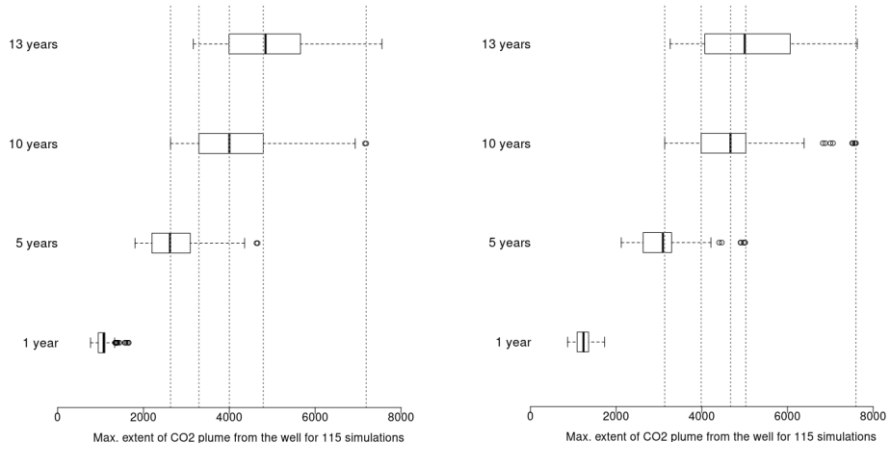

Figure 53 : Box plots (describe results distribution with the median (bold line), percentiles 25 and 75 % (box) and dispersion (segments)) of the maximum extent of CO_2 plume for 115 simulations for several injection periods (1 year, 5 years, 10 years) or post-injection (13 years)). Left, results from one-way simulations; right, results from iterative-coupling simulations.

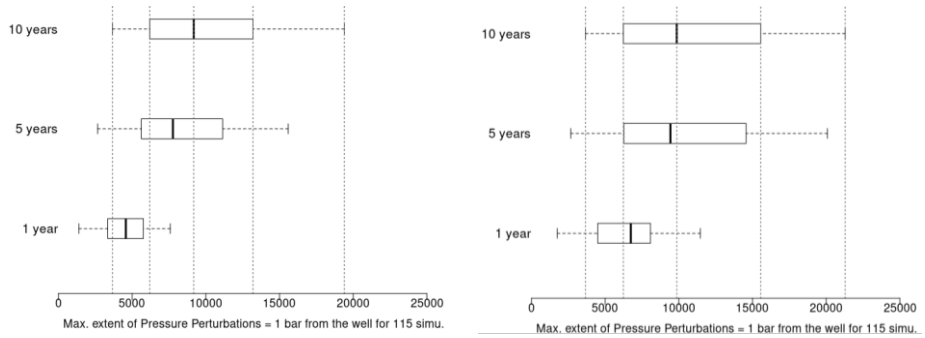

Figure 54 : Box plots (describe results perturbations distribution with the median (bold line), percentiles 25 and 75 % (box) and dispersion (segments)) of the maximum extent of a pressure increase of 1 bar for 115 simulations for several injection periods (1 year, 5 years, 10 years)). Left, results from one-way simulations; right, results from iterative-coupling simulations.

4.1.2.2 Surface displacements results

As previously, the results from one-way simulation **underestimate** the surface displacements compared to iterative-coupling results (Figure 55). For example, the difference in cumulative displacements in the injection area can reach 12 mm after one year or 7 mm after ten years of injection for the 90th percentile. But this difference is more important than the one obtained for the Carbonate scenario.

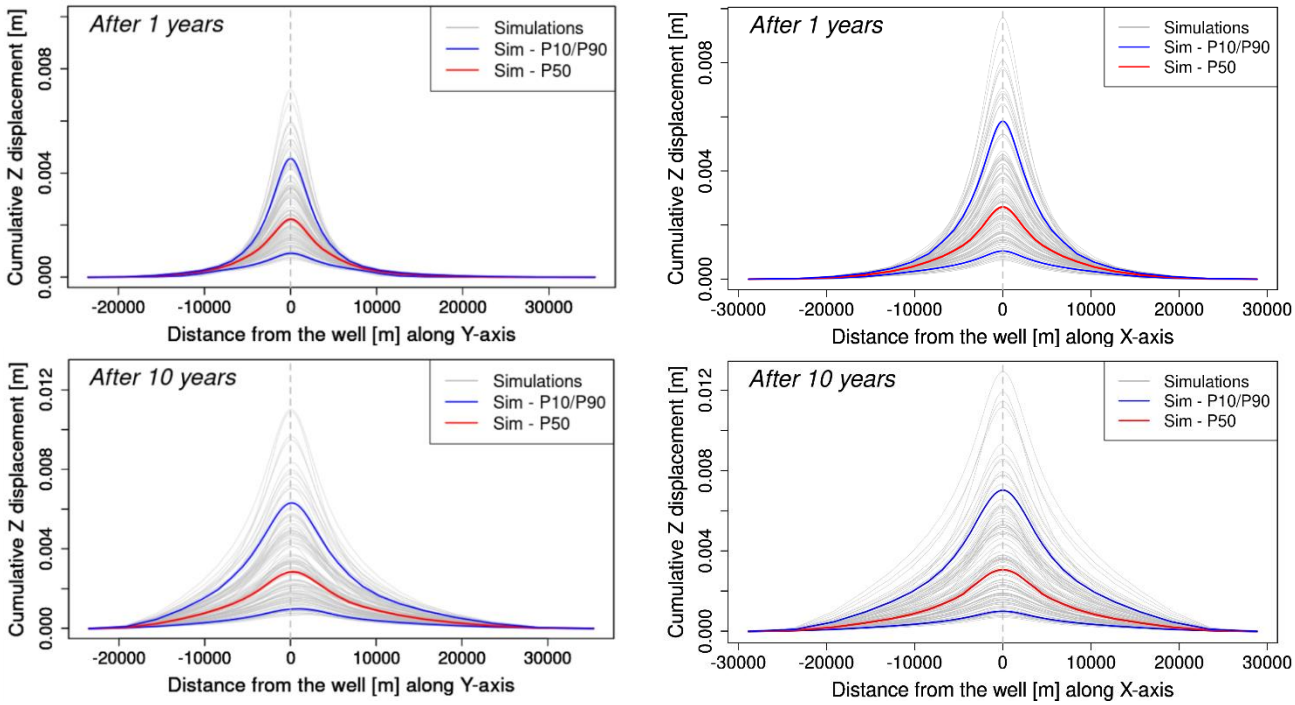

Figure 55 : Cumulative surface displacements function of the distance from the well along the Y-axis (i.e. along the anticline) after one year of injection (top) and after ten years of injection (bottom). In red, the median, in blue P10 and P90 percentiles of the 115 simulations (in grey). Left, results from one-way simulations; right, results from iterative-coupling simulations.

A higher proportion of surface displacements is detectable with InSAR technology from iterative coupling model (Figure 56 and Figure 57). However, for both one-way and iterative models, only results from short-term periods

are above InSAR detection limits. Here, after five years injection, displacements are inferior to the detection limit in both cases (Figure 57).

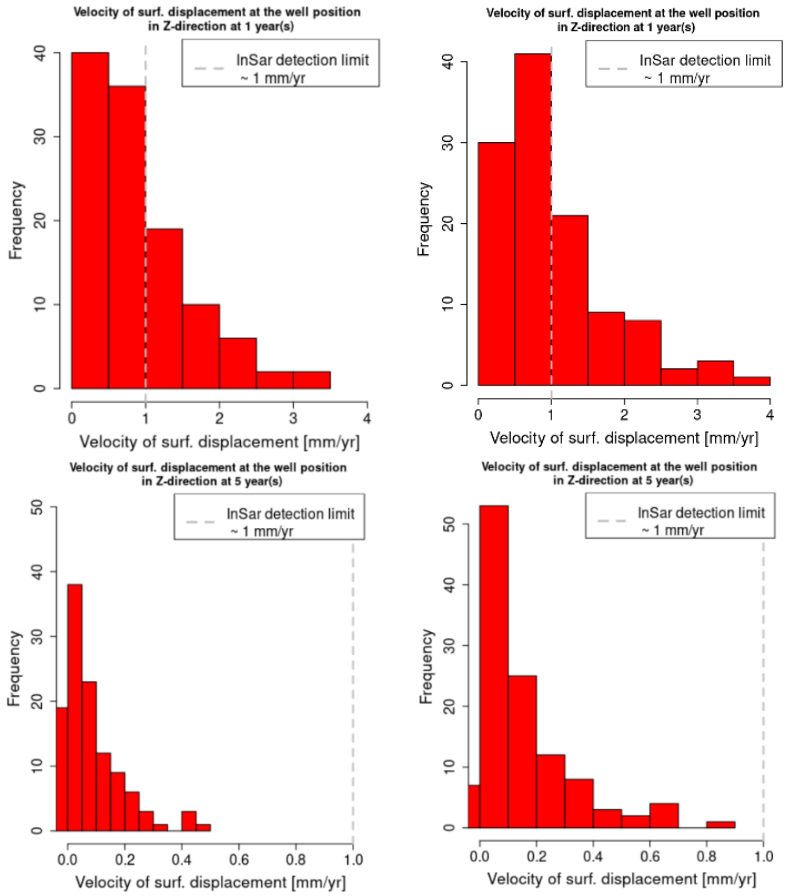

Figure 56 : Distribution of surface displacement velocities above the well after one year of injection (top) and after five years of injection (bottom) with one-way simulations results (left) and iterative-coupling results (right).

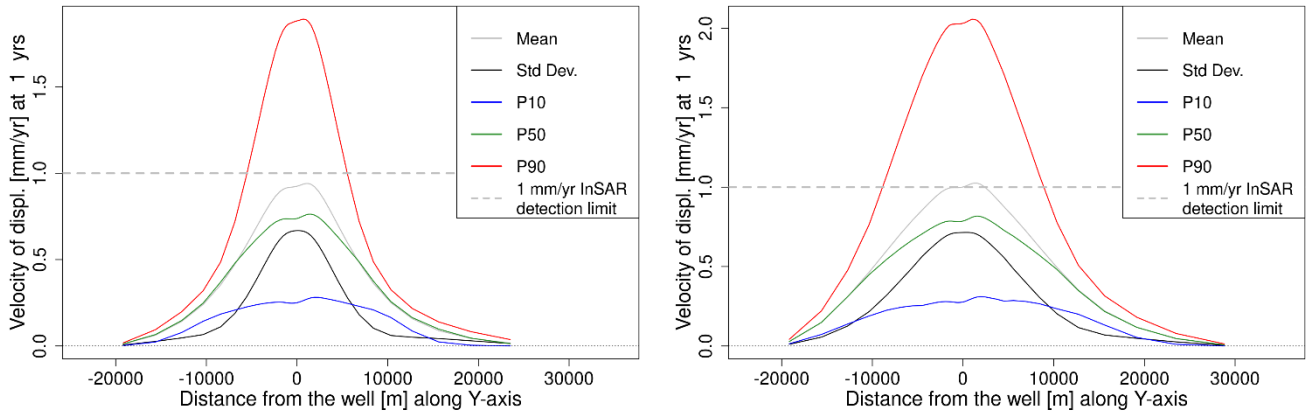

Figure 57 : Uncertainties on the surface displacement velocities (mean, standard deviation, median, quantiles 10% and 90%) related to the uncertainties on the subsurface properties after one year of injection. Left, results from one-way coupling; right, results from iterative coupling. Statistical calculations performed from a Monte-Carlo sampling on metamodels built from the training sample. The detection threshold of the measurement is estimated at 1 mm/year.

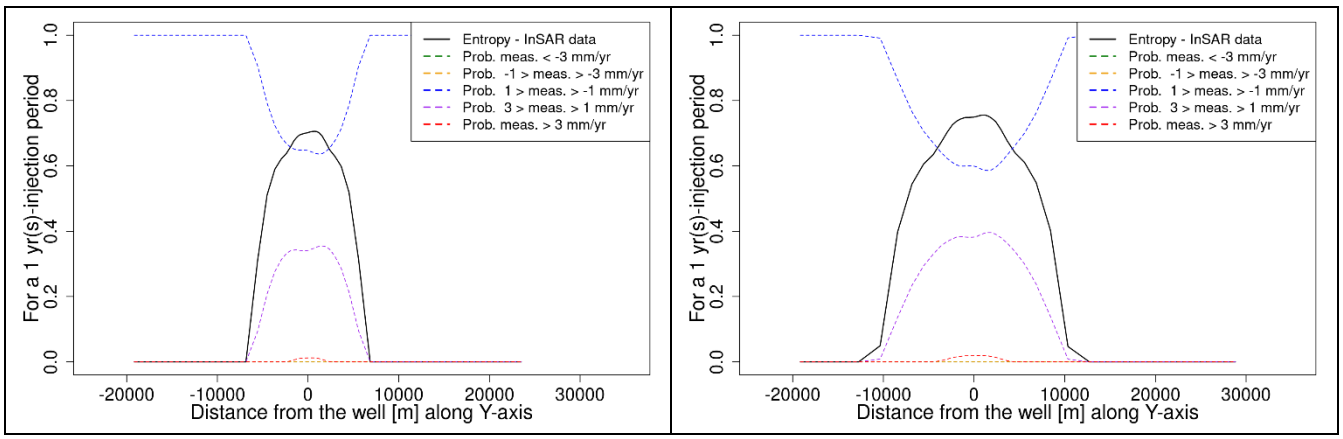

Figure 58 : Shannon entropy for five categories of InSAR surface displacement velocity measurements after one year of injection. The measurement error is estimated at +/- 1mm/year. Shannon entropy is calculated based on one-way results (left) or iterative-coupling results (right).

Again, with iterative results, surface displacements would be detectable on a larger area (Figure 57 and Figure 58). For example, based on the one-way simulations, we would recommend the study area of 9 × 9 km^2 , but if based on the iterative coupling, it is 18 × 18 km^2 (P90 results at one year of injection). Here, the difference in monitoring area recommendation will be a four-fold increase (relatively to a two-fold increase in the Carbonate scenario).

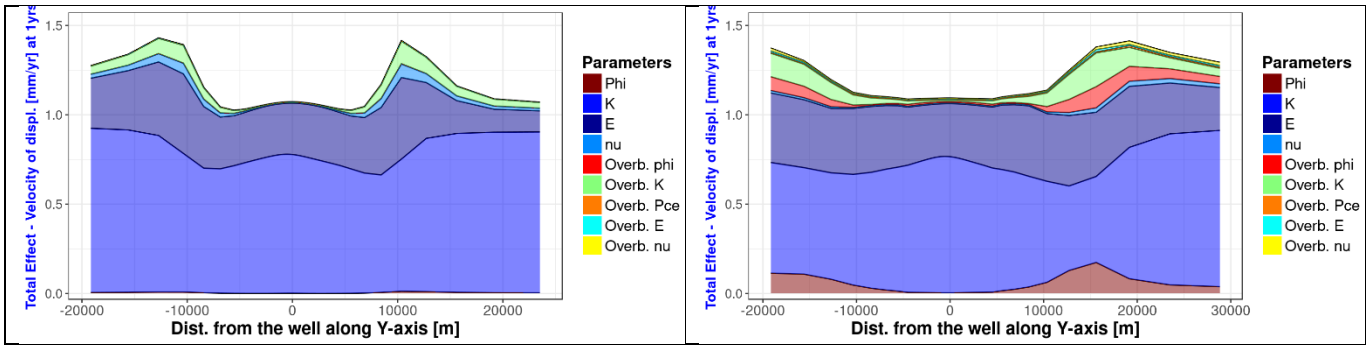

Figure 59 : Total Sobol Indices calculated between uncertain parameters and surface displacements velocities variations after one year of injection based on one-way simulations (left) and iterative-coupling simulations (right).

In Figure 59, the surface results are mostly sensitive to permeability and Young modulus values from the storage formation. The effects are similar for one-way and iterative models.

4.2 Numerical comparison

All the simulations were performed on a IFPEN's super calculator with processors Intel Skylake G-6140 clocked at 2.3 GHz equipped of 96Go RAM. The computing power of solution estimated by a standard benchmark HPL Linpack is of 445 Tflops.

For the code_Aster execution, 32 processors were required and 16 for Puma. In Figure 60, the computational time distributions of 115 simulations for each scenario/coupling model is shown. The corresponding mean values are given in Table 4.

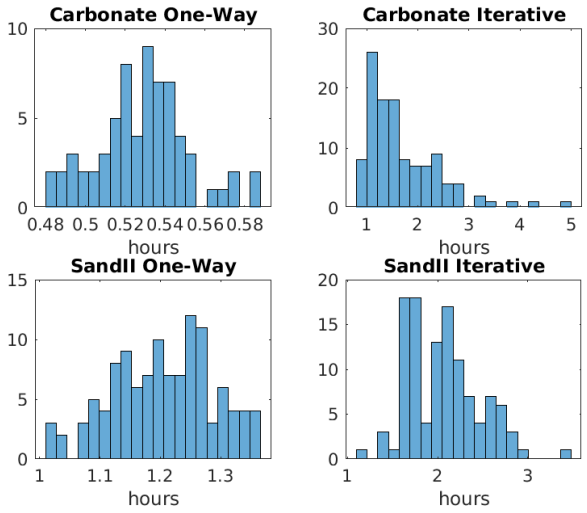

Figure 60 : Computational time statistics for each scenario/coupling model.

	One-way	Iterative
Carbonate	32 min	1h43
Sandstone II	1h12	2h

Table 4 : Mean computational time for each scenario/coupling model over 115 simulations.

Obviously, for iterative model, the computational time can vary according to the convergence criterion between both codes. Even if for the one-way model 12 periods were simulated while for the iterative model only 7 periods were calculated, the computational time from iterative coupling will often be at least twice the time from the one-way. It can even be multiplied in average by three for the carbonate case.

Iterative coupling is more accurate than one-way coupling, but it implies a higher computational cost. A statistical or sensitivity analysis might not always be performed with iterative coupling simulations due to its cost.

5 Surface displacements analysis for anticline cases with faults

The heterogeneities and more specifically a fault network have a strong impact on flows. The goal of this section is to evaluate their impacts considering different realistic hypothesis.

5.1 Geological structures and property values

Synthetic cases including faults and throws are considered in this study. They are built from the conceptual model shown in Figure 61. Three faults are explicitly modeled; two deterministic faults (DF) associated to a throw and a sub-seismic fault (SSF) without throw. For each scenario previously defined (Carbonate, Sandstone I and Sandstone II), we add two characteristics related to the faults with an “open faults” and “sealing faults” cases. “Open faults” means that fluids may flow through the faults versus a “sealing faults” for which no-flow occurs through faults. To summarize, the following cases are considered:

- Homogeneous reservoirs without faults and throws. This case will be used as a comparison case.
- Open faults behavior when throws are associated to the deterministic faults and explicitly modeled. The CO_2 may flow through the faults.
- Sealing faults behavior when throws are associated to the deterministic faults and explicitly modeled. The CO_2 does not flow through the faults but may flow along the fault planes.

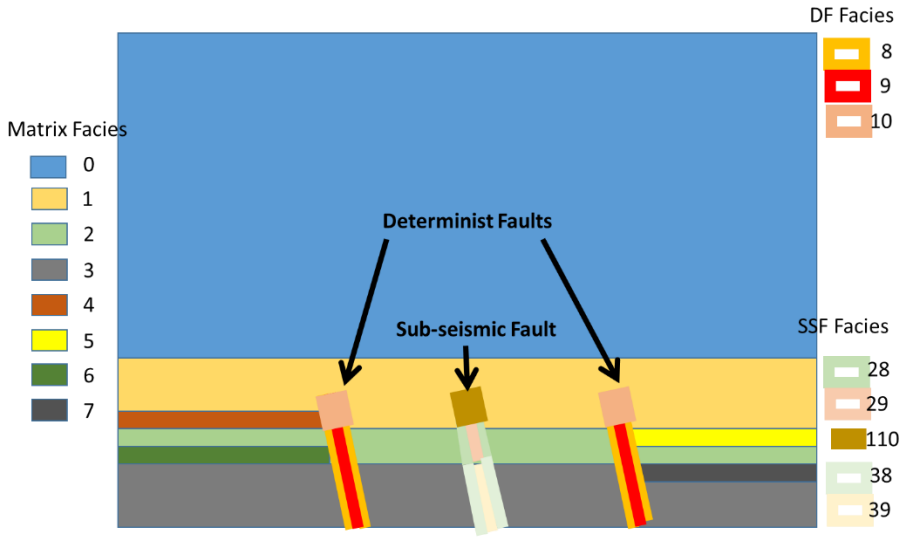

Figure 61 : Conceptual model of faulted scenarios. Facies are defined to quickly build different realistic configurations thanks to an adapted choice of properties values. Facies 4 to 7 are used to model the throws or not. Facies 9, 29 and 39 are used to define a fault core and are useful to model open faults or sealing faults. Facies 8, 28 and 38 are used to model a fracture corridor associated to the faults.

In addition, facies heterogeneities may be added to the fault models. Two facies are defined in both the storage formation and in the overburden. A truncated-gaussian approach is used to model their distributions. The result of this modeling is illustrated Figure 62.

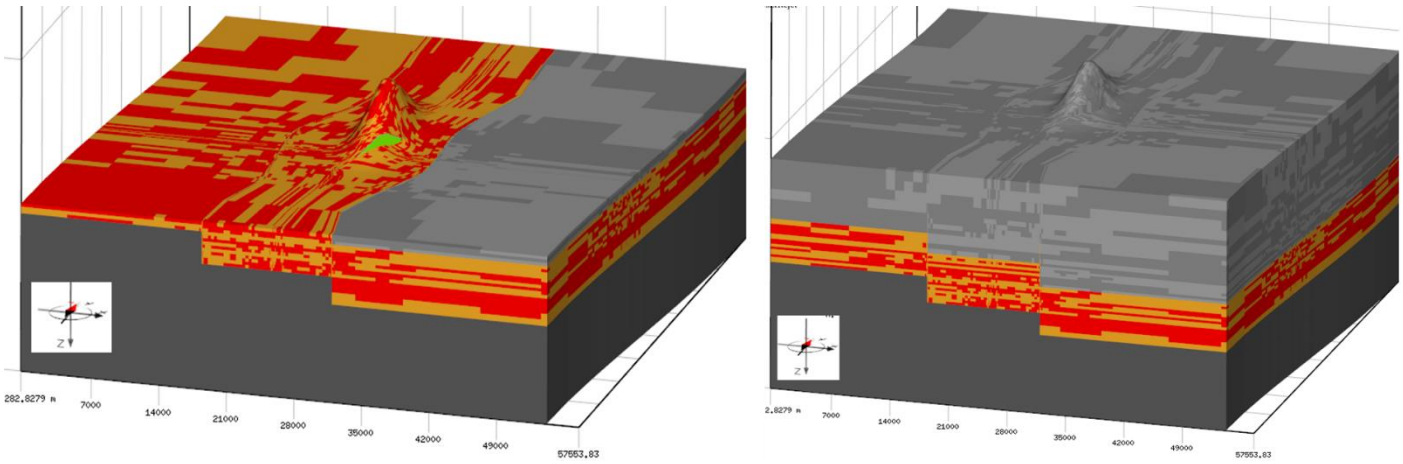

Figure 62 : result of a heterogenous modeling for reservoir and overburden

To define the properties of the facies of the storage formation and overburden, we use the median values from the uncertain interval defined previously.

More detailed description of conceptual models and petrophysical and geomechanical data are contained in the deliverable D2.1 of the SENSE project (Bouquet et al, 2021b).

Finally, for each scenario (Carbonate, Sandstone I and Sandstone II), it is now possible to study different realistic geological structures. A sensitivity study to the following heterogeneity cases is performed and presented in the rest of the report:

- sealing fault for the homogeneous case,
- sealing fault for the heterogeneous case,
- open fault for the homogeneous case,
- open fault for the heterogeneous case,
- homogeneous case without fault and without throw.

5.2 Results

All the simulations were carried out using an iterative coupling.

5.2.1 Injection design and storage capacity

The injection design described in section 2 is used here (Figure 63). Let us remind that only Sandstone II injection is driven by a constant injection flow rate with a maximum bottom hole pressure reached, while Carbonate and Sandstone I injection is driven by a bottom hole pressure.
Heterogeneous storage formation has a better quality in terms of permeability and porosity, that is why

- for a flow rate control, the bottom hole pressure of heterogeneous cases is lower than the bottom hole pressure of the homogeneous ones,
- for a pressure control, the flow rates of heterogeneous cases are higher than for homogeneous ones.

The same remarks can be applied to the open faults and sealing fault cases knowing that the sealing faults drastically decrease the injectivity which is due to the compartmentalization induced by the sealing faults.

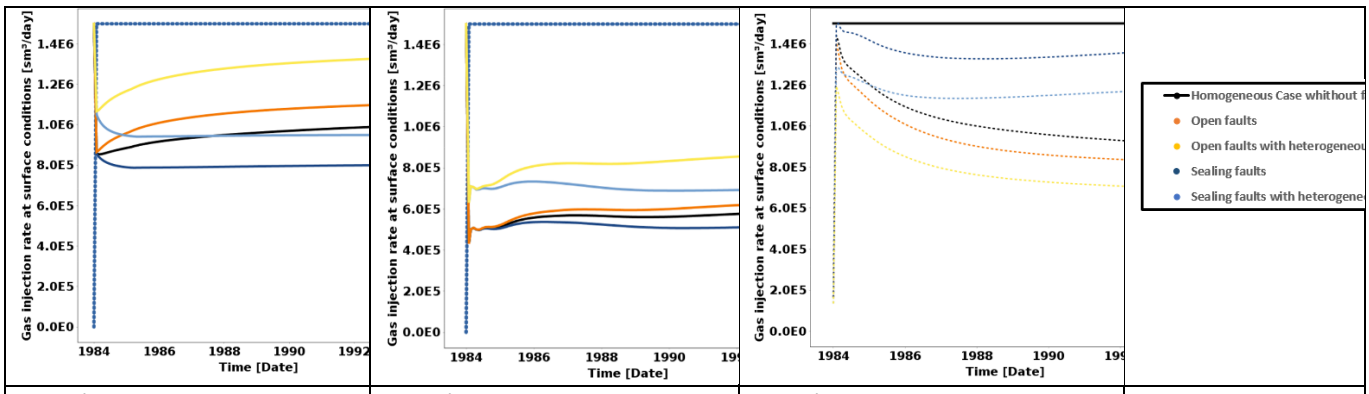

a) Carbonate | b) Sandstone I | c) Sandstone II

Figure 63 : injection pressure (doted lines) and injection rates (continuous lines) for the different scenarios

From a CO_2 volume storage point of view (Table 5), the storage capacity is obviously related to this injectivity. The storage capacity is reduced with the compartmentalization related to the sealing faults. In contrast, heterogeneities (such as defined here with an increase in flow properties) or open faults improve the storage capacity.

Scenario	Homogeneous without fault/throw	Open fault	Open fault (heterogeneous)	Sealing fault	Sealing fault (heterogeneous)
Carbonate	3.47	3.83	4.64	2.91	3.47
Sandstone I	2.04	2.16	2.99	1.88	2.56
Sandstone II	5.47	5.47	5.47	5.47	5.47

Table 5 : Cumulative injected gas at surface conditions [km^3]

5.2.2 Carbonate scenario

A circular shape of the pressure field is observed for the homogeneous case without fault and throw (Figure 64a). On contrary, for the heterogeneous case with sealing faults (Figure 64b), the pressure field is confined by the two deterministic faults. The impact of the sub-seismic fault is also visible by comparing to the homogeneous case without fault/throw, firstly, by an increase in pressure values between this fault and the well location (red circle on Figure 64b) and, secondly, by a decrease in pressure on the right of this sub-seismic fault (light red circle on Figure 64b).

The heterogeneous case with open fault (Figure 64c) is very similar to the homogeneous case but a pressure contrast is observed at the deterministic fault location (located at the right of the reservoir) . This flow barrier behavior is not related to the fault properties but is due to the throw. At this depth, the storage formation (left part of Figure 64c) is in contact with the overburden (right part of Figure 64c) as it was shown in Figure 62.

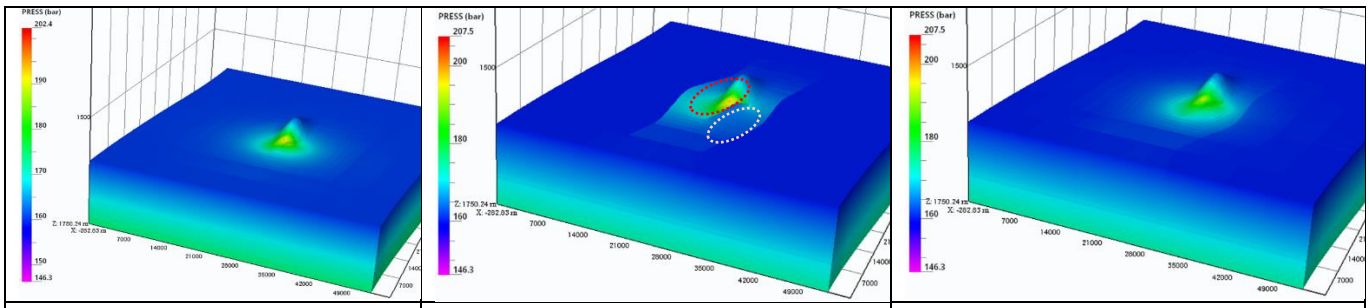

Figure 64 : Pressure field after 10 years of CO_2 injection (carbonate scenario) for homogeneous case without faults (a), heterogeneous case with sealing faults (b) and heterogeneous case with open faults (c).

These different pressure variations have an impact on surface displacements (Figure 65). Considering the same fault behavior (open or sealing), the heterogeneities don't have a huge effect on displacement. Then, if the faults are not a flow barrier (orange and yellow curves, Figure 65), a similar behavior against the homogeneous case without fault/throw (black curve, Figure 65) is observed. Finally, huge impacts are observed when the faults behave as flow barriers (light and dark blue curves, Figure 65). The location of the two deterministic faults may be identified on the curve (around 10 km and 40 km). Between these two faults, a displacement is observed and out of this place no displacement is observed. The shape of the curve changes and are no-more gaussian while the center of the area with a maximum of surface displacements is no-more located on the top of the well. This slight deviation is due to the effect of the sub seismic fault. Since this fault is a flow barrier, CO_2 volume is stopped by the fault and moves away to the fault location. Then the area with a maximum of displacements is no more centered at the top of the well. In this Carbonate scenario, the sealing faults have a strong impact with an increase in pressure between the well and the fault (thus an increase in surface displacement) and without a pressure variation in the other side of the faults (thus a weaker displacement).

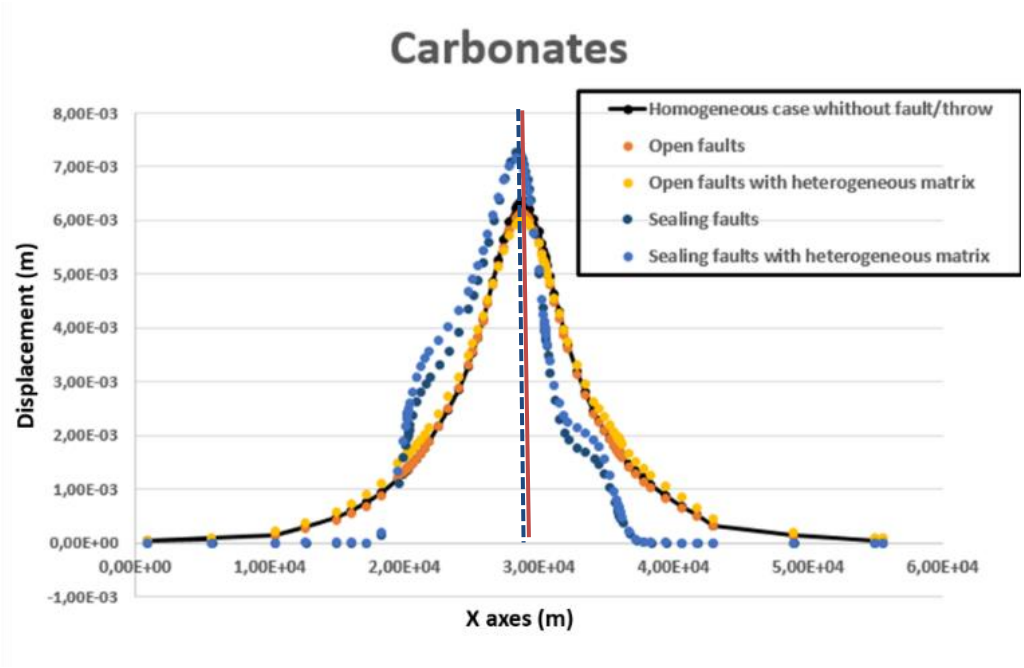

Figure 65 : Cumulative surface displacement along a line crossing the well location and along the X-axis, Carbonate scenario, after 13 years

5.2.3 Sandstone I scenario

Since the reservoir permeability and porosity of Sandstone I scenario are lower than those of the Carbonate scenario, then the corresponding pressure variations are located closer to the injection well. After 10 years of CO_2 injection, Pressure variations seem to not reach the deterministic faults for the three studied scenarios (Figure 66).

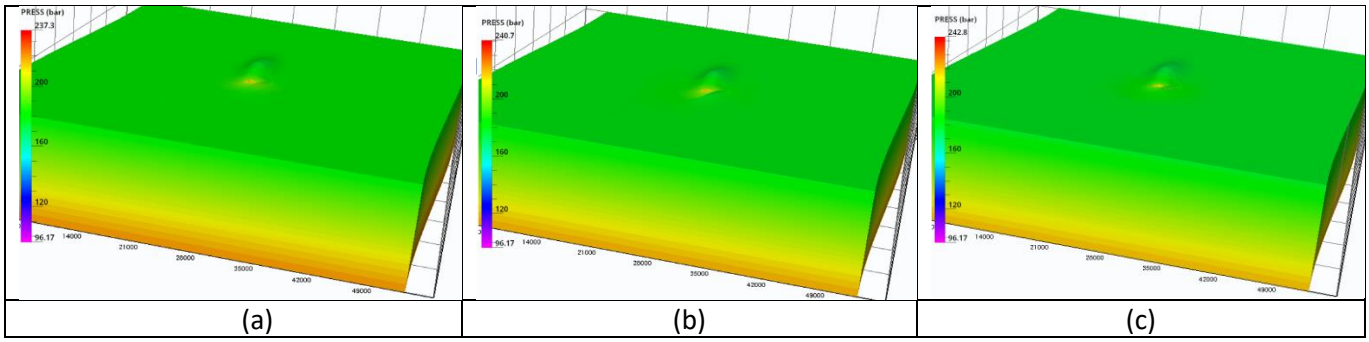

Figure 66: Pressure field after 10 years of CO_2 injection (Sandstone I scenario) for homogeneous case without faults (a), heterogeneous case with sealing faults (b) and heterogeneous case with open faults (c).

The surface displacements curves for all studied cases have a gaussian shape (Figure 67). Only the sub-seismic fault impacts the displacements that may be observed from the surface. Indeed, considering sealing faults, the location of the maximum of displacement is no-more located at the top of the well due to the sealing sub-seismic fault. If the faults are open the displacements have the same behavior than a homogeneous reservoir without faults and throws.

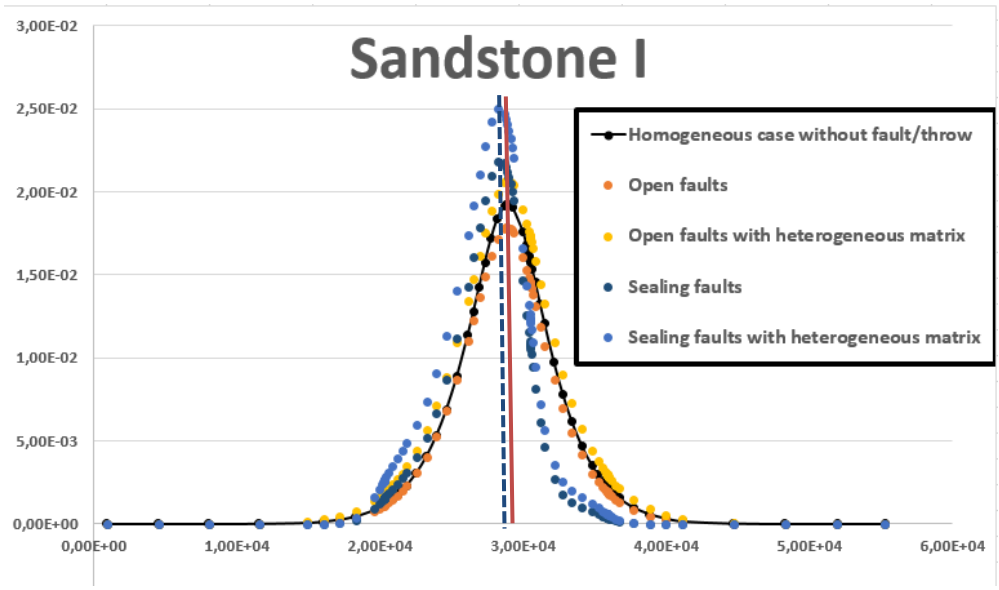

Figure 67 : Cumulative surface displacement along a line crossing the well location and along the X-axis, Sandstone I scenario, after 13 years

5.2.4 Sandstone II scenario

The Sandstone II scenario is now studied. Since the reservoir permeability and porosity are greater than those of the Sandstone I scenario, the pressure variations are no-more located near well but, in this case, they reach the limits of the reservoir. The boundary conditions have a strong influence here and are chosen as constant pressure.

As for the Carbonate case, the sealing faults aim to confine the pressure and the CO_2 between the two deterministic faults. (Figure 68b). For the open fault case, the flow barrier due to the throw is visible (Figure 68c).

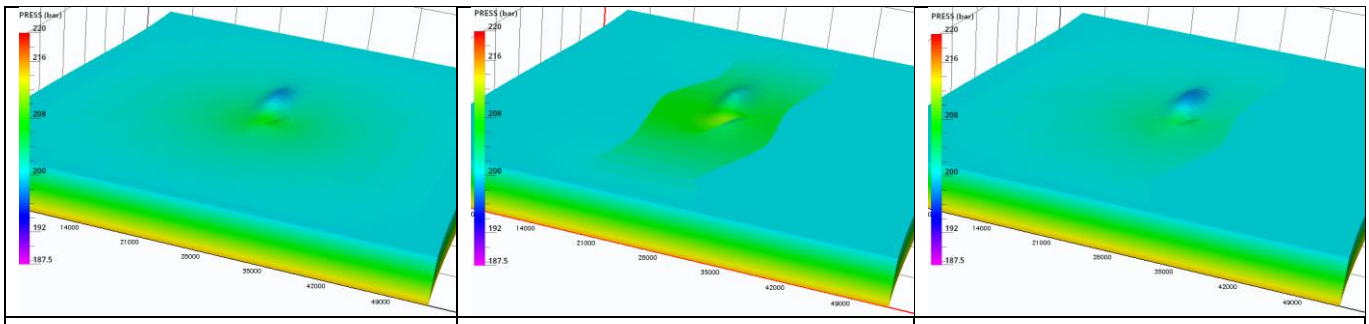

(a)	(b)	(c)

Figure 68 : Pressure field after 10 years of CO_2 injection (Sandstone II scenario) for homogeneous case without faults (a), heterogeneous case with sealing faults (b) and heterogeneous case with open faults (c).

Considering the displacements results, the same comments may be formulated as for the Carbonate scenario. Nevertheless, the impact of sealing deterministic faults is strongly visible (Figure 69). This is due to the reservoir permeability which allow a good pressure diffusion and that is strongly constrained for sealing fault case and not for the open fault case nor for the no fault/no throw case.

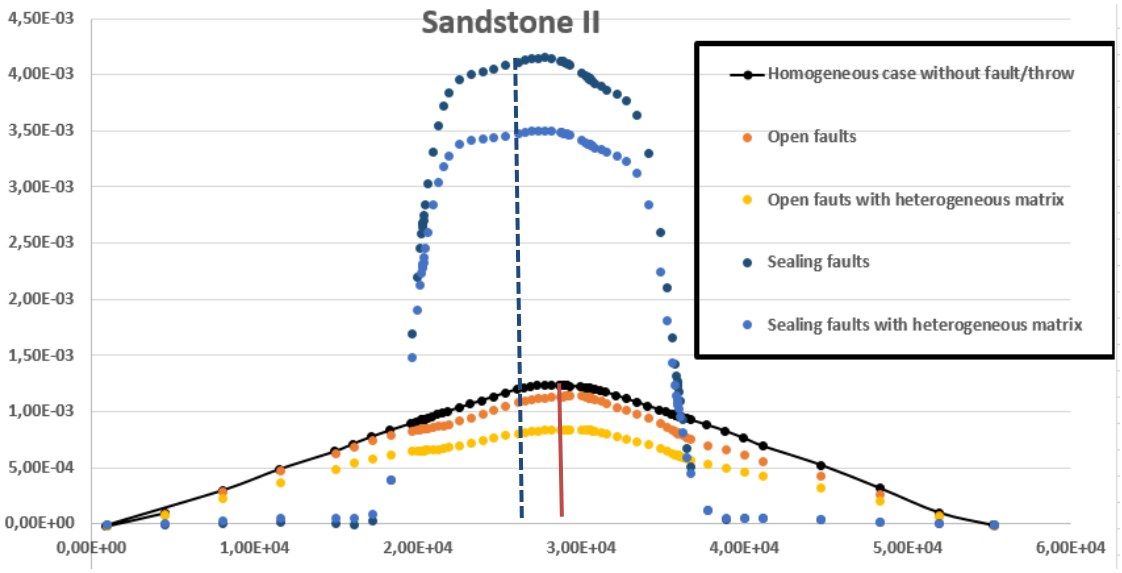

Figure 69 : Cumulative surface displacement along a line crossing the well location and along the X-axis, Sandstone II scenario, after 13 years

5.2.5 Conclusions

To conclude, the sealing faults have a major impact on CO_2 injection. **In order to detect their presence, it is possible to study the shape of the displacements and mostly the location of the center of a maximum of the displacement area that has to be compared to the well location**. In our case, the heterogeneities and the open faults have not a strong impact on the displacements. From a velocity point of view, the sealing cases obviously increase the velocity of the displacements without changing drastically the order of magnitude (Figure 70). The sealing faults presence will help to better observe the displacements from the surface. Nevertheless, as the detectability threshold is 1 mm/year for INSAR, it will be difficult to observe a non-gaussian shape of the curves due to the sealing faults for similar cases.

Scenario	1 year	5 years
a	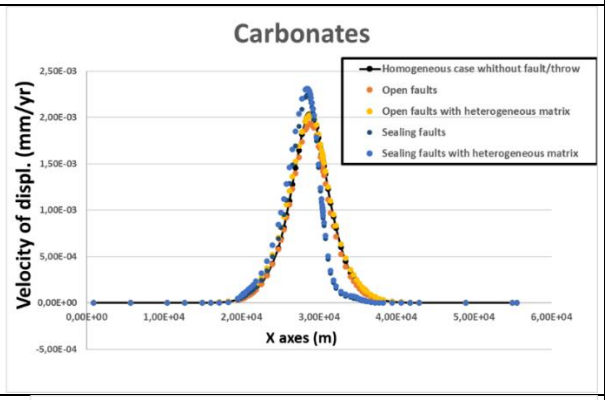	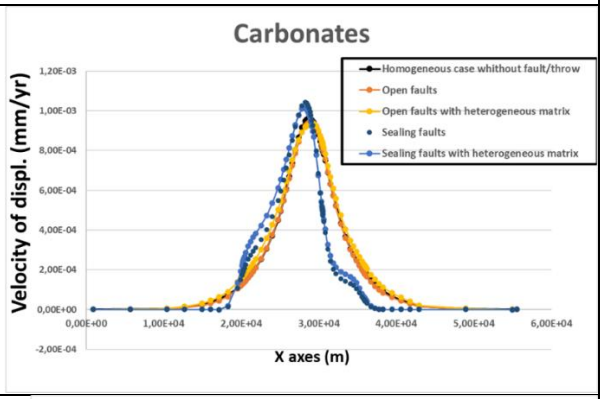
b	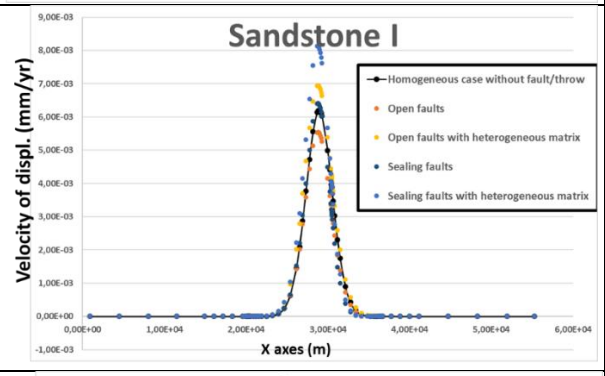	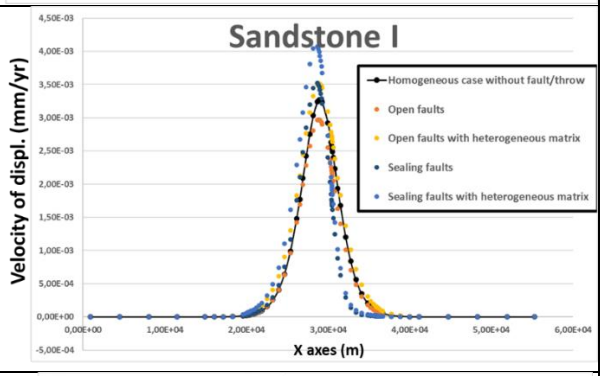
c	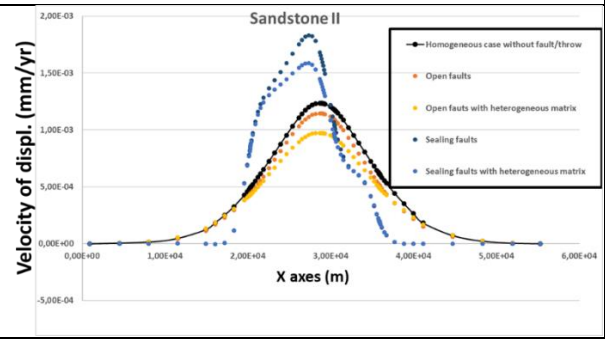	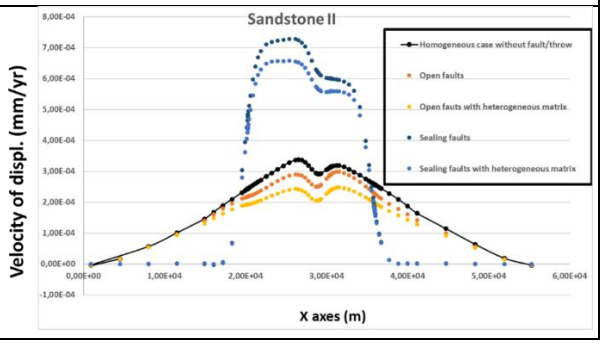

Figure 70 : Velocity of the displacements – Scenario (a) Carbonate, (b) Sandstone I, (c) Sandstone II

5.3 Integrity analysis

Based on the methodology described in section 2.3, caprock and faults integrities has been studied for four stress regimes. For considered porosities, obtained frictions and cohesions for Carbonate, Sandstone I and sandstone II case are given in Table 6.

	Faults		**Caprock (heterogeneous)**				**Caprock (homogeneous)**	
	cohesion (MPa)	***Friction (°)***	***cohesion (Facies 1)***	***friction (Facies 1)***	***cohesion (Facies 2)***	***friction (Facies 2)***	***cohesion***	***Friction***
Carbonate	6.09	17.75	8.91	26.84	11.97	28.63	8.91	26.84
Sandstone I	1.62	20.78	4.89	21	6.67	21	4.89	21
Sandstone II	1.62	20.78	4.89	21	6.67	21	4.89	21

Table 6 : Faults and caprock plastic parameters values

5.3.1 Carbonates scenario

Integrity analysis for Carbonate case is summarized in Table 7. For considered material parameters, initial stress regimes and injection conditions, all tested scenarios remain in the elastic domain (below inner Drucker-Prager criterion) and so no risks are identified for caprock or faults integrities.

	Sealing faults				Open faults			
	Heterogeneous		Homogeneous		Heterogeneous		Homogeneous	
	Caprock	*Faults*	*Caprock*	*Faults*	*Caprock*	*Faults*	*Caprock*	*Faults*
Compressive								
Extensive								
StrikeSlip 1								
StrikeSlip 2								

Table 7 : Integrity analysis results for Carbonate case. Green: all stresses are below inner Drucker-Prager criterion.

On Figure 71, stress distributions with a heterogeneous caprock and sealing faults are presented before injection (present-day) and after 1 and 10 years of injection. A double inner/outer Drucker-Prager criteria (DP) is represented corresponding to the two considered materials in the caprock. The initial stress distribution is more dispersed than for anticline scenarios (without faults). This sparser distribution is due to faults, represented by solid elements with weaker elastic properties (Bouquet et al. 2021) and heterogeneities in caprock and reservoir formations. The stress evolution during injection is less visible and covered by the initial distribution, however, it can be noted that stresses at 10 years of injection remain in the elastic domain and quite far from the most conservative inner DP even for the StrikeSlip 1 regime.

A comparison of stress results obtained with a heterogeneous and a homogeneous caprock is presented on Figure 72. For a homogeneous caprock, the initial stress distribution is less scattered but is still disturbed by the presence of faults. Obtained stress results for the anticline case Figure 37 show a much more regular initial state. Similarly to the heterogeneous case, the stress state during injection remains far away from the inner DP and injection impact is not clearly visible.

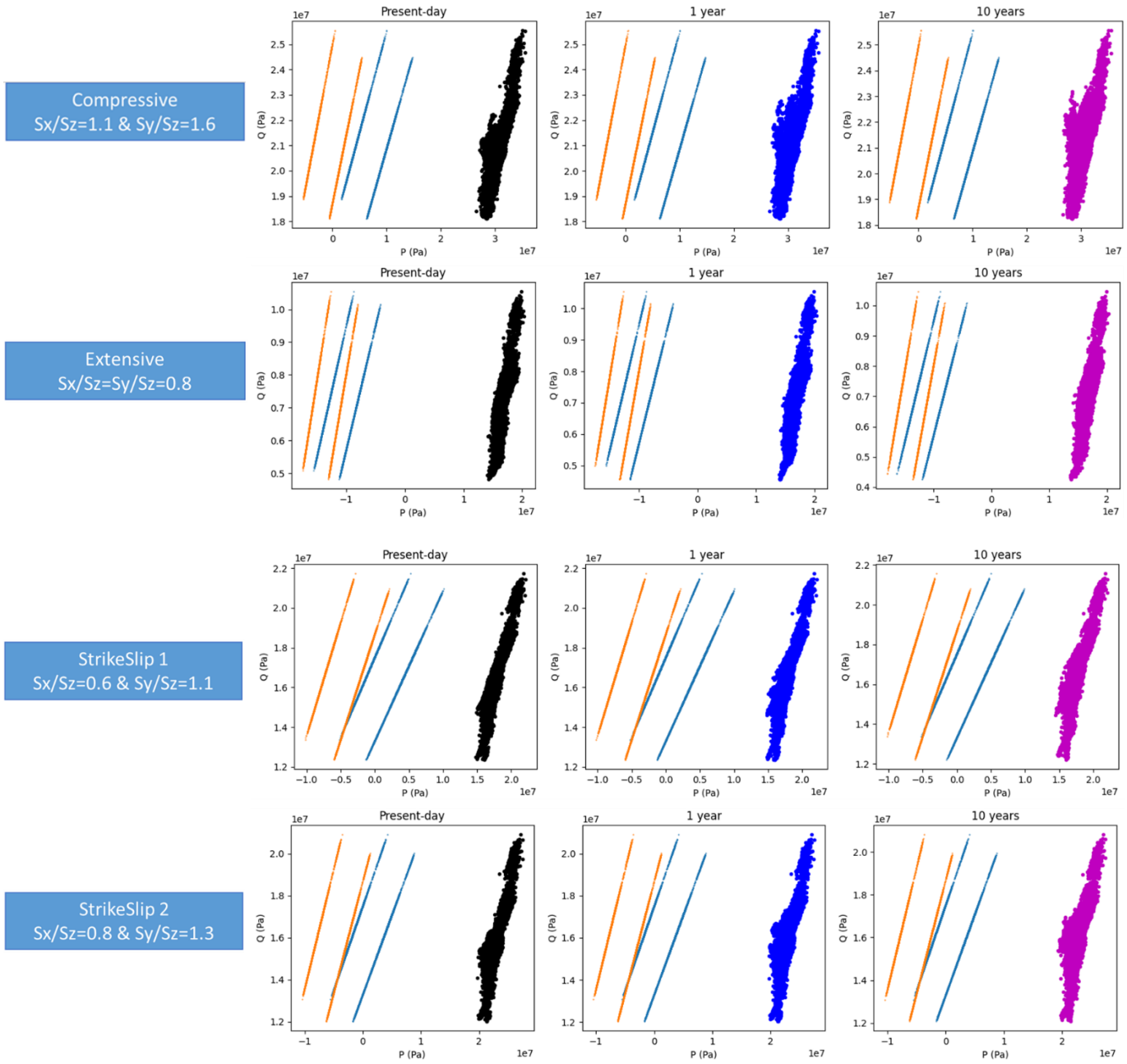

Figure 71 : Stress results in the caprock for the Carbonate scenario with a heterogeneous caprock and sealing faults. Results are presented before injection (present-day), after one year of injection and after ten years of injection for different stress regimes. The points represent a cell results and lines represent Drucker-Prager criteria (outer in orange, inner in blue) for the 2 materials of caprock.

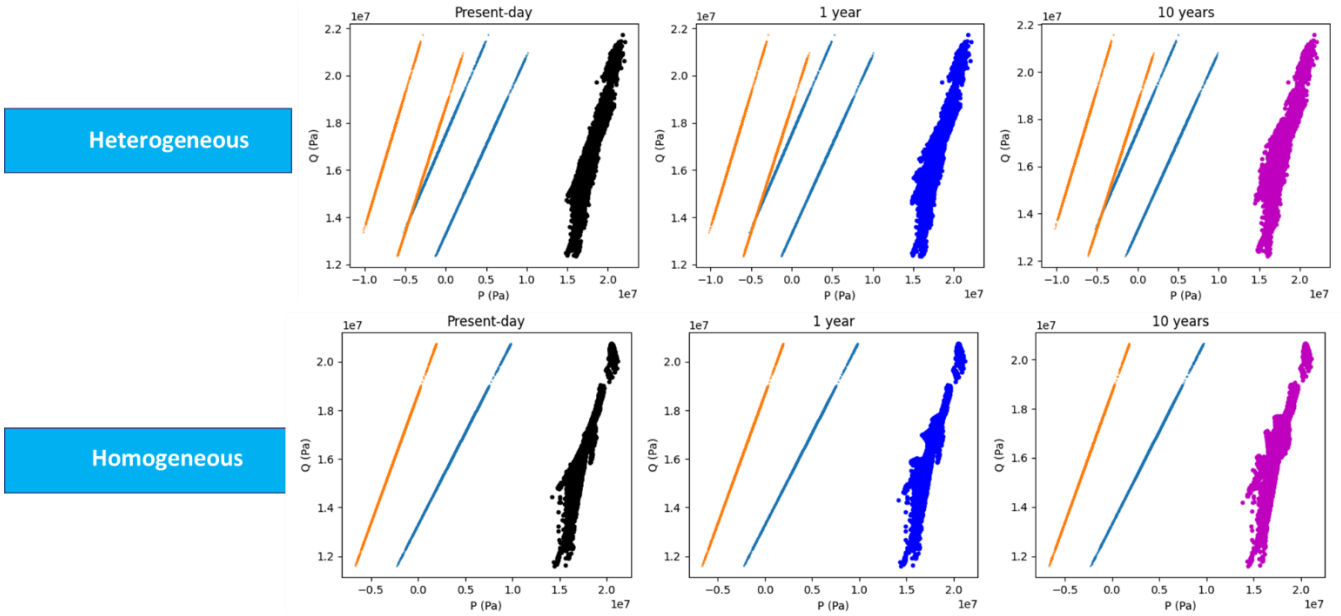

Figure 72 : Stress results in caprock for the Carbonate scenario with sealing-fault for StrikeSlip1 regime. The points represent a cell results and lines represent Drucker-Prager criteria (outer in orange, inner in blue).

Stresses distributions in faults zones are represented on Figure 73. The scatter includes both corridors and core zones of the three considered faults. The same observations than for caprock are made. The initial stress is highly distributed due to heterogeneities, all considered cases remain in the elastic domain, yet for the StrikeSlip 1 regime and after 10 years of injection, some cells are about to cross the inner DP.

In Figure 74, the stress evolutions during injection obtained with sealing and open faults are compared for the StrikeSlip 1 scenario. Two patterns are observed.

- Sealing-faults cases follow an irregular pattern with cells having a decrease in hydrostatic stress with a graduated increase of equivalent stress, getting closer to Drucker-Prager criteria, while other cells exhibit a decrease in equivalent stress with small changes in hydrostatic stress (moving away from the DP).
- Open faults cases show a more regular pattern with a graduated decrease of equivalent and hydrostatic stresses with almost all cells moving slowly closer to DP.

In term of magnitude, induced stresses variations are stronger for sealing faults than for open faults (for both, equivalent and hydrostatic, stresses). Consequently, if a longer injection is considered, instability will be reached sooner for sealing-fault than for open faults.

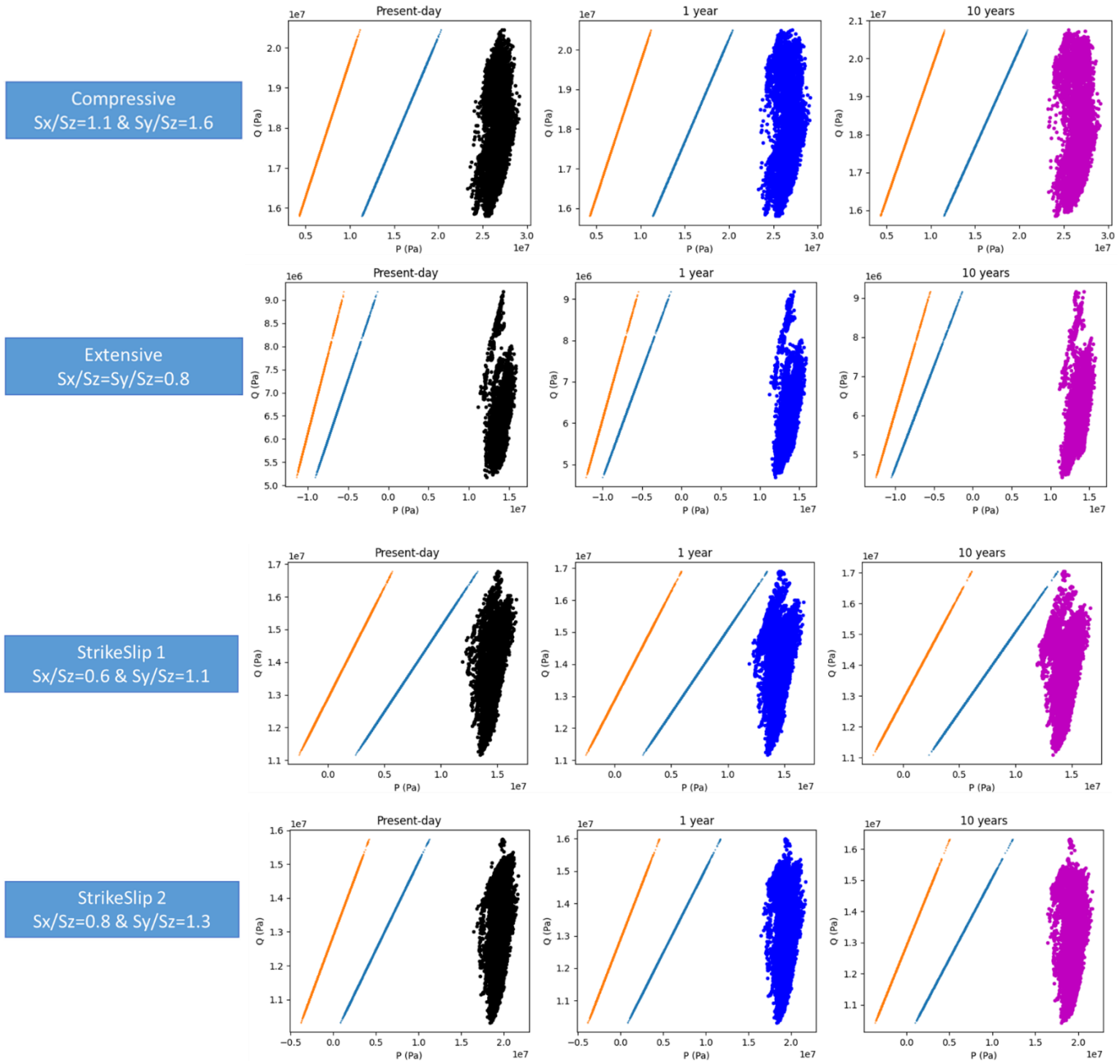

Figure 73 : Stress results in faults for the Carbonate scenario with a heterogeneous caprock and sealing faults. Results are presented before injection (present-day), after one year of injection and after ten years of injection for different stress regimes. The points represent a cell results and lines represent Drucker-Prager criteria (outer in orange, inner in blue).

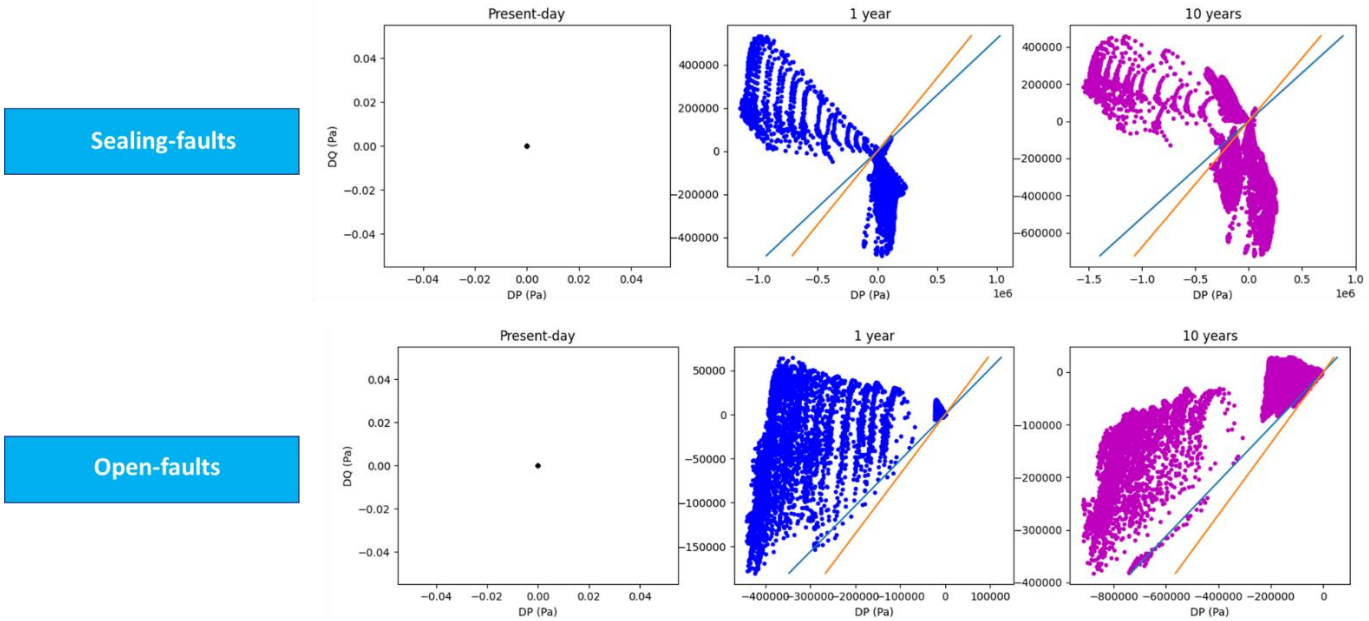

Figure 74 : Stress variations in faults for the Carbonate scenario with a heterogeneous caprock for StrikeSlip1 regime. The points represent a cell results and lines represent shifted along X-axis Drucker-Prager criteria (outer in orange, inner in blue).

5.3.2 Sandstone I scenario

Integrity analysis for Sandstone I scenario highlights several configurations in which integrity of caprock and stability of faults are questionable (Table 8). For caprock integrity, the inner Drucker-Prager criterion has been reached with the StrikeSlip 1 stress regime for all considered configurations (homogeneous or heterogeneous matrix, open or sealing faults). Regarding faults stability, the inner DP is reached for Compressive and StrikeSlip 2, while the outer DP is crossed for StrikeSlip 1 for all considered configurations.

	Sealing faults				**Open faults**			
	Heterogeneous		**Homogeneous**		**Heterogeneous**		**Homogeneous**	
	Caprock	***Faults***	***Caprock***	***Faults***	***Caprock***	***Faults***	***Caprock***	***Faults***
Compressive								
Extensive								
Strike-Slip 1								
Strike-Slip 2								

Table 8 : Integrity analysis results for Sandstone I scenario. Green: all stresses are below inner Drucker-Prager criterion, yellow: some stresses are between inner and outer Drucker-Prager criteria, red: some stresses are beyond outer Drucker-Prager criterion

In Figure 75 and Figure 71, stress distributions with heterogeneous caprock and sealing faults are presented before injection (present-day) and after 1 and 10 years of injection. The same observations as those made in the Carbonate scenario Figure 71 apply here. The initial stress distribution is scattered due to faults and heterogeneities, consequently, stress variations during injection are hardly visible. However, for considered materials properties and stress regimes, obtained stresses are closer to Drucker-Prager criteria than for the Carbonate scenario. The inner DP is locally reached for the StrikeSlip1 regime. In Figure 76, we can see that cells crossing the inner DP are all a part of the same material (facies (1) on Table 13) with stronger porosity and weak cohesion. The stress distribution with a homogeneous caprock is quite similar and does not show any noticeable differences.

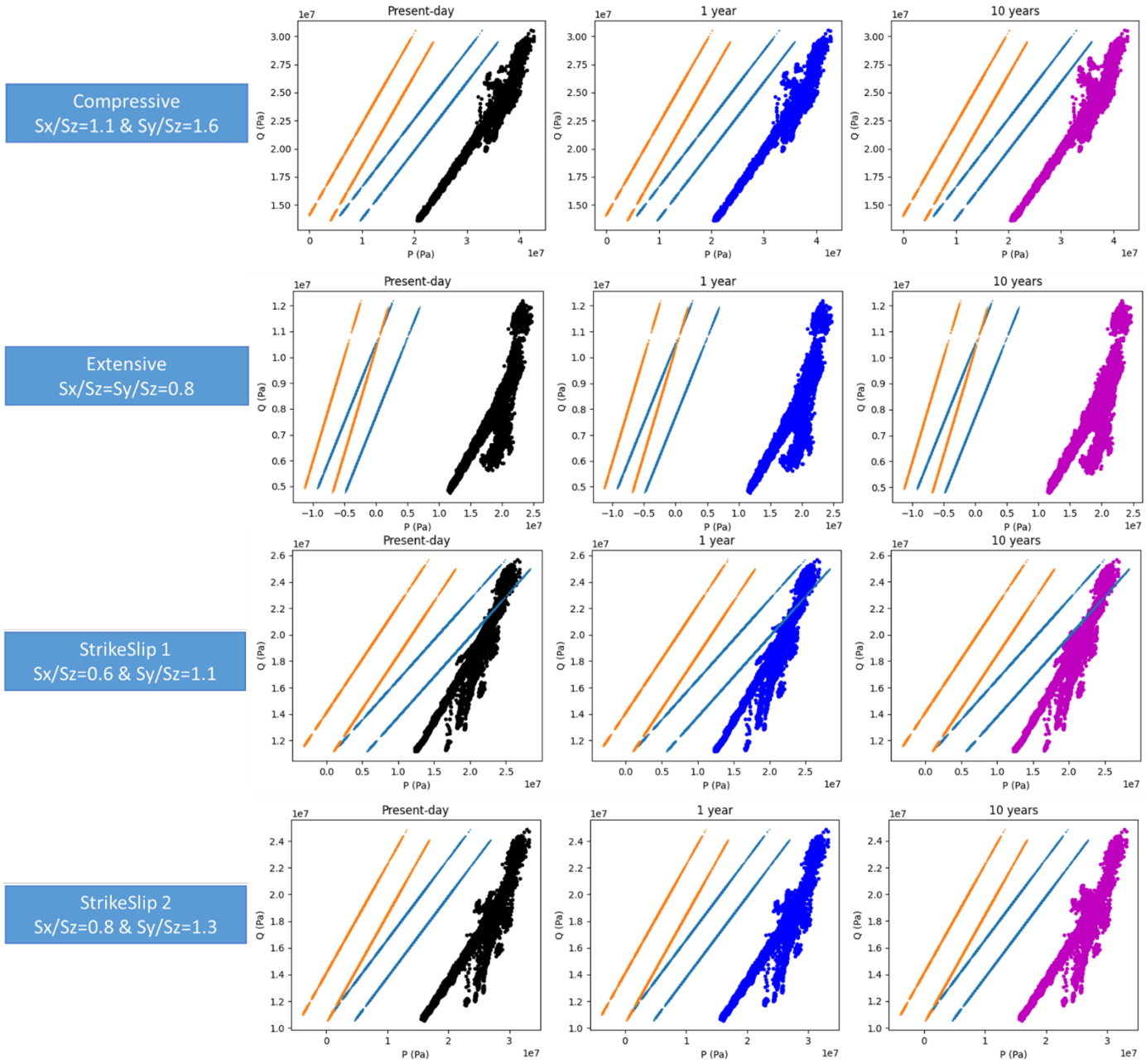

Figure 75 : Stress results in the caprock for the Sandstone I scenario with a heterogeneous caprock and sealing faults. Results are presented before injection (present-day), after one year of injection and after ten years of injection for different stress regimes. The points represent a cell results and lines represent Drucker-Prager criteria (outer in orange, inner in blue) for the 2 materials of caprock.

In Figure 77, stresses in faults zones are observed. Distributions are more scattered than for Carbonate scenario, and initial stress is critical for several regimes. For Compressive and StrikeSlip 2 regimes, the inner DP is reached at present-day and remain below outer DP during injection, with weak variation induced by the injection as seen in Figure 78. For StrikeSlip 1, the initial stress is beyond the outer DP. It means that the initial stress field is not plastically admissible. The distance (see Section 2.3.1) in terms of hydrostatic stress between the stress state at 10 years of injection and outer DP is displayed in Figure 79, the sub-seismic fault is closer to the criterion and tends more to be reactivated.

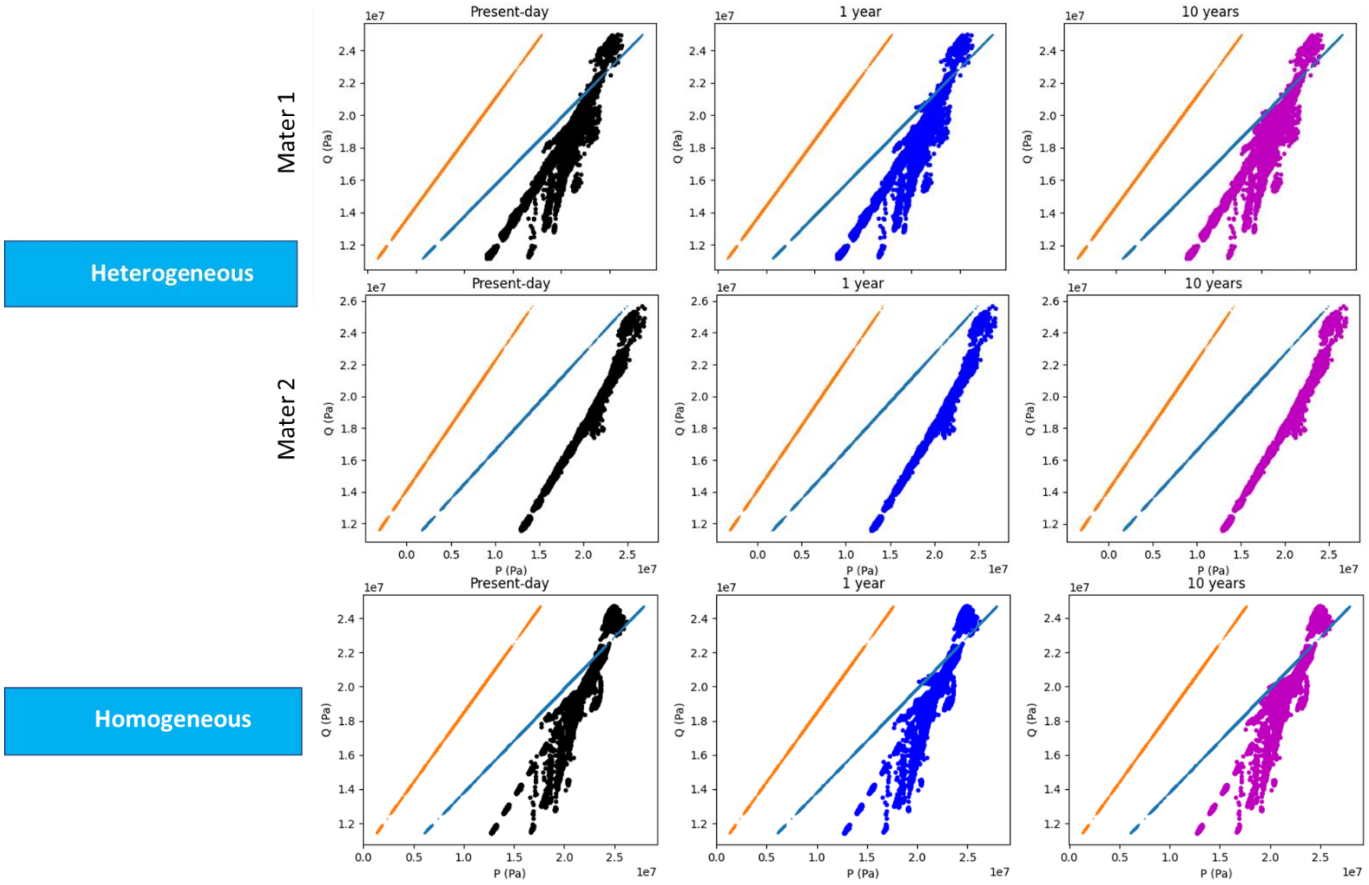

Figure 76 : Stress results in caprock for the Sandstone I scenario with sealing-fault for StrikeSlip 1 regime. Heterogenous caprock is separated in one figure per considered material. The points represent a cell results and lines represent Drucker-Prager criteria (outer in orange, inner in blue).

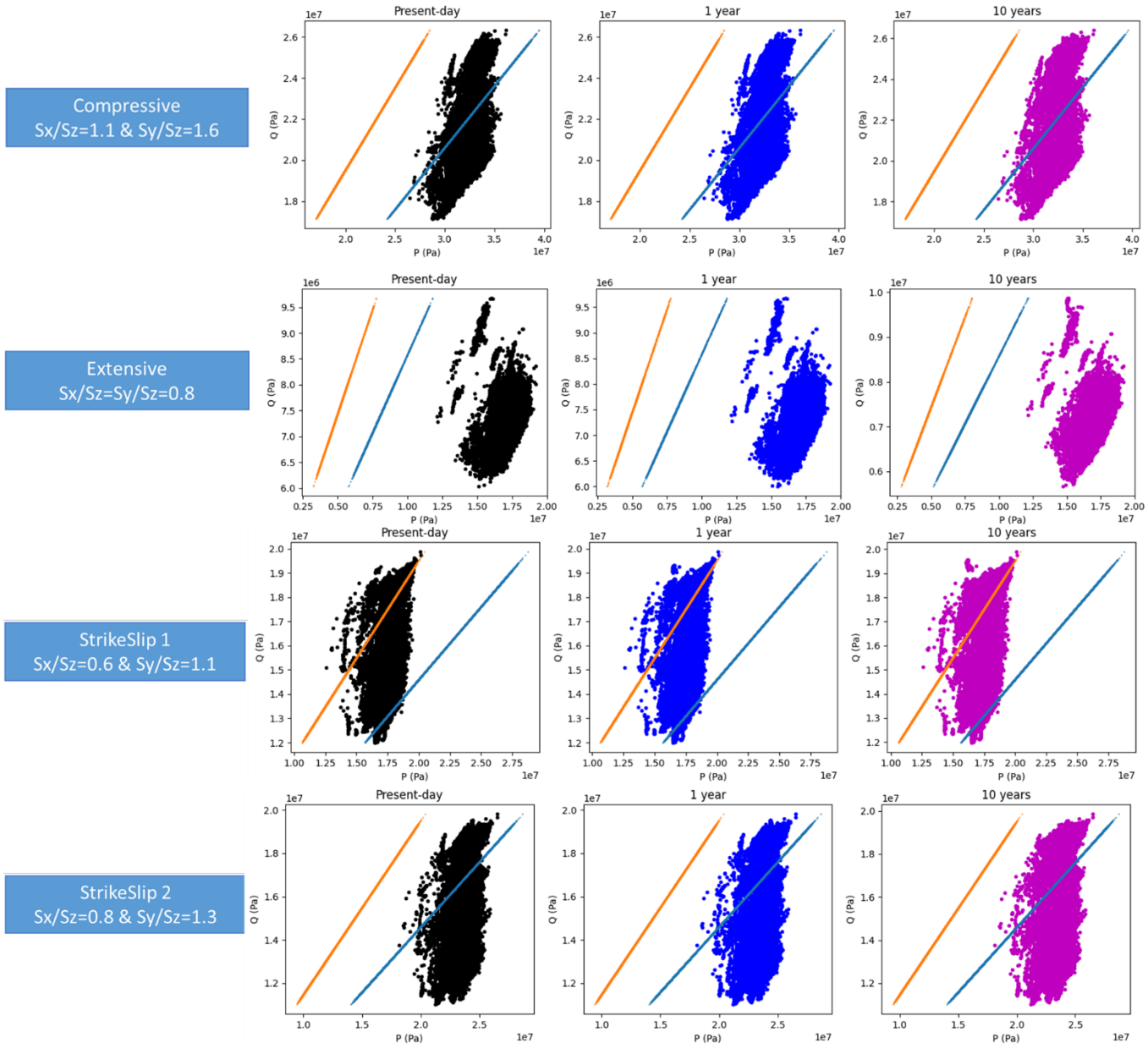

Figure 77 : Stress results in faults for the Sandstone I scenario with a heterogeneous caprock and sealing faults. Results are presented before injection (present-day), after one year of injection and after ten years of injection for different stress regimes. The points represent a cell results and lines represent Drucker-Prager criteria (outer in orange, inner in blue).

In Figure 78, stress variations for sealing and open faults are compared for the Compressive regime. Similarly to the Carbonate scenario (Figure 74), variations for sealing-faults are less regular but stronger than for open-faults. The impact of the injection on stress is weaker for the Sandstone 1 than for the Carbonate scenario. It should be noticed that for sealing or open faults cases, in the context of a Compressive initial regime, almost all stress points move towards the Drucker-Prager criteria during injection.

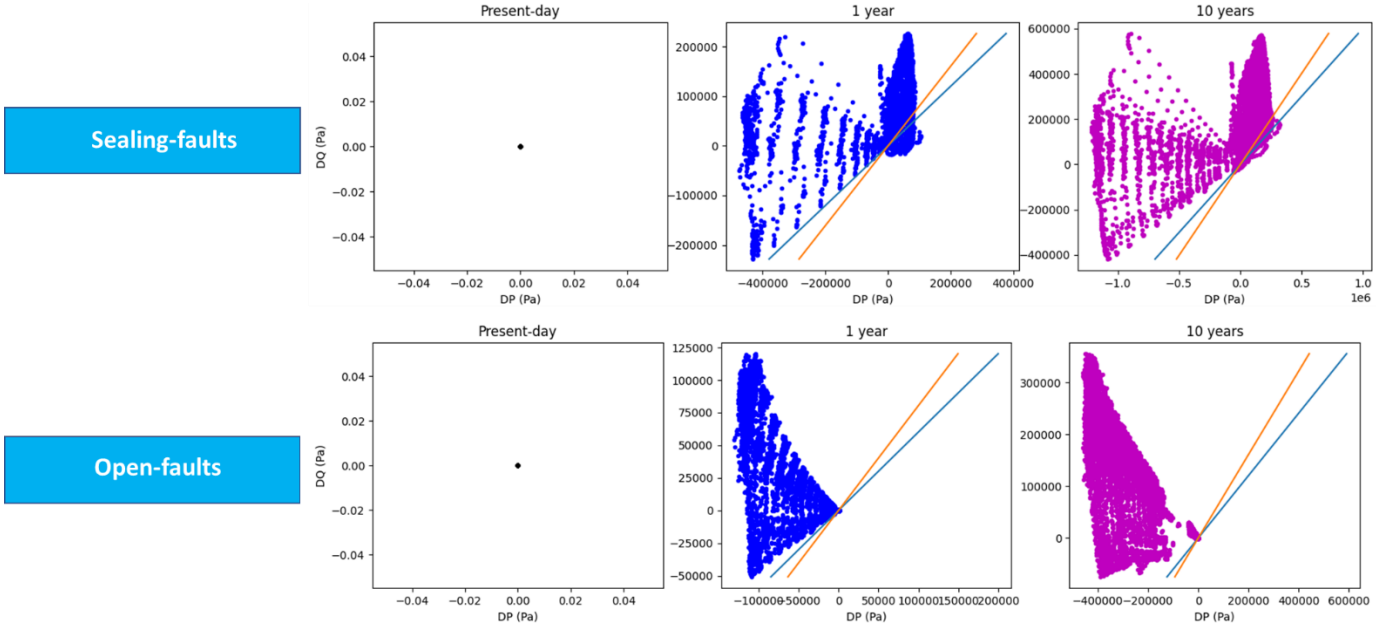

Figure 78 : Stress variations in faults for the Sandstone I case with a heterogeneous caprock for Compressive regime. The points represent a cell results and lines represent shifted along X-axis Drucker-Prager criteria (outer in orange, inner in blue).

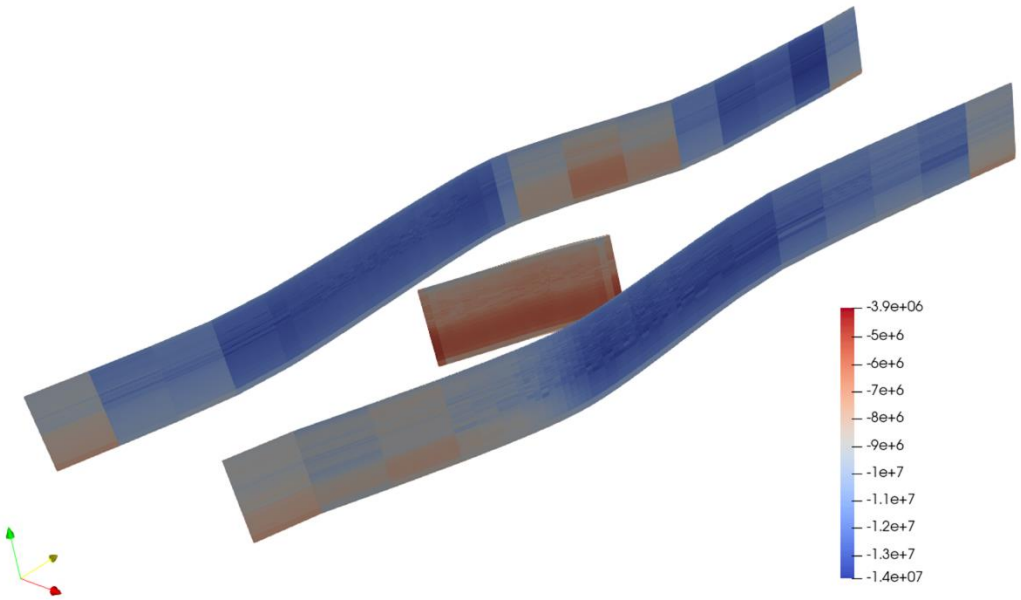

Figure 79 : Distance (Pa) from the outer Drucker-Prager criterion at 10 years of injection for Compressive regime and sealing faults.

5.3.3 Sandstone II scenario

Sandstone II is the most critical scenario in term of integrity. The inner DP is crossed for almost all considered configuration (except for caprock in an Extensive regime), and for several cases the initial stress is beyond the outer DP and plastically not admissible.

	Sealing faults				Open faults			
	Heterogeneous		Homogeneous		Heterogeneous		Homogeneous	
	Caprock	*Faults*	*Caprock*	*Faults*	*Caprock*	*Faults*	*Caprock*	*Faults*
Compressive								
Extensive								
StrikeSlip 1								
StrikeSlip 2								

Table 9: Integrity analysis results for Sandstone II scenario. Green: all stresses are below inner Drucker-Prager criterion, yellow: some stresses are between inner and outer Drucker-Prager criterion, red: some stresses are beyond outer Drucker-Prager criterion.

For the heterogeneous caprock with sealing faults, initial stress distributions in the caprock are more scattered than Carbonate and Sandstone I, moreover stress variations induced by injection are negligible (Figure 80). Inner DP is crossed for both StrikeSlip 1 and 2 regimes while isolated cells are beyond outer DP for Compressive regime.

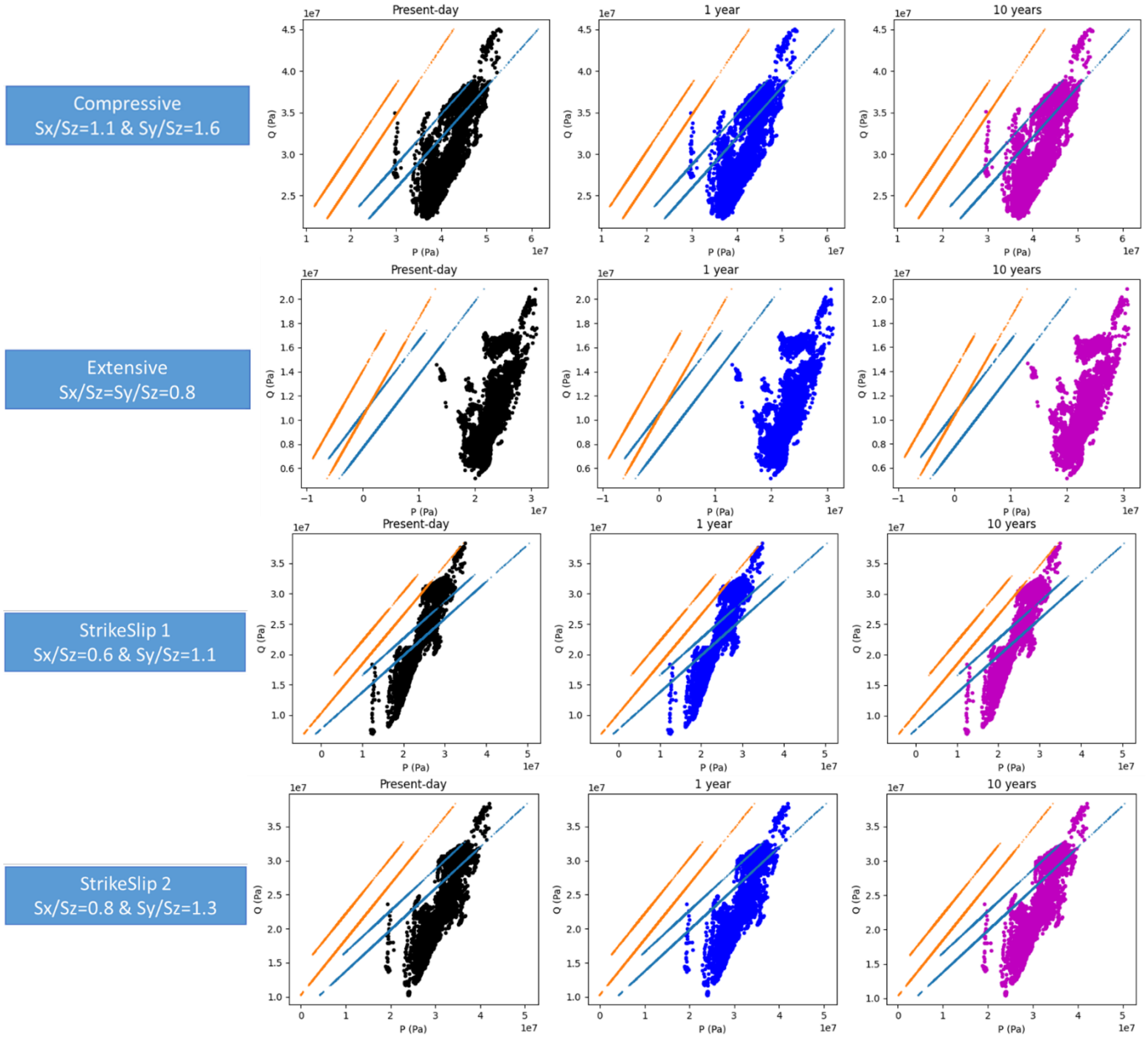

Figure 80 : Stress results in the caprock for the Sandstone II scenario with a heterogeneous caprock and sealing faults. Results are presented before injection (present-day), after one year of injection and after ten years of injection for different stress regimes. The points represent a cell results and lines represent Drucker-Prager criteria (outer in orange, inner in blue) for the 2 materials of caprock.

Differences in stress distributions are observed between heterogeneous and homogeneous caprock in Figure 81. Both cases are beyond the inner DP and very close to the outer DP. As observed for Sandstone I scenario, in the heterogeneous case, cells of facies1 are more subjected to integrity issues.

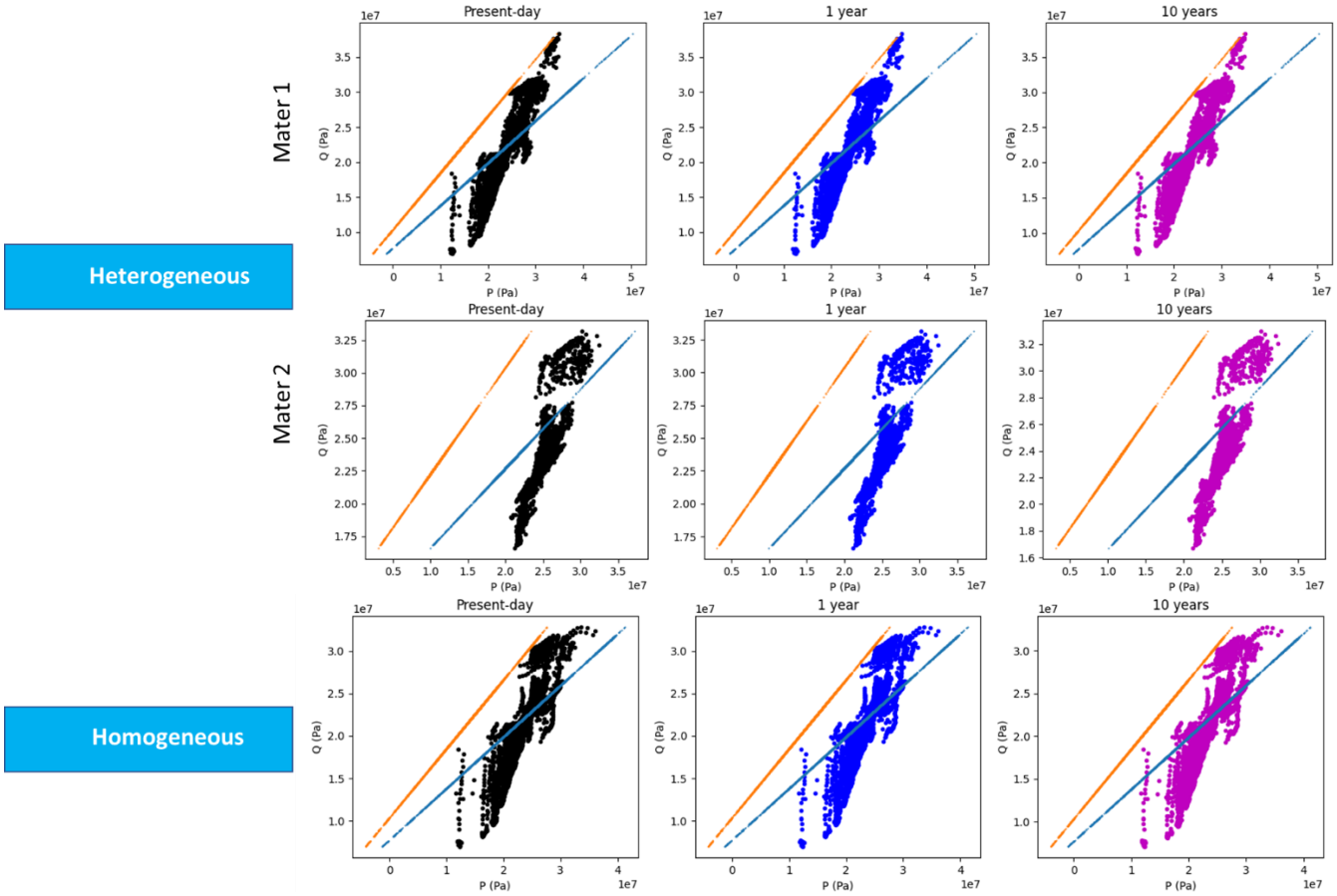

Figure 81 : Stress results in caprock for the Sandstone I case with sealing-fault for StrikeSlip1 regime. Heterogenous caprock is separated in one figure per considered material. The points represent a cell results and lines represent Drucker-Prager criteria (outer in orange, inner in blue).

Regarding distributions in faults zones (Figure 82 and Figure 73), obtained stresses are critical for all considered regimes. StrikeSlip 1 and 2 are beyond the outer DP, Compressive and Extensive regimes are beyond the inner DP and very close to the outer DP. The stress distribution is highly sparsed for Extensive regime. In Figure 84, we can see that the upper part of faults is far for the outer DP (>10MPa from the criterion in term of hydrostatic stress), while the lower part is very close (<1MPa from the criterion), the same behavior is observed on both principal and sub-seismic faults.

Stress variations for sealing and open faults are compared for the Extensive regime (Figure 83). For sealing faults, an irregular pattern is observed. Similarly to the other considered scenarios, some cells move to the criteria with a decreasing hydrostatic stress and a wide range of variation in equivalent stress, while other cells observe a drop in equivalent stress for a quasi-constant hydrostatic stress (moving away from criteria). For open faults almost all cells undergo a decrease of both hydrostatic and equivalent stresses moving away from Drucker-Prager criteria. Although induced variations magnitudes are weak (<0.5MPa after 10 years of injection), the pattern differ completely from that which is observed with a Compressive regime (Figure 78) and highlight the impact of the initial stress regime on the stress evolution during injection.

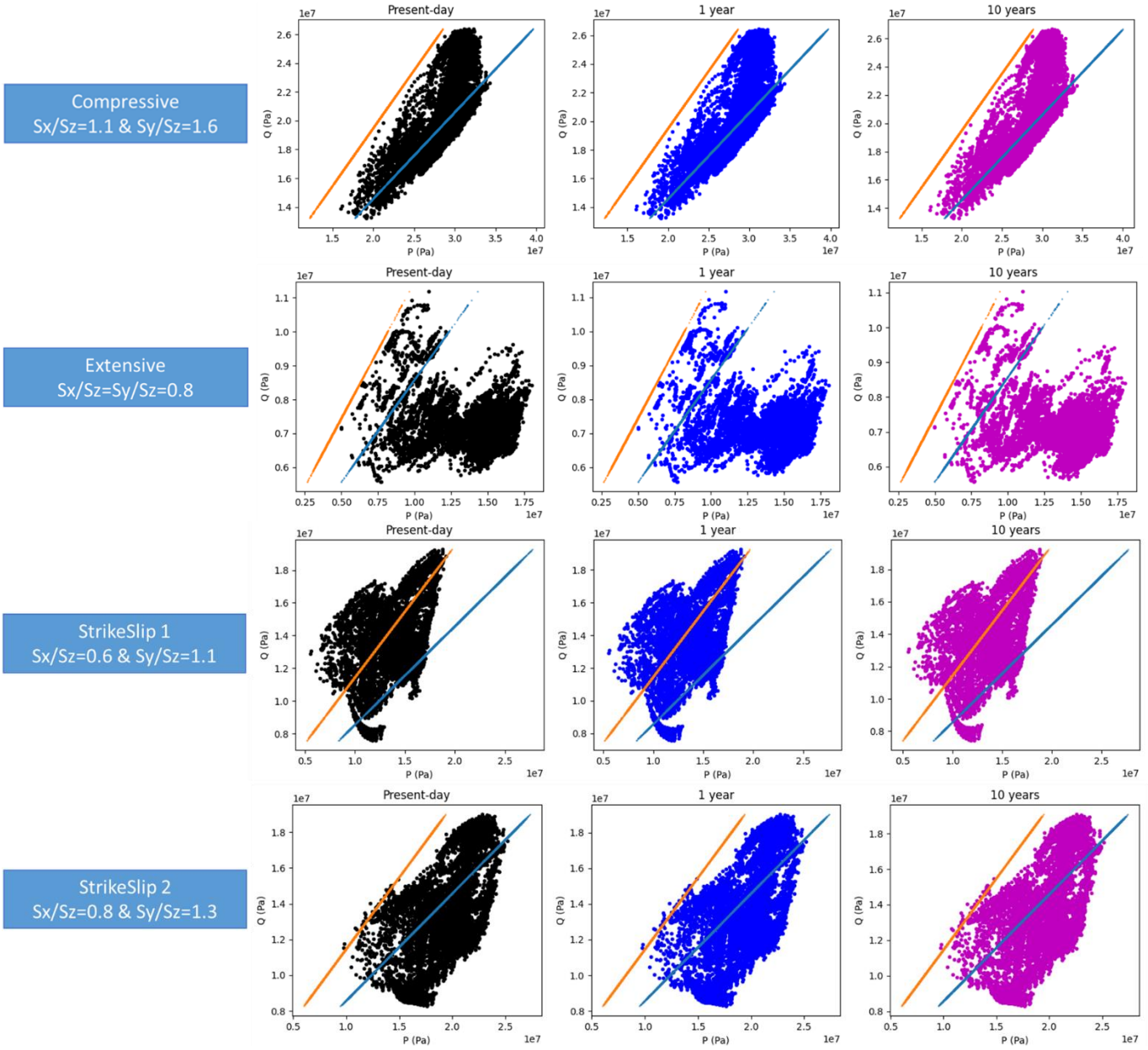

Figure 82 : Stress results in faults for the Sandstone II scenario with a heterogeneous caprock and sealing faults. Results are presented before injection (present-day), after one year of injection and after ten years of injection for different stress regimes. The points represent a cell results and lines represent Drucker-Prager criteria (outer in orange, inner in blue).

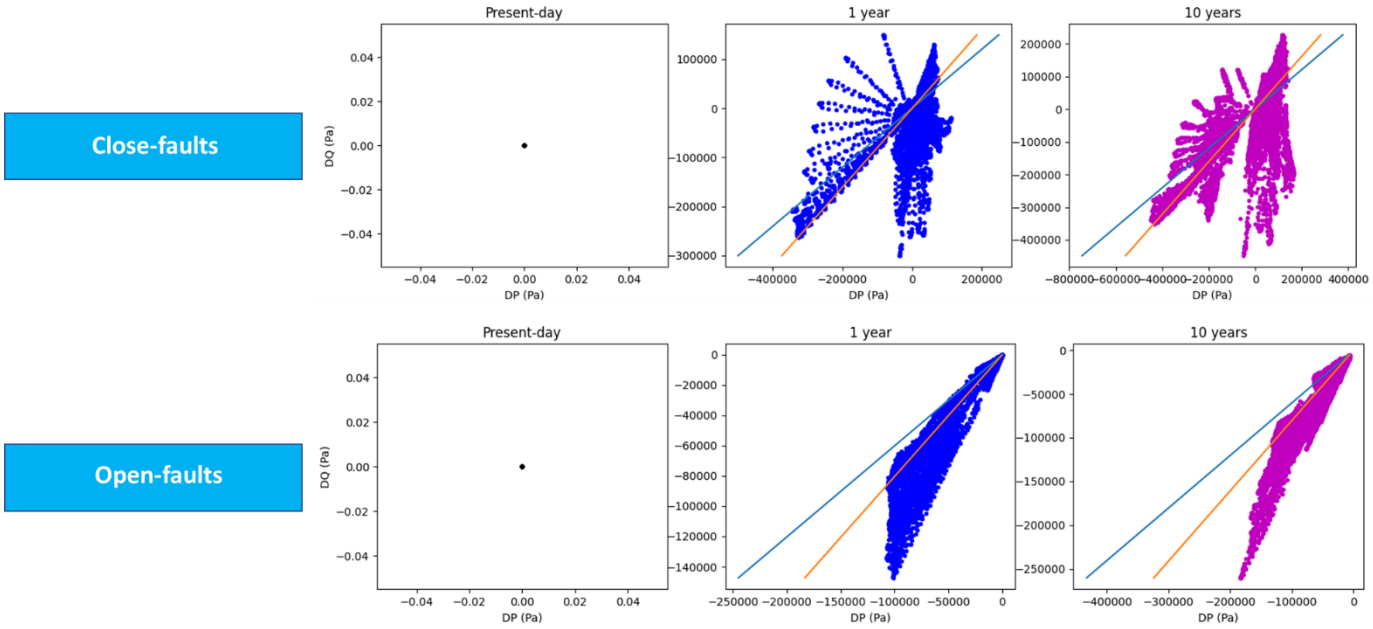

Figure 83 : Stress variations in faults for the Sandstone II scenario with a heterogeneous caprock for Extensive regime. The points represent a cell results and lines represent shifted along X-axis Drucker-Prager criteria (outer in orange, inner in blue).

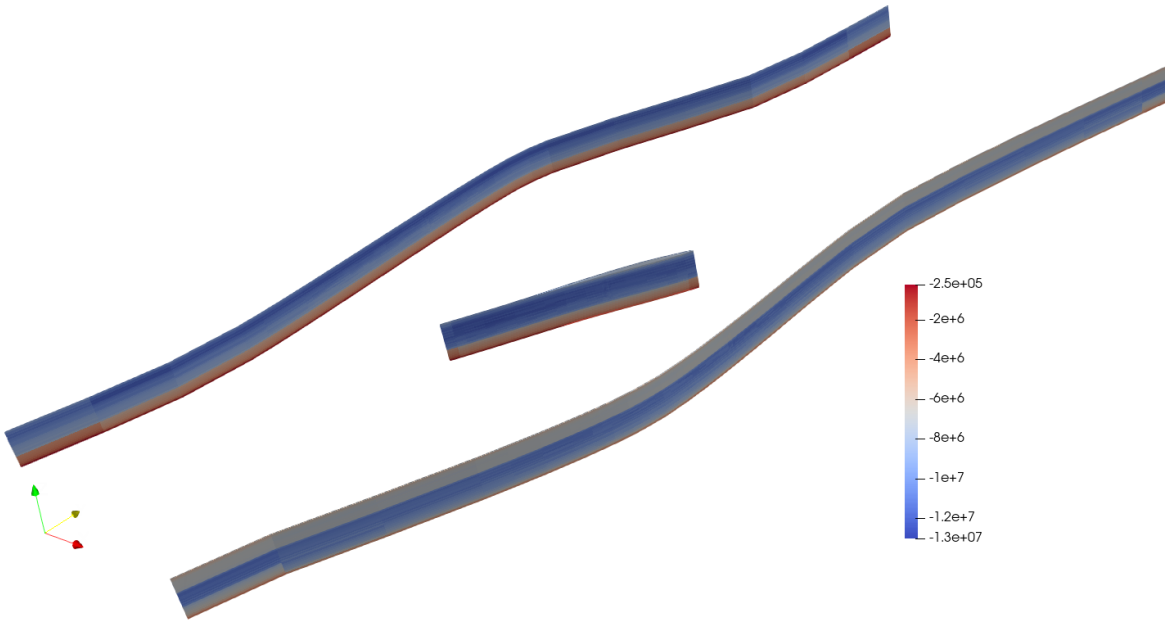

Figure 84 : Distance (Pa) from the outer Drucker-Prager criterion at 10 years of injection for Extensive regime and sealing faults.

5.3.4 Conclusions

Obviously, sealing faults have the strongest impact on the flow with a flow compartmentalization effect. Nevertheless, open faults aim to add additional heterogeneities in the reservoir that explain more dispersive scatter plot of stress results than for no-faulted cases.

The following observations are made from this integrity analysis.

- The initial stress regime is critical since it define the initial distance to the considered criterion (Section 2.3.1). In several cases, and particularly for Sandstone II scenario, the storage is already at risk (or maybe damaged) before the injection.
- The initial stress regime as well as the fault hydraulic behavior are strongly impacted by the stress variations induced by the injection. Various patterns have been observed, such as with an Extensive regime and open faults. Stress in faults move away from the Drucker-Prager criteria, on the contrary to a Compressive regime with sealing faults when stress evolve toward the criteria.
- The hydraulic behavior of faults has an impact on induced stress variation magnitude. For all considered scenarios, stress variation during injection is stronger with sealing faults.
- The chosen heterogeneity model in the reservoir and the caprock formation has a small impact of initial stress distribution (more scattered with heterogeneities), whereas impact on induced stress variation is negligible.

Regarding the considered fault scenario, we can conclude:

- for Carbonate cases, injection in all considered stress regimes is safe;
- for Sandstone I cases, injection in the Extensive regime is safe, while injection in Compressive and StrikeSlip 2 regimes present a risk and requires an advanced analysis on faults stability;
- for Sandstone II cases, even in Extensive regime the stability of faults may be jeopardized, injection should be avoided.

6 Conclusions and Recommendations

6.1 Conclusions

Developing techniques of geological CO_2 storage sites monitoring is crucial for both, the long-term safety of the sites themselves and the widespread deployment of this technology to be accepted as a reliable method of reducing CO_2 emissions worldwide. The SENSE project aims to develop reliable, continuous and cost-effective monitoring based on ground motion detection combined with modelling and geomechanical inversion, using new technological developments, data processing optimization and interpretation algorithms. In this context, we presented a methodology based on coupled flow-geomechanical simulations which, from the uncertainties on the subsurface properties and on the measurements, can reproduce measurements from different surface monitoring tools.

By carrying out an uncertainty study on simulations results and taking into account the advantages and disadvantages of each of these tools, a monitoring strategy can be designed such that the tools will record potential displacements at the most sensitive periods and locations, taking into account their respective accuracies. Based on this methodology, a workflow is developed and applied in this work to several conceptual models in order to identify which conditions induce different surface displacements and thus may require specific surface monitoring strategy. These conceptual models are built using several structural models and considering different sedimentary deposits contexts to cover different aspects of surface displacements that can be encountered at storage sites. A 10-years CO_2 injection (at a maximum 1 Mt/year constrained by a maximum overpressure of 50 bar) is defined for three on-shore scenarios:

- **Carbonate Case**, inspired from Brindisi and Michigan Basin storage sites
- **Sandstone I case**, inspired from In Salah and Gorgon projects.
- **Sandstone II case**, inspired from Snøhvit, Decatur and Otway storage sites.

First, an anticline structure without faults is considered for all the scenarios. For each of them, 115 coupled hydro-mechanical simulations are launched with a one-way coupling scheme. Simulated surface displacement results are significantly different between scenarios with an expected uplift can reach the centimeter-scale for Sandstone I, while for Sandstone II most of the expected uplifts would be far below the centimeter at the end of injection. These surface displacements can be directly related to the subsurface behavior: pressure and CO_2 migration but without directly identifying the geological formations where the pressure and gas saturation variations are located.

If the intensity of surface displacement is sufficient to be recorded by the surface monitoring tools thus, we would have an efficient subsurface monitoring tool based only on surface recording. INSAR technology and tiltmeters are studied in this simulation work to analyze their usefulness by estimating both the area and time period of validity for the three scenarios. Thus, we conclude that a monitoring area of 3 km radius from the well would be adapted for the Carbonate and Sandstone I scenarios based on a detection limit of 1 mm/year for INSAR measurements while for Sandstone II the monitoring area radius could reach 4.5 km. However, we can expect to obtain discriminating results for subsurface properties characterization only for Sandstone I due to a low standard deviation compared to the tool precision for Carbonate and Sandstone II scenarios. One interesting point for Sandstone II, though, is that the effect of anticline structure to CO_2 migration may be visible by the INSAR technology and may be recorded in some cases (asymmetrical displacement relatively to the well location).
Temporal monitoring recommendations are also estimated for the INSAR tool based on vertical displacement velocities over the well as a function of time. For all simulations and scenarios, the fastest vertical displacements occur near the well. While for the Sandstone II and Carbonate scenarios most of the displacement occurs at the early stage of the injection with results above the detection up to 2 or 3 years, for the Sandstone I case there is no restriction with time. For post-injection period, the simulation results show that subsidence behavior could be monitored via InSAR data in most cases for Sandstone I and Carbonate.

For tiltmeters, it would be recommended to locate the sensors about 1.5 km from the well for short- and long- term monitoring for Carbonate case. The same recommendation applied for Sandstone I but extra-tiltmeters could be also located further away, at about 8 km from the well. For Sandstone II case, the recommendations would be to locate sensors further away from the well, around 5 km and 10 km from the well, to monitor surface displacement over time.

The next step is designing the surface displacements monitoring plan. We propose a methodology for estimating the most sensitive locations that we apply only for tiltmeters (with a 50 nanorads detection limit) on the Carbonate case. First, the storage formation permeability and the Young modulus of the overburden are defined as the most sensitive uncertain parameters by a sensitivity analysis. To optimize the monitoring design with the objective to better constrain these subsurface properties, we propose in the workflow to select tiltmeters locations at locations corresponding to high dependency (HSIC value) between tiltmeters measurements and uncertain properties in addition to locations with the highest variance for tiltmeters measurement based on uncertainty analysis and related simulations. Based on this method, we select seven locations for observation data along the Y-axis for the Carbonate case. For each set of simulations, these selected locations allow to better constraint the *a posteriori* distribution close to the real subsurface properties than using random locations.

Then, we propose to analyse a storage integrity with failure criteria to define the locations where a risk of damage is identified. In this stage, four different initial stress regimes were applied: Extensive regime, StrikeSlip 1 and 2, Compressive regime. For all scenarios (Carbonate, Sandstone I and II), the failure criteria are never reached in the Extensive regime. On the contrary, for all scenarios, the inner failure criterion is reached for a significant part of simulations, even at the initial state in the StrikeSlip 1 context. That context is the most unfavorable one, for which CO_2 storage may not be sustainable whatever the injection design. Those differences emphasize the importance of properly defining the initial stress regime. For the two others stress regimes, the risk of failure is quite different depending on the considered geological scenario. For each area where the failure criterion is reached, we recommend to put additional measurement points to monitor an eventual change in the surface displacements due to fracturation in subsurface.

One-way coupling simulations were performed for the previous statistical and sensitivity analyses. However, one-way coupling may lack of accuracy in terms of surface displacements or flow simulation results compared to more intensive computational methods such as iterative coupling. To quantify the loss of accuracy and the gain in computational time for the one-way coupling, we compare performances between both methods for the Carbonate and Sandstone II scenarios. For both scenarios, the one—way coupling may underestimate the extents predictions for CO_2 plume and pressure distribution (about few hundred meters for CO_2 plume and few kilometers for pressure perturbations for Carbonate scenario and several hundreds of meters for CO_2 plume, and several kilometers for pressure perturbation for Sandstone II). The same effect is observed for the surface displacements. Consequently, the difference in monitoring area recommendation will be a four-fold increase (relatively to a two-fold increase in the Carbonate scenario) using iterative coupling. Thus, surface displacements would be detectable on a larger area and for a longer time period with iterative results. *A contrario*, a sensitivity analysis conducts to the same conclusion. Iterative coupling is more accurate than one-way coupling, but it implies a higher computational cost (twice or four times in the studied cases).

Considering faulted reservoirs, the sealing faults have a major impact on CO_2 injection. The surface displacements may have a non-gaussian shape and faults presence may be detected thanks to a move of the area with a maximum surface displacement.
Without these kinds of workflow giving information of the displacement magnitude, it is difficult to predict what will be observable from the surface. For studied faulted synthetic cases, only a variation of the area of a maximum surface displacement (not center on the well) seems to be observable considering sealing faults while matrix heterogeneities and the open faults have not a strong impact on the displacements. Nevertheless, open faults as additional heterogeneities in the reservoir are characterized by more dispersive scatter plots of stress results than for no-faulted cases.

The initial stress regime stays a critical input to study the reservoir integrity while the hydraulic behavior of faults has an impact on induced stress variation magnitude. For all considered scenarios, stress variation during injection is stronger with sealing faults. Regarding the considered fault scenario, injection in the studied Carbonate case seems to be safe and for Sandstones I with Extensive regime too. Other scenario needs an advanced analysis or more precise modeling. Some of these conclusions differ from the results of the first no-faulted cases. However, analysis was done considering a critical simulation case to underline a mechanical behavior for homogeneous cases while the median values from the previous uncertain analysis were chosen to underline the fault impacts for faulted cases. Moreover, the open-fault and homogeneous cases differ since the open-fault case contain throws. This last remark highlights the fact that CO_2 injection must be carefully studied taking into account geological structures, initial stress, and heterogeneities.
From a surface monitoring point of view, these results also showed the importance to study first the near well surface displacements. Indeed, a shift between the location of the center of the maximal surface displacement area and the top of the well might indicate the presence of a strong heterogeneity. Similarly, an evolution of this shift would indicate an evolution of the heterogeneity properties (typically a fault aperture increase) and a possible CO_2 migration through it.

Thus, these works allowed to define some storage conditions where soil surface monitoring can be useful for CCS even if they should be continued to improve the results with (1) a sensitivity study to the injection conditions, the heterogeneity scale and the sub-seismic characteristics and (2) the assessment of the most informative dates with the same statistics methodology as for the surface displacement measurement locations one. Moreover, this study was based on synthetic cases which allow to work in different storage conditions but with simplified models. The results give an overview of the storage behavior, but the next step should be to extend this study to a real case, which is planned in the WP2.3 of the SENSE project.

Nevertheless, this study allowed us to highlight that if surface displacements are measurable and sufficiently sensitive to subsurface properties then this type of monitoring will be very useful for operators and regulators:

- to monitor the subsurface deformations that is one of the impacts of the CO_2 injection,
- to have a numerical model able to predict the long-term CO_2 storage fate
    - by better constraining the most sensitive subsurface properties and pressure propagation and possibly subsurface behavior such as plume migration and storage capacity,
    - by analyzing the surface deformation shape to better know the subsurface structure and heterogeneities as static objects if they are detectable by this surface data.
- consequently, to be able to give early warning of an unexpected behavior if the monitored surface deformation does not correspond to the expected one estimated by simulation and quickly define the actions of remediation.

Compared to data measured locally at the wells, the main advantage of the soil surface data is either to give 2D information of the subsurface behavior with the INSAR technology at time frequency that can be high or local information along lines with tiltmeters in informative or risky areas. The 2D or 3D seismic technology gives the same advantages but at a lower time frequency due to higher costs.

This work was also useful

- to define a workflow to help designing the surface displacement monitoring plan,
    - definition of the area where (and the period of time when) surface displacements are measurable with a tiltmeter and INSAR technology
    - determination of the most sensitive uncertain parameters for which the soil surface displacement data would be the most informative
    - design (location of measurements) of an optimized monitoring plan to better constrain the sensitive parameters.
    - determination of additional points of monitoring with a risk analysis based on a failure criteria

- to highlight the necessity to have information regarding the initial stress regime for faults to reduce the simulation result uncertainty,
- to analyze the benefit of each type of coupling for the fluid flow geomechanical simulation (one-way, iterative).

6.2 Set of recommendations and guidelines

We recommend to operators and regulators:

- to use the surface deformation data as monitoring data both to improve the knowledge and to monitor the CO_2 storage behavior,
- to use the workflow developed in this study to help designing the surface displacement monitoring plan,
- to acquire the critical data listed previously to minimize the uncertainty of the simulated surface displacement and the risk analysis,
- to adapt the type of coupling as function of its usefulness
    - A statistical or sensitivity analysis might not always be performed with iterative coupling simulations due to its cost,
    - if any elements at risk exists in the uncertainty range, one would have to consider using iterative coupling to improve the risk analysis.

For the monitoring tools, we draw the following recommendations:

<u>For satellite measurements:</u>

- The area of interest for surface displacement data processing should be limited to the expected extent of surface displacements. This would avoid unnecessary processing knowing that processing time is directly proportional to data size/amount and limit the memory requirements. Same kind of recommendations can be drawn by defining time periods of interest (when surface displacements remain above InSAR detection limit)
- On expected displacements intensity:
    - the intensity of mean and maximum surface displacements should be defined in absolute values. This should define if specific requirements are needed, e.g. requirements to improve the accuracy of satellite data, recommendations for processing algorithm, temporal sampling, or recommendations for corner reflectors installation if surface displacements remain low compared to detection limit.
    - The expected displacements intensity is function of simulated spatial displacement variability. This would impact the spatial resolution and thus the satellite type to be used.
    - The expected displacements intensity is function of local sensitivity. Location of corners-reflectors could be also focused on areas with a high sensitivity or displacements variations.
- Monitoring strategy with InSAR data would have to be adapted to the considered context with
    - Temporal definition and Spatial Definition
    - InSAR precision
        - Specific high precision requirements for Sandstone II (*e.g.* consider installing corner-reflectors which will improve the accuracy for precision requirements or use more precise satellite data such as TerraSar-X (0.75 m x 0.25 m) compared to Sentinel-1 (5 m x 20 m) but at higher cost).
        - Given the small variations for the Carbonate case, it could be interesting to consider locating corner-reflectors (which will improve the accuracy) in the areas of high uncertainties.

These specifications could be of high values to better constrain the time-consuming processing of InSAR data and related cost (including type of InSAR data, use of corner-reflectors,

use of supplementary monitoring techniques). For example, InSAR data could be used to constrain heterogeneous values of elastic properties of the medium. Different uses of data for inversion are possible depending on their degree of accuracy: use of all types of data simultaneously, or, for example, use of the result of the calibration of InSAR data as *a priori* for the calibration of tiltmeter or GNSS data.

For tiltmeters:

- Sufficient and necessary monitoring resolution for the storage site is function of simulated displacements: locating tiltmeters in areas with sufficient simulated displacements relatively to sensors resolution,
- Defining the most promising locations for sensors, *i.e.* ones with lateral and vertical displacement, with a high variability and/or sensitivity function of uncertainties and considered scenarios. For example, tiltmeters could be located at the expected flanks of the surface uplift.

7 Bibliography

Baroni, A., Estublier, E., Deflandre, J.-P., Daniel, J.-M. (2011). Modelling surface displacements associated with CO_2 reinjection at Krechba. 45th US Rock Mechanics / Geomechanics Symposium.

Baroni, A., Estublier, A., Vincké, O., Delprat-Jannaud, F., Nauroy, J-F., (2015). Dynamic Fluid Flow and Geomechanical Coupling to Assess the CO_2 Storage Integrity in Faulted Structures. Oil & Gas Science and Technology - 70 (4), pp.729-751.

Barros, E., Leeuwenburgh, O. and Boullenger B. (2020). Practical quantitative monitoring strategy assessment for conformance verification of CO2 storage projects. 82nd EAGE Conference and Exhibition 2020, Amsterdam, The Netherlands, December 8-11.

Bouquet, S., Frey, J., Malinouskaya, I., Soulat, A., Estublier, A., Fourno, A., (2021a). Analysis of Surface Movement through Conceptual and Coupled Flow-Geomechanics Models an Example of Surface Monitoring Assessment for CCS Project. SINTEF Proceedings;7, Chapter. Bouquet S., Fourno A., Estublier, A., Frey, J., Malinouskaya, I., (2021b). Assuring integrity of CO2 storage sites through ground surface monitoring (SENSE) – WP2.1: Presentation of conceptual models (Delivrable D2.1).

Cook, P.J., (2014). Geologically Storing Carbon: Learning from the Otway Project Experience. CSIRO Publishing, Melbourne, ISBN: 978-1-118-98618-9.

Coussy, O. (1991) Mécanique des milieux poreux', chapitre VIII. pp. 346.

Da Veiga, S. (2015). Global sensitivity analysis with dependence measures. Journal of Statistical Computation and Simulation, 85(7):1283–1305.

Deflandre, J.-P., Estublier, A., Baroni, A., Fornel, A., Clochard, V., Delépine, N. (2013). Assessing field pressure and plume migration in CO_2 storages: Application of case-specific workflows at in Salah and Sleipner. Energy Procedia, 37, pp. 3554-3564. doi: 10.1016/j.egypro.2013.06.248

De Lozzo, M., Marrel, A. (2017). New improvements in the use of dependence measures for sensitivity analysis and screening. Journal of Statistical Computation and Simulation. DOI :10.1080/00949655.2016.1149854

Drucker, D.-C., Prager, W., (1952): Soil mechanics and plastic analysis or limit design. Quart. Appl. Math. 10, 157–175.

Dsurizin, D. (2003). A comprehensive approach to monitoring volcano deformation as a window on the eruption cycle. Reviews of Geophysics, 41, 1 / 1001, American Geophysical Union, doi:10.1029/2001RG000107.

EDF. Code_aster, Analyse des Structures et Thermo-mécanique pour des Études et des Recherches. www.code-aster.org [consulté le 05/10/2020]

Estublier, A., Lackner, A.F.(2009). Long-term simulation of the Snøhvit CO_2 storage, Energy Procedia, Volume 1, Issue 1, Pages 3221-3228, ISSN 1876-6102, https://doi.org/10.1016/j.egypro.2009.02.106.

Feraille, M., Marrel, A. (2012). Prediction under Uncertainty on a Mature Field. Oil & Gas Science and Technology – Rev. IFP Energies Nouvelles, Vol 67, No. 2, pp. 193-206. DOI: https://doi.org/10.2516/ogst/2011172

Flett, M. et al. (2008). Gorgon Project: Subsurface evaluation of carbon dioxide disposal under Barrow Island. SPE Asia Pacific Oil and Gas Conference, Perth, Australia, October 20-22 . SPE 116372.

IFP Energies nouvelles (2018). PumaFlow 10.0 reference manual. France.

Mainguy, M, Longuemare, P. (2002) Coupling Fluid Flow and Rock Mechanics: Formulations of the Partial Coupling Between Reservoir and Geomechanical Simulators, Oil & Gas Science and Technology - Rev. IFP, 57 4 355-367

McColpin, G. (2009). Surface Deformation Monitoring As a Cost Effective MMV Method. Energy Procedia 1(1):2079-2086. DOI: 10.1016/j.egypro.2009.01.271

McKay, M.D., Beckman, R., Conover, W. (1979). A Comparison of Three Methods for Selecting Values of Input Variables in the Analysis of Output from a Computer Code. In Technometrics, Vol. 21, No. 2, pp. 239-245. DOI: https://doi.org/10.1080/00401706.1979.10489755

Michael, K., Golab, A., Shulakova, V., Ennis-King, J., Allinson, G., Sharma, S., Aiken, T (2010). Geological storage of CO_2 in saline aquifers-A review of the experience from existing storage operations, International Journal of Greenhouse Gas Control, 4 (4), pp. 659-667. doi: 10.1016/j.ijggc.2009.12.011

Niemi, A., Bear, J., Bensabat, J. (2017). Geological Storage of CO_2 in Deep Saline Formations, Volume 29 de Theory and Applications of Transport in Porous Media, Springer.

Rutqvist, J., Rinaldi, A. P., Vilarrasa, V., Cappa, F. (2019). Chapter 10 - Numerical Geomechanics Studies of Geological Carbon Storage (GCS), Editor(s): Pania Newell, Anastasia G. Ilgen, Science of Carbon Storage in Deep Saline Formations, Elsevier, Pages 237-252, ISBN 9780128127520, https://doi.org/10.1016/B978-0-12-812752-0.00010-1.

Schembre-McCabe, J.M., Kamath, J., Gurton, R. (2008). Mechanistic Studies of CO_2 Sequestration. International Petroleum Technology Conference. Dubai, UAE, December 4-6. IPTC 11391.

Schweizer, D., Blum, P., Butscher, C. (2017). Data assimilation and uncertainty assessment in 3D geological modeling. Solid Earth Discussions, 1-23.

Skerlec, G.M., (1999). Treatise of Petroleum Geology / Handbook of Petroleum Geology: Exploring for Oil and Gas Traps. Chapter 10: Evaluating Top and Fault Seal, AAPG Special Volumes. https://wiki.aapg.org/Fault_seal_behavior

Sobol, I.M, (1993). Sensitivity analysis for non-linear mathematical models, Mathematical modelling and computational experiment (translated from Russian: I.M. Sobol', sensitivity estimates for nonlinear mathematical models. Matematicheskoe Modelirovanie 2 (1990), 112–118 407–414).

Szulczewski, M.L., MacMinn, C.W., Juanes, R. (2014). Theoretical analysis of how pressure buildup and CO_2 migration can both constrain storage capacity in deep saline aquifers, International Journal of Greenhouse Gas Control, Volume 23, Pages 113-118, ISSN 1750-5836, https://doi.org/10.1016/j.ijggc.2014.02.006

Touhidi-Baghini A. (1998) Absolute permeability of McMurray formation oil sands at low confining stress, PhD Thesis, Department of Civil and Environmental Engineering, Univ. of Alberta.

Tremosa, J., Castillo, C., Vong, C.Q., Kervévan, C., Lassin, A., Audigane, P. (2014). Long-term assessment of geochemical reactivity of CO_2 storage in highly saline aquifers: Application to Ketzin, In Salah and Snohvit storage sites. International Journal of Greenhouse Gas Control,Elsevier, 2014, 20, pp.2-26..

Vasco, D., Ferretti, A., Rucci, A., Samsonov, S., & White, D. (2019). Monitoring the Deformation Associated with the Geological Storage of CO_2. In T. Davis, M. Landrø, & M. Wilson (Eds.), Geophysics and Geosequestration (pp. 93-114). Cambridge University Press. DOI 10.1017/9781316480724.007

Zhou, Q., Birkholzer, J.T., Mehnert, E., Lin, Y.-F. and Zhang, K. (2010), Modeling Basin- and Plume-Scale Processes of CO_2 Storage for Full-Scale Deployment. Groundwater, 48: 494-514. doi:10.1111/j.1745-6584.2009.00657.x

Annex A - Literature study

1. Figures table

2. Tables table